EXPERIMENTS WITH A FOUR-BLADED CYCLIC PITCH STIRRING MODEL ROTOR

Part III of First Yearly Report under Contract NAS2-76`3

Prepared for the Ames Directorate, AMRDL,
at Ames Research Center, Moffett Field, California

by

K. H. Hohenemser

and

S. T. Crews

Department of Mechanical and
Aerospace Engineering

Washington University
School of Engineering and Applied Science
St. Louis, Missouri

June, 1974

EXPERIMENTS WITH A FOUR-BLADED CYCLIC PITCH STIRRING MODEL ROTOR

Part III of First Yearly Report under Contract NAS2-7613

Prepared for the Ames Directorate, AMRDL,
at Ames Research Center, Moffett Field, California

by

K. H. Hohenemser

and

S. T. Crews

Department of Mechanical and
Aerospace Engineering

Washington University
School of Engineering and Applied Science
St. Louis, Missouri

June, 1974

Preface to First Yearly Report under Contract NAS2-7613

Work under Contract NAS2-7613 started on July 1, 1973. It is a continuation of research conducted since February 1, 1967, under Contract NAS2-4151. Phase VII-A, B and C Reports of June, 1973, titled, "Concepts for a Theoretical and Experimental Study of Lifting Rotor Random Loads and Vibrations", are the final reports under Contract NAS2-4151 and list the 9 preceding reports and 11 published articles and papers prepared under the contract.

Meanwhile 2 further papers generated under this Contract have been published:

Crews, S. T., Hohenemser, K. H. and Ormiston, R. A., "An Unsteady Wake Model for a Hingeless Rotor", Journal of Aircraft Vol. 10, No. 12, Dec. 1973, pp. 758-760.

Hohenemser, K. H. and Prelewicz, D. A., "Computer Experiments on Periodic Systems Identification Using Rotor Blade Transient Flapping-Torsion Responses at High Advance Ratio", AHS/NASA Ames Specialists Meeting on Rotorcraft Dynamics, Moffett Field, California, February 1974.

The first paper which has been generated under the new Contract NAS2-7613 is:

Hohenemser, K. H. and Yin, S. K., "On the Use of First Order Rotor Dynamics in Multiblade Coordinates", presented at the 30th Annual National Forum of the American Helicopter Society, May 1974, Preprint 831.

II

The research goals stated in Contract NAS2-7613 are

(a) Assess analytically the effects of fuselage motions on stability and random response. The problem is to develop an adequate but not overly complex flight dynamics analytical model and to study the effects of structural and electronic feedback, particularly for hingeless rotors.

(b) Study by computer and hardware experiments the feasibility of adequate perturbation models from non-linear trim conditions. The problem is to extract an adequate linear perturbation model for the purpose of stability and random motion studies. The extraction is to be performed on the basis of transient responses obtained either by computed time histories or by model tests.

(c) Extend the experimental methods to assess rotor wake-blade interactions by using a 4-bladed rotor model with the capability of progressing and regressing blade pitch excitation (cyclic pitch stirring), by using a 4-bladed rotor model with hub tilt stirring, and by testing rotor models in sinusoidal up or side flow.

The first yearly report under Contract NAS2-7613 is subdivided into 3 parts, whereby Parts I, II, and III are related to the research goals (a), (b), and (c) respectively. The authors and titles of the three parts are:

Part I, Hohenemser, K. H. and Yin, S. K., "Methods Studies Toward Simplified Rotor-Body Dynamics".

Part II, Hohenemser, K. H. and Yin, S. K., "Computer Experiments in Preparation of System Identification from Transient Rotor Model Tests".

Part III, Hohenemser, K. H. and Crews, S. T., "Experiments with a Four-Bladed Cyclic Pitch Stirring Model Rotor".

Part I considers a number of simplifications in rotor-body dynamics and applies the various analytical models to a hypothetical compound hingeless rotorcraft with and without feedback into cyclic and collective controls.

Part II deals with the problem of rotor parameter identification from noise polluted transient blade flapping responses. Computer experiments are used in order to gain some insight into the efficiency of various identification schemes to be later applied to rotor model flapping transients.

Part III summarizes the test results obtained with the 4-bladed cyclic pitch stirring model rotor. The analytical blade flapping responses without considering the rotor wake are compared to the measured responses which include the wake-blade interactions.

IV

EXPERIMENTS WITH A FOUR-BLADED CYCLIC PITCH STIRRING MODEL ROTOR

Part III of First Yearly Report under Contract NAS2-7613

Abstract

The experimental work with the 2-bladed 16-inch diameter model rotor reported in Phase VII-C Report under Contract NAS2-4151 of June 1973 has been continued with a 4-bladed 16.5 inch diameter rotor capable of progressing and regressing cyclic pitch excitation (cyclic pitch stirring). Advance ratios of 0, .19 and .38 were tested at rotor speeds corresponding to non-dimensional blade natural frequencies of 1.14 and 1.19. The results are presented in the form of the first 5 Fourier components of the periodic response modulating function which for a periodic system takes the place of the complex response amplitude ratio of a constant system. In addition, the first and second hormonics of the trim response are presented. The test data are compared to analytical data without rotor wake and to the test data obtained earlier with the two bladed rotor model of half the blade solidity ratio. The larger wake effect of the 4-bladed rotor at the same collective pitch setting is evident. Dynamic downwash data at zero advance ratio are presented. In addition to the test data obtained to date with the 4-bladed model rotor, this report includes a brief description of work which has been done in preparation of future experiments with this model rotor.

EXPERIMENTS WITH A FOUR-BLADED CYCLIC PITCH STIRRING MODEL ROTOR

Part III of First Yearly Report under Contract NAS2-7613

Table of Contents

Nomenclature

e	equivalent hinge off-set
$F_R(t) + iF_I(t)$	complex valued periodic response modulating function
$F_{Rcn} + iF_{Icn}$ $F_{Rsn} + iFIsn$	complex valued Fourier coefficients
F_{cn} , F_{sn}	absolute values of complex valued Fourier coefficients
F_Ω , $F_{2\Omega}$	absolute values of first and second trim harmonics, normalized by dividing by θ_o
F_{ω_f}	first harmonic of rotor downwash
I	blade moment of inertia
R	rotor radius
β	blade flapping angle
γ	blade Lock number
θ	blade pitch angle
μ	rotor advance ratio
σ	rotor solidity ratio
ϕ_{cn} , ϕ_{sn}	arguments of complex valued Fourier coefficients
ψ	blade azimuth angle
Ω	rotor angular speed
ω_1 or P	blade natural frequency, rotating, unit Ω
ω	frequency of excitation in rotating system
ω_f	frequency of excitation in fixed system

Nomenclature (continued)

Subscripts

I, II	multiblade variables
c	cyclic pitch stirring amplitude
k	kth blade
o	collective pitch
β_1 , β_2	first, second flap frequency, non rotating
θ_1 , θ_2	first, second blade torsion frequency
ζ_1	first blade chordwise frequency, non rotating

Introduction

Tests with the two-bladed rotor model of 16 inch diameter are described in References [1] to [4]. An analytical unsteady wake model for zero advance ratio and its comparison with the test results is presented in Reference [5]. The problem of unsteady rotor wake analysis is treated more extensively in Reference [6] and analytical results are compared with model frequency response tests presented in Reference [7]. In all references except Reference [2] only the rotor tilting response has been measured and presented. In Reference [2] and in this report the first 5 Fourier components of the complex valued periodic modulating function have been evaluated, so that the zero, first and second harmonics of this function are available together with their comparison with analytical data. The first and second harmonic of the trim response is also presented. In many cases where fluctuations of the data occur from period to period, mean and standard deviation for several periods have been obtained.

It was discovered that the non-zero advance ratio tests of Reference [2] - but not the zero advance ratio tests of Reference [5] - had a common constant error in rotor rpm due to a not recognized instrument bias. Thus the values of advance ratio and of the non-dimensional blade natural flapping frequencies needed corrections together with the analytical data. The rpm bias

error was the same for the two bladed rotor tests of Reference [2] and for the 4-bladed rotor tests of this report. Thus the test results are comparable, though the advance ratios are not as intended .20, .40 etc. but somewhat smaller. The charts in this report contain the corrections for both the previous 2-bladed and the new 4-bladed rotor tests, and also the corrections of the analytical data. All of these corrections are rather minor.

No effort has been made to correlate one of the available unsteady wake theories with the extensive test results. Attempts at doing this have not been very successful because of the wide frequency range of the tests. It is planned to limit future correlation efforts to a frequency range which corresponds approximately to the frequencies encountered in flight dynamics, up to .3 or .4. In this range first order rotor dynamics in multiblade coordinates is approximately applicable, as shown in Part I of this Yearly Report. It is also planned to recover the relevant parameters for the various rotor wake models by identification algorithms from transient tests, beginning with the simple use of an equivalent Lock number. After correcting the analytical model in this empirical fashion for rotor wake effects, improved analytical data will be available to compare with the experimental data of this report.

Rotor Model Description

The four-bladed pitch stirring rotor is sketched in Figs. 17 and 18 of Phase VII-C Report under Contract NAS2-4151. These figures are included herein as Fig. 1 and 2. A photo of the new rotor set up for hovering tests is presented in Fig. 3.

The new rotor has 4 feathering bearings and 2 bearings in the pitch stirring mechanism, as opposed to 2 feathering and one pitch stirring bearing in the previously tested 2-bladed rotor. The rotor radius is increased from 8.0 inches to 8.25 inches, which results in an increase of the Lock number from 4.0 to 4.25. In spite of small parts in the rotor hub which called for micro-precision machine work no major mechanical assembly problem arose.

The new rotor hub screws onto the old rotor shaft. Its two pitch stirring bearings mate with an eccentric in which is attached to the eccentric shaft. Two eccentrics have been manufactured, 0° and 1.5°. The 0° eccentric is necessary for establishing the 0° collective pitch condition and for tracking the rotor. The zero collective pitch setting is accomplished by finding the position for minimum absolute downwash reading of the hot wire anemometer with all blades tracked. Once this reference setting has been established, collective pitch changes can be achieved without further tracking.

Each blade root carries a mirror which is used to reflect light from a parallel light source on to a scale marked in

degrees. This system cannot be used for initially setting collective pitch (because of small mechanical variations from blade to blade) but is adequate in moving from one collective pitch setting to a new one.

After the 0° reference collective pitch setting has been established, one is free to remove the 0° eccentric (which is done by removing the rotor head and pulling out tne eccentric), install the $\pm$ 1.5° eccentric, and wire up the instrumentation by soldering 7 wires.

The fully assembled rotor even after 16 hours of operation shows no noticeable play in the pitch excitation system. During the initial 16 hours of operation the 4-bladed pitch stirring rotor was easy to work with and free of mechanical trouble.

Geometric and dynamic characteristics of the 2 and 4 bladed rotors are compared in the following table. The natural frequencies are measured at zero rotor speed.

	2-bladed	4-bladed
D	16.0	16.5
σ	.080	.154
ω_{β_1}	12.6	14.0 cps
ω_{β_2}	160	166 cps
ω_{θ_1}	170	180.5
ω_{θ_2}	-	271.0
ω_{ζ_1}	-	114
γ	4.0	4.25
θ_c	1.70	1.495°

The frequency measurement was made by exciting the blade near the root with a variable frequency magnetic field and observing the response amplitude peaks of the strain gage instrumented hub flexures.

A finite element analysis with 20 stations from blade tip to hub center, with 7 stations on the hub flexure was used to study blade dynamics. Theoretical stiffness values were adjusted until theoretical first and second flapping frequencies at 0 rotor rpm agreed with the measured values. Once the correct theoretical stiffnesses were determined, the program was used to find the first and second flapping frequencies and the moment distributions at various rpms. It was found that at the center of the blade-hub flexure the moment per inch of tip deflection varies little with rpm. Theoretical values follow:

rpm	lb_f-in/in tip deflection	P
0	.580	-
729	.579	1.55
1458	.581	1.20
2187	.578	1.12
2916	.570	1.096

The measured value of moment per inch of tip deflection at 0 rpm was .58 lb_f-in/in tip deflection. This number was used as the calibration number in the flapping response analysis.

By selecting proper gear ratios the following exciting frequencies could be obtained: ω = .2, .4, .6, .8, .9, .9033, 1.067, 1.1, 1.2, 1.4, 1.6 and 1.8.

For all testing conducted, flapping and torsion measurements were made in the rotating reference frame. Only the flapping data are presented herein. For the μ = 0 test, downwash measurements were made in non rotating reference frame with a linearized constant temperature hot wire anemometer. The probe can be seen in Figure 3 together with the ground plate.

Test Results on Blade Flapping Responses

As explained in Reference [2] the flapping response to a pitch input

$$\theta = \exp it(1-\omega_f) = (\cos t + i \sin t) \exp(-it\omega_f)$$

is of the form

$$\beta = [F_R(t) + i F_I(t)] \exp(-i\omega_f t)$$

Input and response are written in a rotating reference system. The bracket expression in the flapping response is the complex modulating function which, for a periodic system, takes the place of a complex amplitude ratio for constant systems. The modulating function has the period 2π. The modulating function is expanded into a Fourier series

$$F_R(t) + i\,F_I(t) = \sum_{n=0}^{\infty} [(F_{Rcn} + iF_{Icn})\cos nt + (F_{Rsn} + i\,F_{Isn})\sin nt]$$

A method to determine the Fourier coefficients is given in Reference [2]. The test results and the analytical results are given in terms of the absolute values of the complex Fourier coefficients and of their arguments:

$$F_{cn} = (F_{Rcn}^2 + F_{Icn}^2)^{1/2}, \quad F_{sn} = (F_{Rsn}^2 + F_{Isn}^2)^{1/2}$$

$$\phi_{cn} = \arg(F_{Rcn} + iF_{Icn})$$

$$\phi_{sn} = \arg(F_{Rsn} + iF_{Isn})$$

Because of the small errors in the results presented in Reference [2] and discussed in the introduction, the previously obtained test data for the two bladed rotor have been reprocessed and are presented here together with the results for the four bladed rotor. The format of the presentation is the same as in Reference [2]. The absolute values of the first 5 Fourier components of the modulating function are shown vs. cyclic pitch excitation frequency ω in the rotating system. $\omega < 1$ corresponds to a progressing mode, $\omega > 1$ to a regressing mode. In addition to the absolute values of the first 5 complex Fourier components of the modulating function F_{co}, F_{c1}, F_{s1}, F_{c2}, F_{s2},

the arguments of the cos t and sin t terms, ϕ_{c1} and ϕ_{s1}, are also given. In addition, the first and second harmonics of the trim response (absolute values) are shown. For zero advance ratio downwash data are given and will be discussed in the subsequent section. The list of Figure Captions is followed by a table which relates the letters a - h in the figure designations to the quantity shown in each figure.

Figs. 4 to 7 present the data for the 4-bladed model rotor. The collective pitch is $\theta_o = 2°$. Blade flap frequencies are P = 1.14 and 1.19. The advance ratios are 0, .191 and .382. Figs. 8 to 10 show comparisons for the 4-bladed and 2-bladed rotors for $\theta_o = 2°$, P = 1.19 and μ = .190 and .380, and P = 1.21 and μ = 0. Figs. 11 to 16 show the revised data for the 2-bladed rotor for P = 1.105 and 1.182, $\theta_o = 2°$ and 5°, and μ = .192, .382, .555 and .740. All charts except those for the trim coefficients F_Ω and $F_{2\Omega}$ and except Figs. 13 and 14 show in addition to the test data points also curves obtained analytically without rotor downwash consideration. In Figs. 13 and 14 the curves without symbols represent test results for $\theta_o = 2°$ also shown in Figs. 8 and 9.

The largest deviations in the response from the analytical values without downwash occur at zero advance ratio, Figs. 4, 7 and 10. Only at resonance, when inertia and restoring blade moments balance, is there almost no effect of downwash, and the phase angle is about zero. As Fig. 10 shows, the downwash

effects are larger for the 4-bladed rotor with its higher rotor solidity ratio.

At medium advance ratio, μ = .19, Figs. 5, 8 and 11, the F_{c1} and F_{s1} components are still very much affected by the downwash, more so for the 4-bladed rotor, as is evident from Fig. 8. At higher advance ratio, μ=.38, Figs. 6, 9 and 12, the downwash effect is smaller, though not insignificant. Again the 4-bladed rotor shows the larger deviations from the analytical values. While the first harmonics F_{c1} and F_{s1} of the modulating function are in the entire advance ratio regime and between ω = .7 and 1.3 quite different from the analytical responses, the second harmonics are in this frequency range small and reasonably well predicted by the analysis.

Higher values of the collective pitch were only tested for the two bladed rotor and are shown in Figs. 13 and 14. With the linear theory collective pitch has no effect on the cyclic pitch response. Actually the responses for θ_o = 2° and 5° differ from each other, the higher collective pitch producing larger deviations from the analytical values. Only at resonance are the three responses - the analytical one and those for θ_o = 2 and θ_o = 5° - almost identical.

Figs. 15 and 16 show for two blades the responses at high advance ratios, μ = .555 and .740. Even here the downwash effects, though again smaller than at μ = .38, are quite evident. In particular the peculiar shape of the F_{s1}

curve with its two peaks is retained up to the highest advance ratio.

The absolute values of the first and second trim harmonics shown in the -h graphs have been normalized by dividing by θ_o. From Figs. 13h and 14h it is seen, that the trim harmonics are approximately proportional to the collective pitch angle, since the curves for $\theta_o = 2°$ and $\theta_o = 5°$ nearly coincide.

Test Results on Rotor Downwash Measurements at Zero Advance Ratio

Downwash measurements at $\mu = 0$ with a ground plate distance of $h/D = .65$ are shown for $\theta_o = 2°$ in Figs. 4c, 7c and 10c. The probe was located at .82R from the rotor center and at .20R below the rotor plane. Fig. 17 gives the average downwash velocity at this station vs. P in ft/sec. Lower P values correspond to higher rotor speed and, therefore, show higher downwash velocity. The downwash amplitudes shown in Figs. 4c, 7c, 10c and 18 are non-dimensional based on the average downwash velocity at the respective P values. The blade flapping frequency is approximately

$$P = \sqrt{1 + e/R + (14/\Omega)^2}$$

where for the model rotor the equivalent hinge off-set $e/r = .116$.* The aerodynamic blade moment at the rotor center is approximately

$$M_{aer}/I = \beta(P^2 - \omega^2)$$

*This approximate equation was not used for determining P. Instead, the procedure described in the Section "Rotor Model Description" was applied.

and should be zero at resonance, when P = ω. Fig. 18 shows the non-dimensional downwash amplitude (absolute value of first harmonic in ω_f) for ω = 1.2 vs. P. The standard deviations over several subsequent cycles are also indicated. It is seen that the downwash is fluctuating considerably. It is also seen that a minimum downwash amplitude is obtained for P = 1.2 at resonance. Fig. 19 presents a series of oscilloscope photographs taken at decreasing P values for ω = 1.2. In the upper trace each vertical mark represents one rotor revolution. The lower trace represents the dynamic downwash with a period of 5 rotor revolutions. The amplitude diminishes as resonance at P = 1.2 is approached.

Figs. 4c, 7c and 10c show a very peculiar change of the non-dimensional downwash velocity with the exciting frequency ω. The minimum value at approximately resonance, P = ω, is clearly seen in these figures and explained by the absence of an aerodynamic blade moment. The β responses, as mentioned before, show for this point approximate agreement with the analytical responses computed without dynamic wake. For the 4-bladed rotor both Figs. 4c and 7c show another downwash minimum at ω = .8. At lower ω the downwash increases considerably. As Fig. 10c indicates, the two bladed rotor has similar downwash characteristics though the increase at lower ω is not as pronounced. The standard deviations for

each point are not large enough to mask this trend. When comparing the analytical and test responses in the vicinity of $\omega = .8$ it is seen from Figs. 4c, 7c, 10c that they deviate most from each other when the dynamic downwash is smallest. The downwash characteristics presented may be typical of the selected probe location and tests with other probe locations will be conducted to find out whether or not the same trend with ω exists.

Status of Work in Preparation of Future Experiments

In addition to flow visualization of dynamic wakes and of more complete downwash measurements at $\mu = 0$ there are three new types of tests being presently prepared, which will be briefly discussed in the following.

1. Multiblade Coordinate Measurements

Circuit designs have been completed for measuring simultaneously the multiblade coordinates β_0, β_I and β_{II}. This is done by instrumenting each blade hub flexture with 4 parallel and non-overlapping strain gages with 2 gages on each side of the flexture. Those 2 gages are both parallel with and equidistant from the blade quarter cord line.

Two gages on each flexture are used to generate β_I and β_{II}. Opposing blades are wired together so that $(\beta_1 - \beta_3)$ and $(\beta_2 - \beta_4)$ are directly generated with torsional and edgewise moments canceling out in the bridge construction. 2400 cps 10VP-P power is supplied to each bridge through the slip ring assembly. The $(\beta_1 - \beta_3)$ and $(\beta_2 - \beta_4)$ signals are passed through a resolver on the rotor shaft which directly generates $\beta_I = (\beta_1 - \beta_3) \cos \psi + (\beta_2 - \beta_4) \sin \psi$ and $\beta_{II} = (\beta_1 - \beta_3) \sin \psi + (\beta_2 - \beta_4) \cos \psi$, where the blade β_1 is aft for $\psi = 0$. These signals are then put through strain gage amplifiers where the carrier frequency is filtered out with a low-pass filter. Linearity of voltage transfer across the resolvers has been measured and found to be adequate for the very small voltage levels which will be passing through them in the test. The voltage transfer is also quite linear at higher voltage levels. Phase shifts have been measured through the circuiting and have been found to be less than 3° at 2400 cps which is well within the range the amplifiers can handle.

Two gages on each flexture are used to generate β_o.

$$\beta_o = \beta_1 + \beta_2 + \beta_3 + \beta_4$$

Power to this bridge and the bridge output pass through the slip ring assembly. Again, the bridge is wired so that torsional and edgewise moments cancel cut.

Two flextures have been successfully instrumented with the 4 gage set up. With the 4-gage set up a single blade flapping response can also be generated. An extra flexture will be instrumented in torsion so that one can switch quickly from multiblade measurements of β_o, β_I and β_{II} to single blade measurements of flapping and torsion.

2. Cyclic Pitch Stirring Transients

Different exciting frequencies are now generated by a gear train which links the pitch and rotor control shafts together. Changing gear ratios changes the excitation frequency. Thus only discrete values of excitation frequencies are available. This was necessary because of the large number of rotor revolutions the method of analysis required. Drift could not be tolerated.

When using system identification methods, transients can be used. The first transient which will be generated in future tests is a frequency of excitation transient. In the rotating system the frequency ranges of $\omega = 1 + 2$ and of $\omega = 1 + 0$ will be swept with different accelerations. This will be achieved in the following way. The gear train will be disconnected, and a variable speed motor will be connected to the pitch control shaft. The motor and the motor-shaft coupling, are already available. The maximum acceleration that can be achieved with the pitch control motor is approximately 80

cps per second. With this acceleration the frequency will change from $\omega = 1$ to 1.2 in 1 rotor revolution. The acceleration should be adequate for exciting the important rotor modes.

Resolvers will have to be linked with the pitch control and rotor control shafts to generate point by point values of the state of the excitation.

3. Normal Flow Transients

The tunnel section for producing normal flow transients is shown in Figures 20a to 20c. The Washington University wind tunnel in an open-return tunnel thus the test section static pressure is less than atmospheric pressure, consequently the test section must remain sealed at all times. If the test section area is kept constant downstream of the oscillating vanes then the flow oscillations quickly die out. If the section widens downstream of the oscillating vanes then the flow oscillations can be maintained. The new test section provides variable volume expansion chambers. It also provides for variable area slotted upper and lower walls downstream of the oscillating vanes. The photos Fig. 2a to c show the test section with one half of the section fitted with slotted walls.

The flow oscillations are produced with a NACA 0012, fourty percent flap vane with a 10 in cord. The

motor which oscillates the flaps is a variable speed 1/2 hp motor. The calculated first natural frequency in torsion of the flap is 90 cps. The flaps have been excited at 20 cps with no trouble. Testing frequencies will usually be below 10 cps. Steady as well as transient oscillations can be produced.

The photos Fig. 20 show the test section set up for excitation with 2 flaps in parallel (the front 60% of the lower airfoil has been removed). The holes can be seen for setting up the tunnel for 3 flap excitation. Flap oscillation amplitudes up to 10° can be achieved by adjusting the eccentric mounted on the motor.

Initial tests will be conducted for measuring the flow oscillation characteristics of the tunnel with different volume expansions and different slot sizes, to determine the best arrangement for the model tests.

Conclusions

The flapping responses to cyclic pitch stirring were measured for a 2 and 4-bladed model rotor and the following conclusions were drawn:

1. Because of almost twice the solidity ratio of the 4-bladed model rotor as compared to the 2-bladed model rotor, the dynamic downwash effects are larger as indicated by larger deviations of the experimental frequency responses in blade flapping from the analytical values obtained without rotor dynamic downwash. The type of deviations is, however, the same for the 4-bladed and for the 2-bladed rotor.
2. The deviations between experimental and analytical frequency responses are greatest for zero advance ratio, but they remain substantial in the entire advance ratio range measured up to .74.
3. At $\theta_o = 2°$ both 4 and 2-bladed model rotors show a peculiar characteristics of the first harmonic sine component of the modulating function. In addition to a response peak at resonance $\omega = P$, there is a second flapping response peak between $\omega = .8$ and .9 evident at all advance ratios. For $\theta_o = 5°$ the second response peak does not occur.
4. In the frequency range $\omega = .7$ to 1.3 the second harmonics of the modulating function are small and in reasonable agreement with the analytical values.

5. Downwash measurements with a linearized hot wire anemometer conducted at zero advance ratio show a minimum at the blade flapping resonance frequency. At this frequency the analytical response computed without dynamic downwash agrees with the measured response. Another downwash minimum occurs at about $\omega = .8$. At this frequency the analytical response deviates most from the measured response. The phenomenon is the same for the 4 and the 2-bladed rotor and at present cannot be explained even qualitatively. It may be typical of the selected probe location .82R radially out and .20R below the rotor plane.
6. The first two measured trim harmonics show approximate proportionality to the collective pitch angle, which is in agreement with the linear theory at zero rotor angle of attack.
7. In addition to more extended dynamic rotor downwash measurements at zero advance ratio and to flow visualization studies work is progressing to equip the rotor model with the capability for multiblade coordinate measurements, and for cyclic pitch stirring transients. Work is also progressing to equip the wind tunnel with the capability of producing in the test section normal flow waves and normal flow transients.

References

1. Hohenemser, K. H. and Crews, S. T., "Experiments with Progressing/Regressing Forced Rotor Flapping Modes", Phase VI-B Report under Contract NAS2-4151, June 1972.
2. Hohenemser, K. H. and Crews, S. T., "Further Experiments with Progressing/Regressing Rotor Flapping Modes", Phase VII-C Report under Contract NAS2-4151, June 1973.
3. Hohenemser, K. H. and Crews, S. T., "Unsteady Wake Effects on Progressing/Regressing Forced Rotor Flapping Modes", AIAA 2nd Atmospheric Flight Mechanics Conference, Palo Alto, California, September 1972, AIAA Paper No. 72-957.
4. Hohenemser, K. H. and Crews, S. T., "Model Tests on Unsteady Rotor Wake Effects", Journal of Aircraft, Vol. 10 No. 1, January 1973, pp. 58-60.
5. Crews, S. T., Hohenemser, K. H. and Ormiston, R. A., "An Unsteady Wake Model for a Hingeless Rotor", Journal of Aircraft, Vol. 10 No. 12, Dec. 1973, pp. 758-760.
6. Peters, D. A., "Hingeless Rotor Frequency Response with Unsteady Inflow", Proceedings Specialists Meeting on Rotorcraft Dynamics, AHS/NASA Ames, Moffett Field, CA, February 1974.
7. Kuczynski, W. A., "Experimental Hingeless Rotor Characteristics at Full Scale First Flap Mode Frequencies", Lockheed Report LR 25491, October 1972.

Figure Captions

Fig. 1 Schematic Side View of Four Bladed Rotor Model

Fig. 2 Schematic Top View of Four Bladed Rotor Model

Fig. 3 Photo of Rotor Model over Ground Plate with Downwash Probe

Fig. 4 a-c Fourier Coefficient, Phase Angles, and Downwash, 4 Blades, $P = 1.14$, $\theta_o = 2°$, $\mu = 0$

Fig. 5 a-h Fourier Coefficients and Phase Angles, 4 Blades, $P = 1.14$, $\theta_o = 2°$, $\mu = .191$

Fig. 6 a-h Fourier Coefficients and Phase Angles, 4 Blades, $P = 1.14$, $\theta_o = 2°$, $\mu = .382$

Fig. 7 a-c Fourier Coefficients, Phase Angles, and Downwash, 4 Blades, $P = 1.19$, $\theta_o = 2°$, $\mu = 0$

Fig. 8 a-h Fourier Coefficients and Phase Angles 4 and 2 Blades, $P = 1.19$, $\theta_o = 2°$, $\mu = .190$

Fig. 9 a-h Fourier Coefficients and Phase Angles, 4 and 2 Blades, $P = 1.19$, $\theta_o = 2°$, $\mu = .380$

Fig. 10 a-c Fourier Coefficients, Phase Angles and Downwash, 4 and 2 Blades, $P = 1.21$, $\theta_o = 2°$, $\mu = 0$

Fig. 11 a-h Fourier Coefficients and Phase Angles, 2 Blades, $P = 1.105$, $\theta_o = 5°$, $\mu = .192$

Fig. 12 a-h Fourier Coefficients and Phase Angles, 2 Blades, $P = 1.105$, $\theta_o = 5°$, $\mu = .382$

Fig. 13 a-h Fourier Coefficients on Phase Angles, 2 Blades, $P = 1.182$, $\theta_o = 2$ and $5°$, $\mu = .186$

Fig. 14 a-h Fourier Coefficients and Phase Angles, 2 Blades, $P = 1.182$, $\theta_o = 2$ and $5°$, $\mu = .373$

Fig. 15 a-h Fourier Coefficients and Phase Angles, 2 Blades, $P = 1.182$, $\theta_o = 2°$, $\mu = .555$

Fig. 16 a-h Fourier Coefficients and Phase Angles, 2 Blades, $P = 1.182$, $\theta_o = 2°$, $\mu = .740$

Fig. 17 Average Downwash Velocity at $\mu = 0$ for $\theta_o = 2°$ vs. P, 4 Blades

Fig. 18 Downwash Amplitude for $\omega = 1.2$ at $\mu = 0$ for $\theta_o = 2°$ vs. P, 4 Blades

Fig. 19 Oscilloscope Pictures of Downwash at Various P Values, $\mu = 0$, $\theta_o = 2°$, 4 Blades

Fig. 20 a-c New Wind Tunnel Section

For Figs. 4 to 16 the letters a-h refer to the following quantities:

$\mu = 0$ (Figs. 4, 7 and 10)

- a Flapping over cyclic pitch amplitude
- b Phase lag between tip path plane and swashplate
- c Normalized downwash first harmonic

$\mu \neq 0$ (Figs. 5, 6, 8, 9, 11 to 16)

- a Zero Response Harmonic
- b Absolute value of first cosine response harmonic
- c Argument of first cosine response harmonic
- d Absolute value of first sine response harmonic
- e Argument of first sine response harmonic
- f Absolute value of second cosine response harmonic
- g Absolute value of second sine response harmonic
- h Absolute values of first and second trim harmonics

Figure 1 Side View-Pitch Stirring Rotor

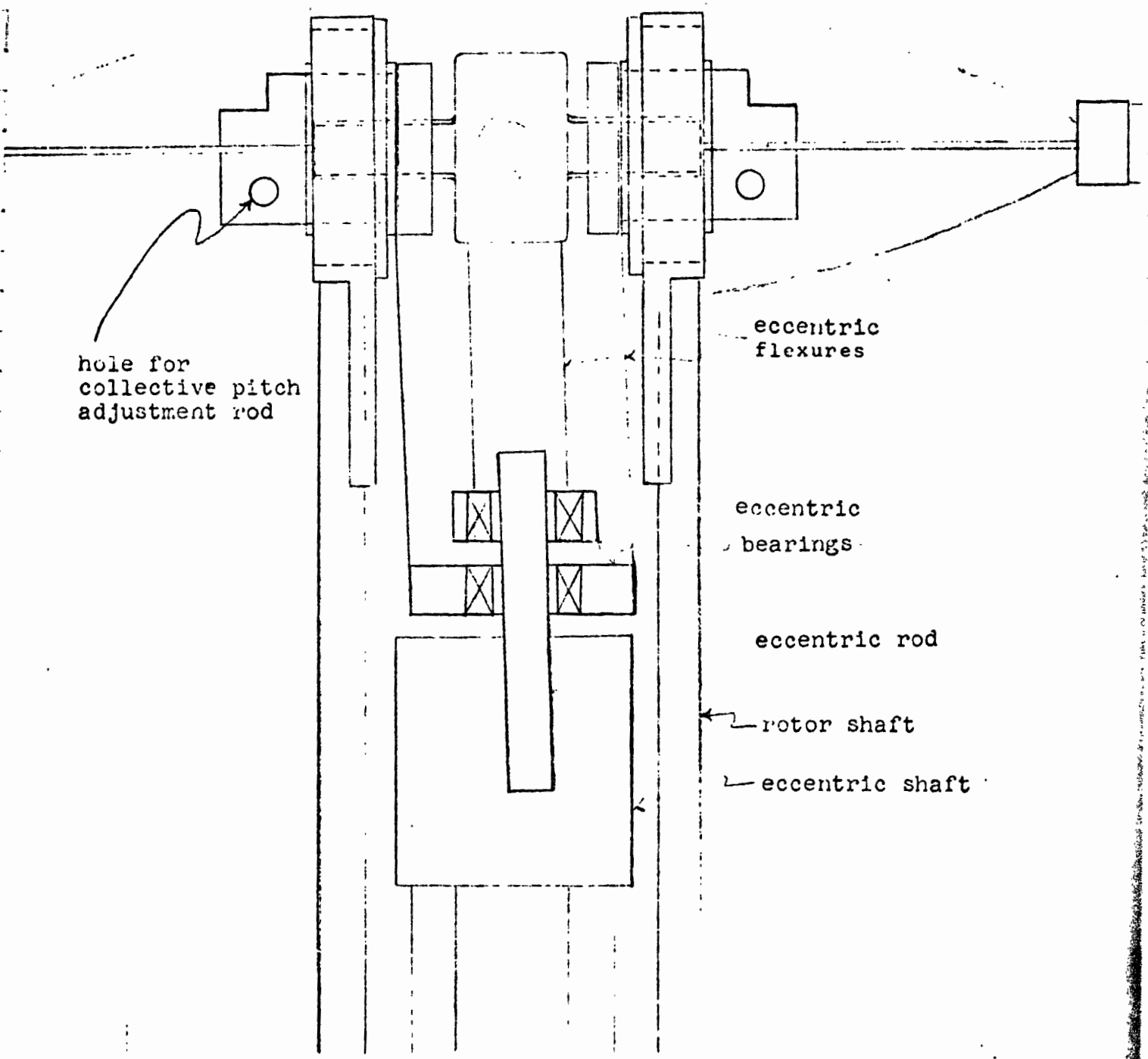

Figure 2 Top View-Pitch Stirring Rotor

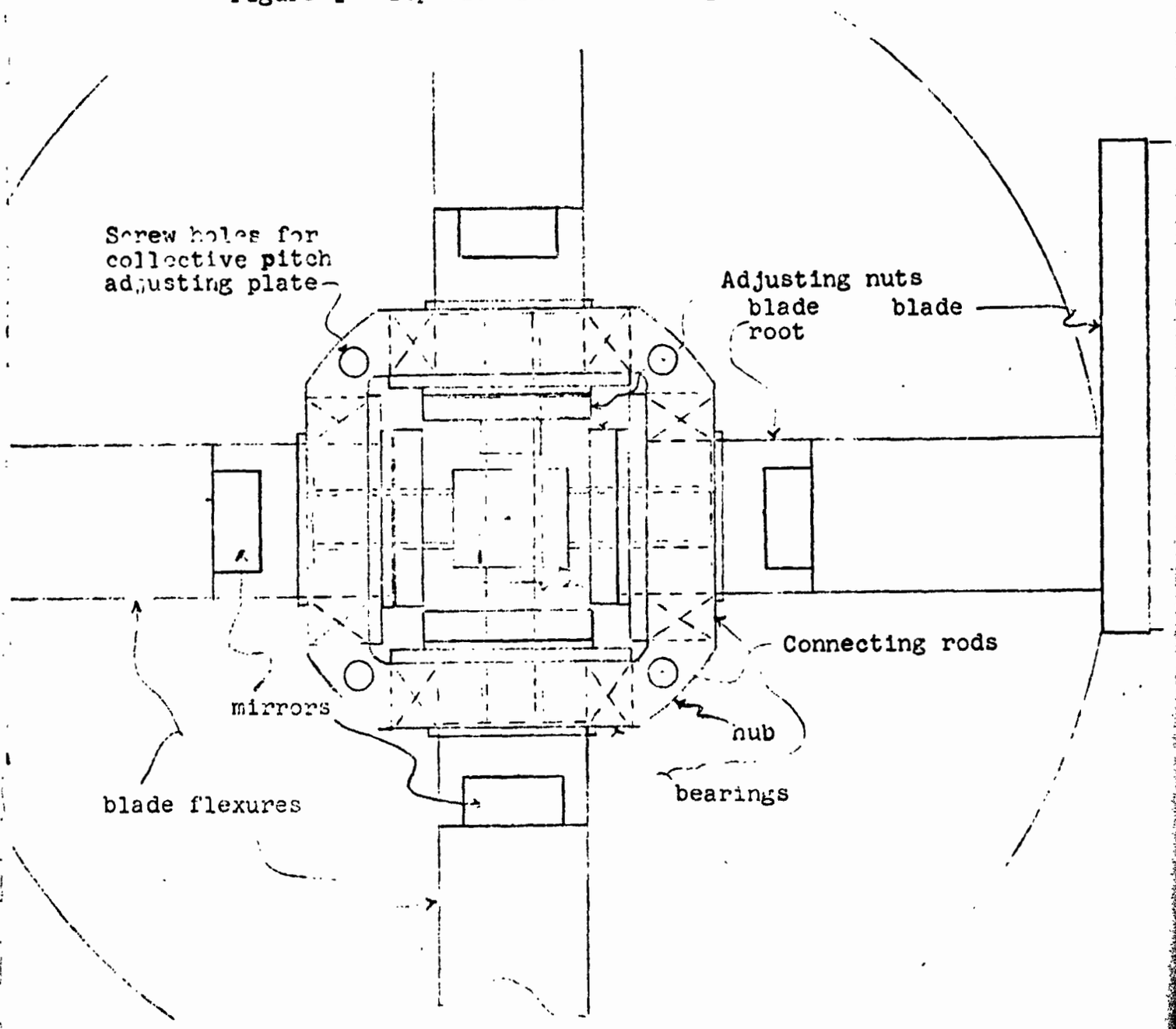

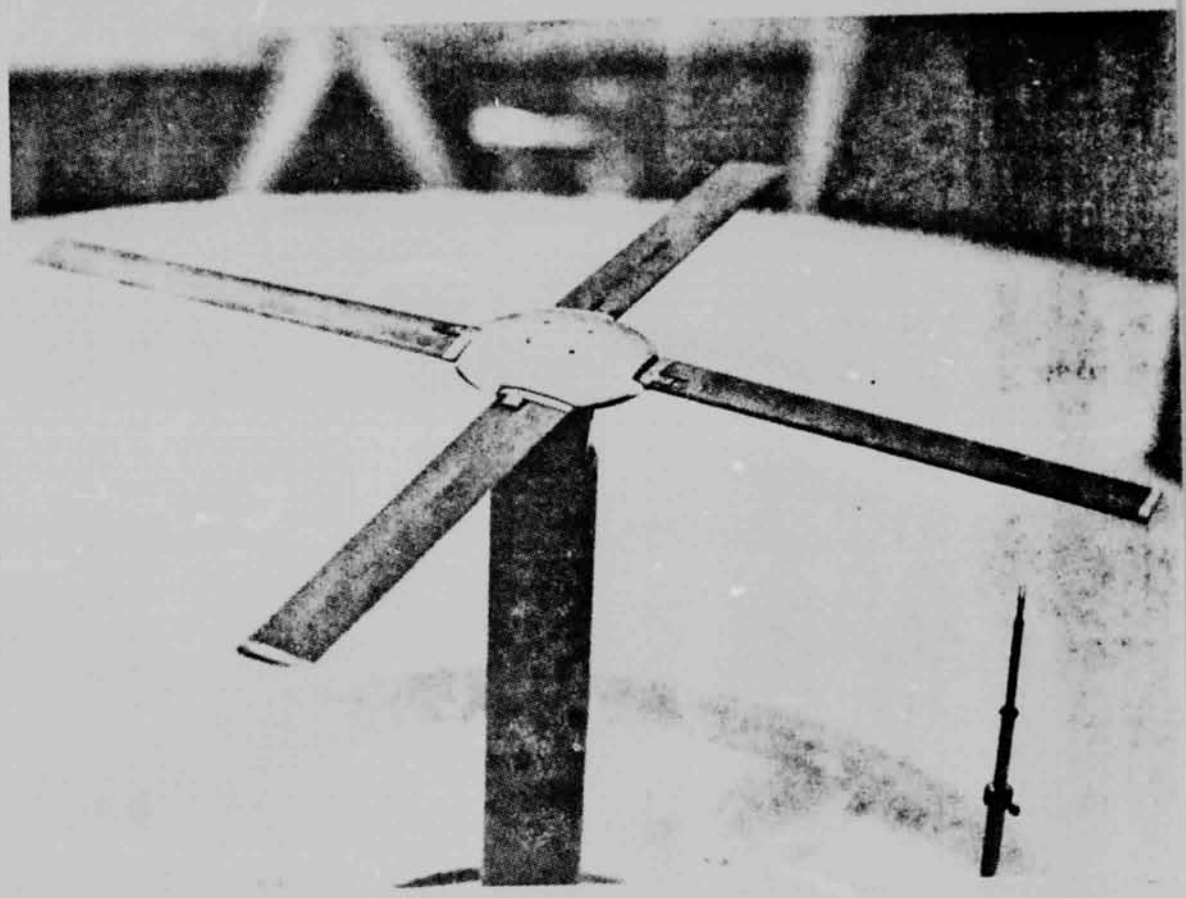

Figure 3

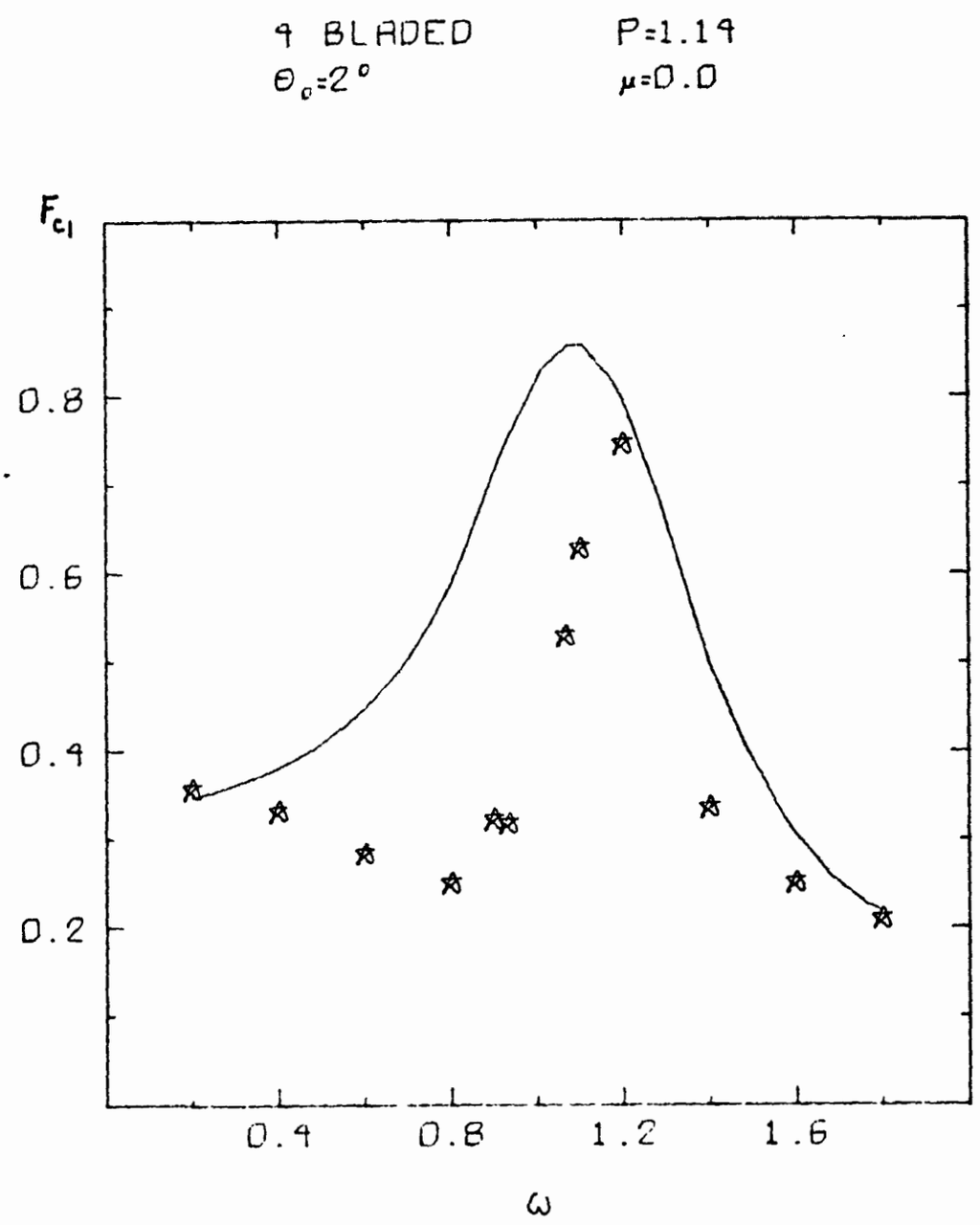

Figure 4a

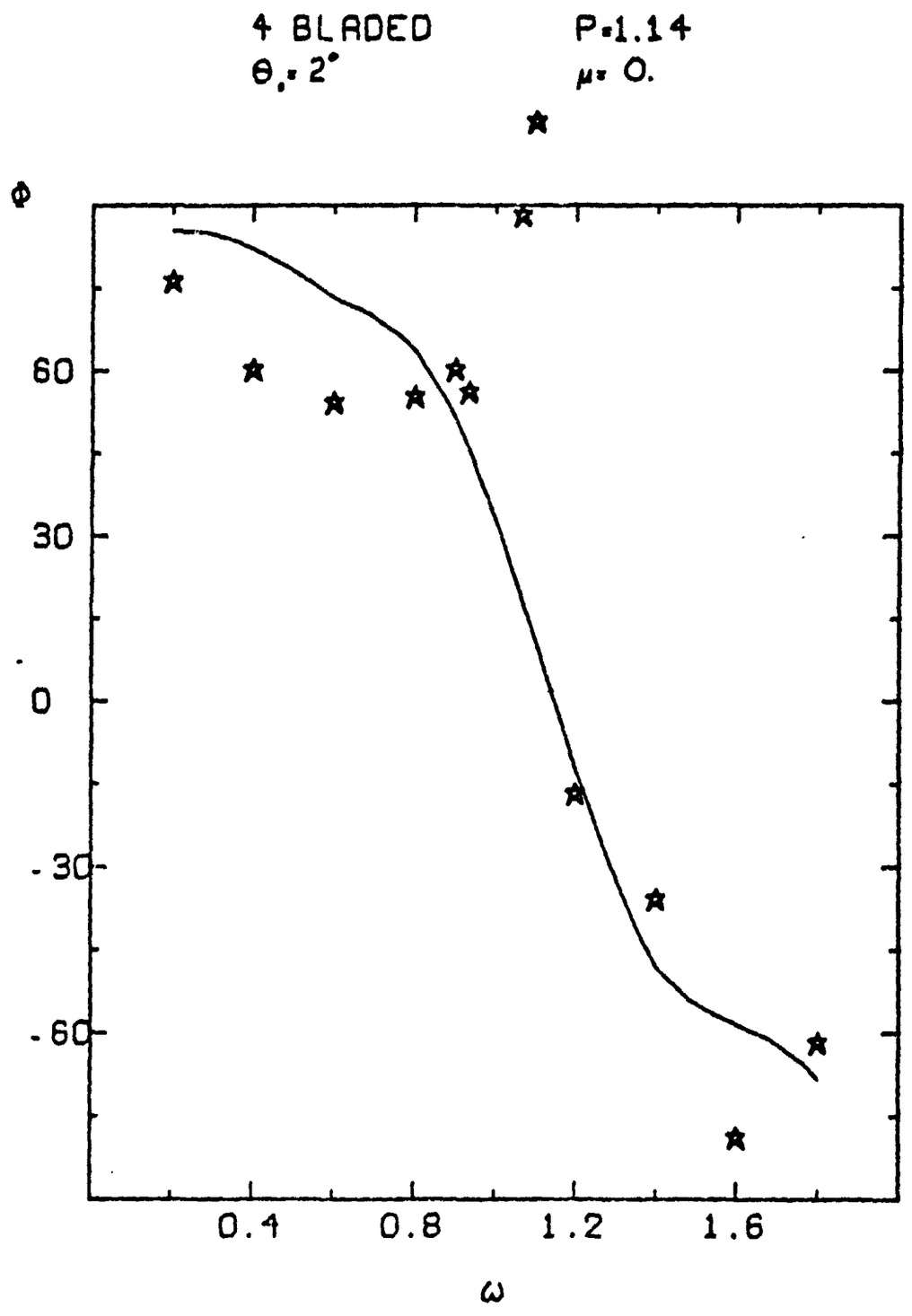

Figure 4b

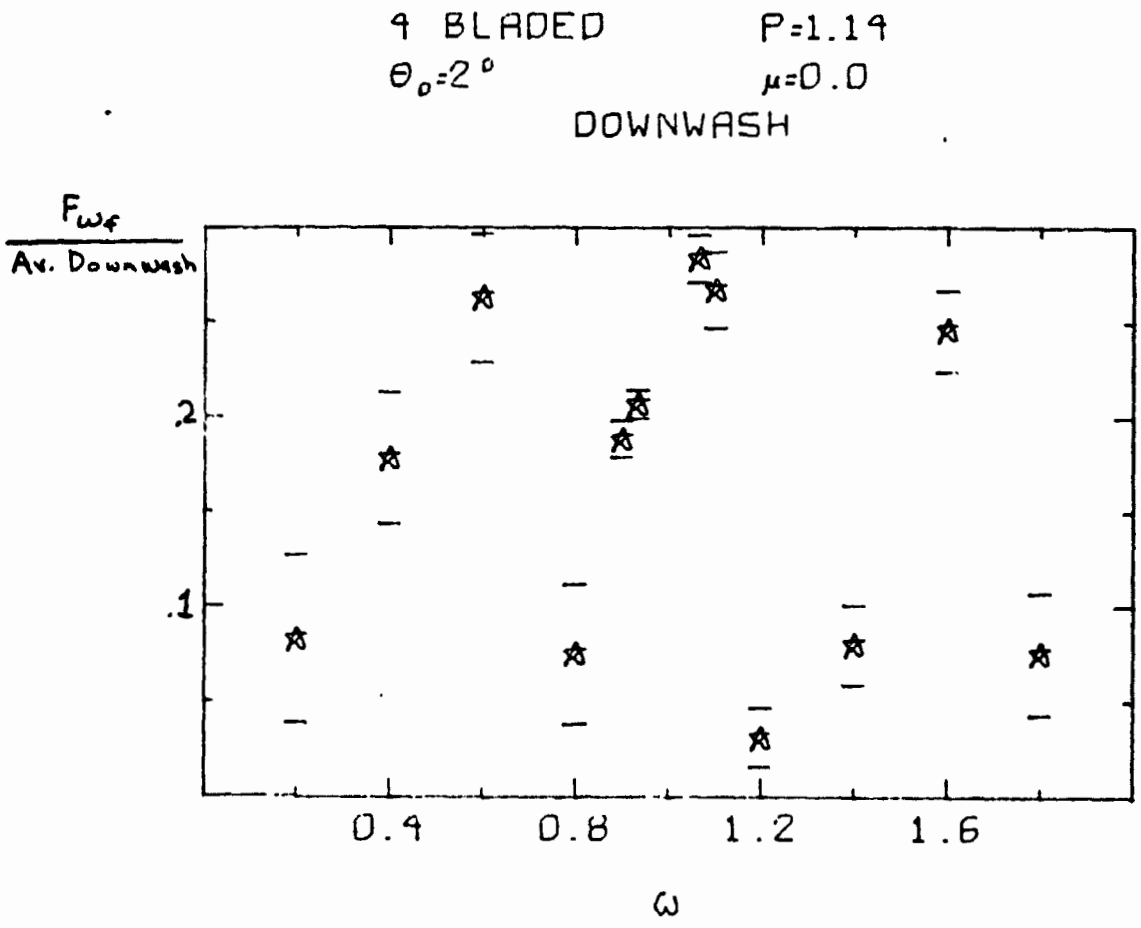
4 BLADED
P=1.14
θ_0=2°
μ=0.0
DOWNWASH
$\frac{F_{\omega_4}}{\text{Av. Downwash}}$
.2
.1
0.4
0.8
1.2
1.6
ω

Figure 4c

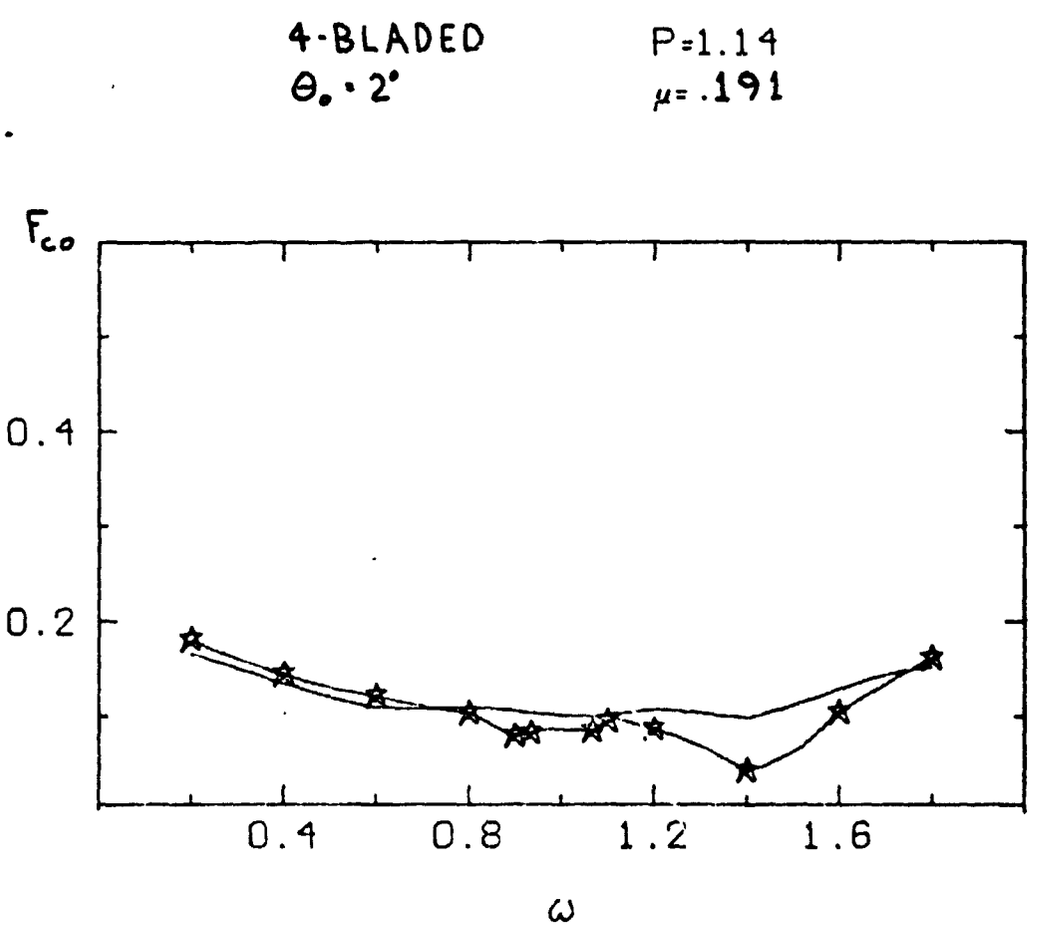

Figure 5a

4 BLADED $\theta_o = 2^\circ$ P=1.14 μ=.191

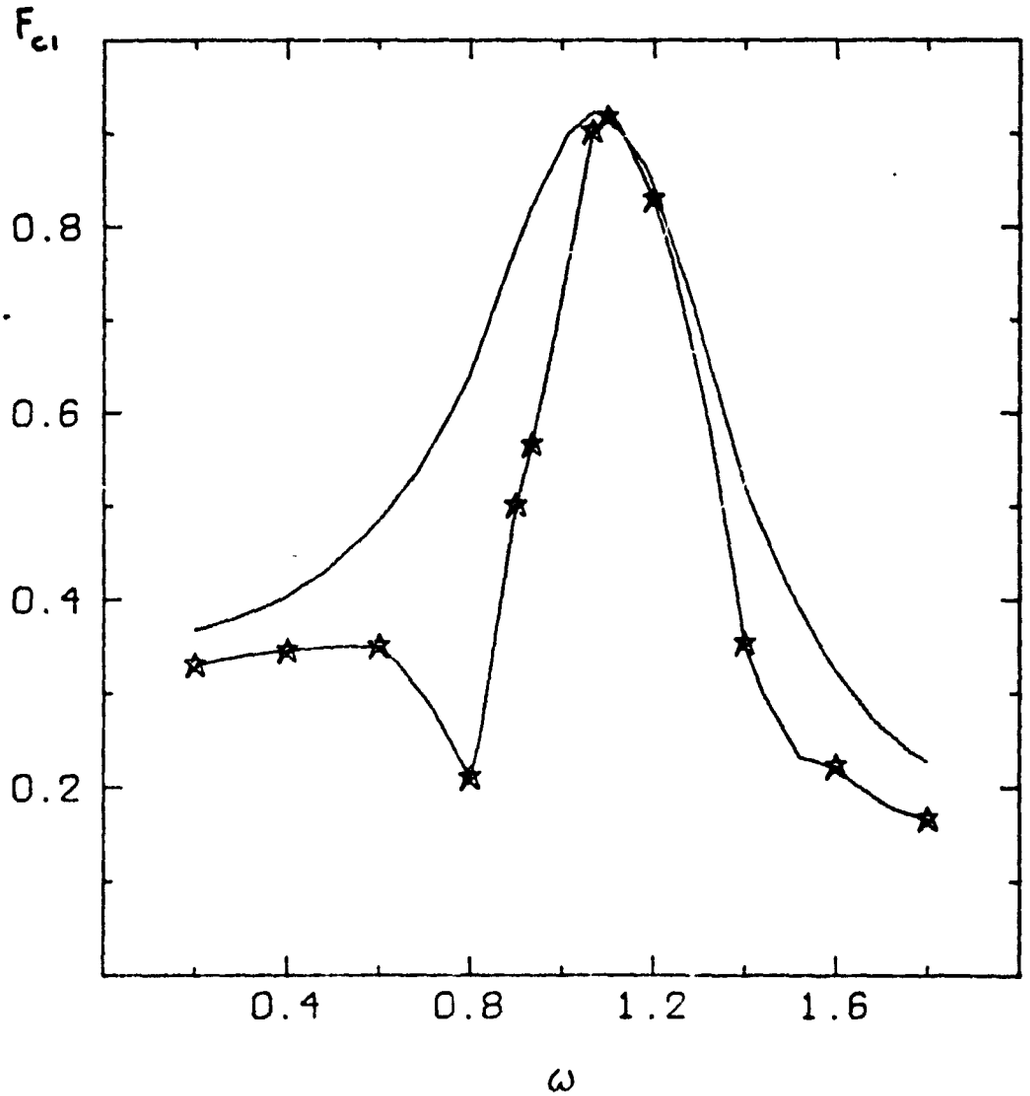

Figure 5b

4 BLADED P=1.14
θ_0= 2° μ=.191

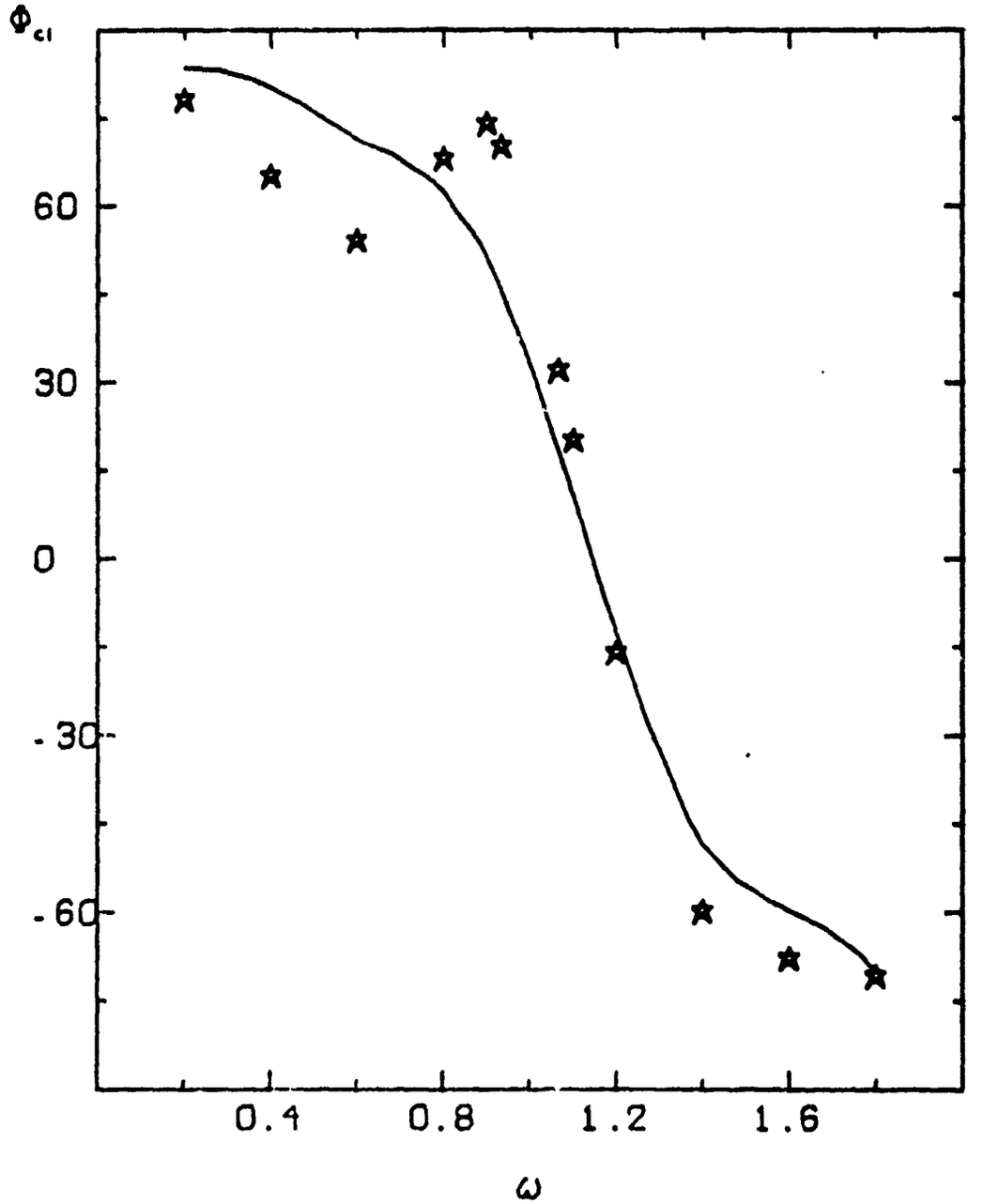

Figure 5c

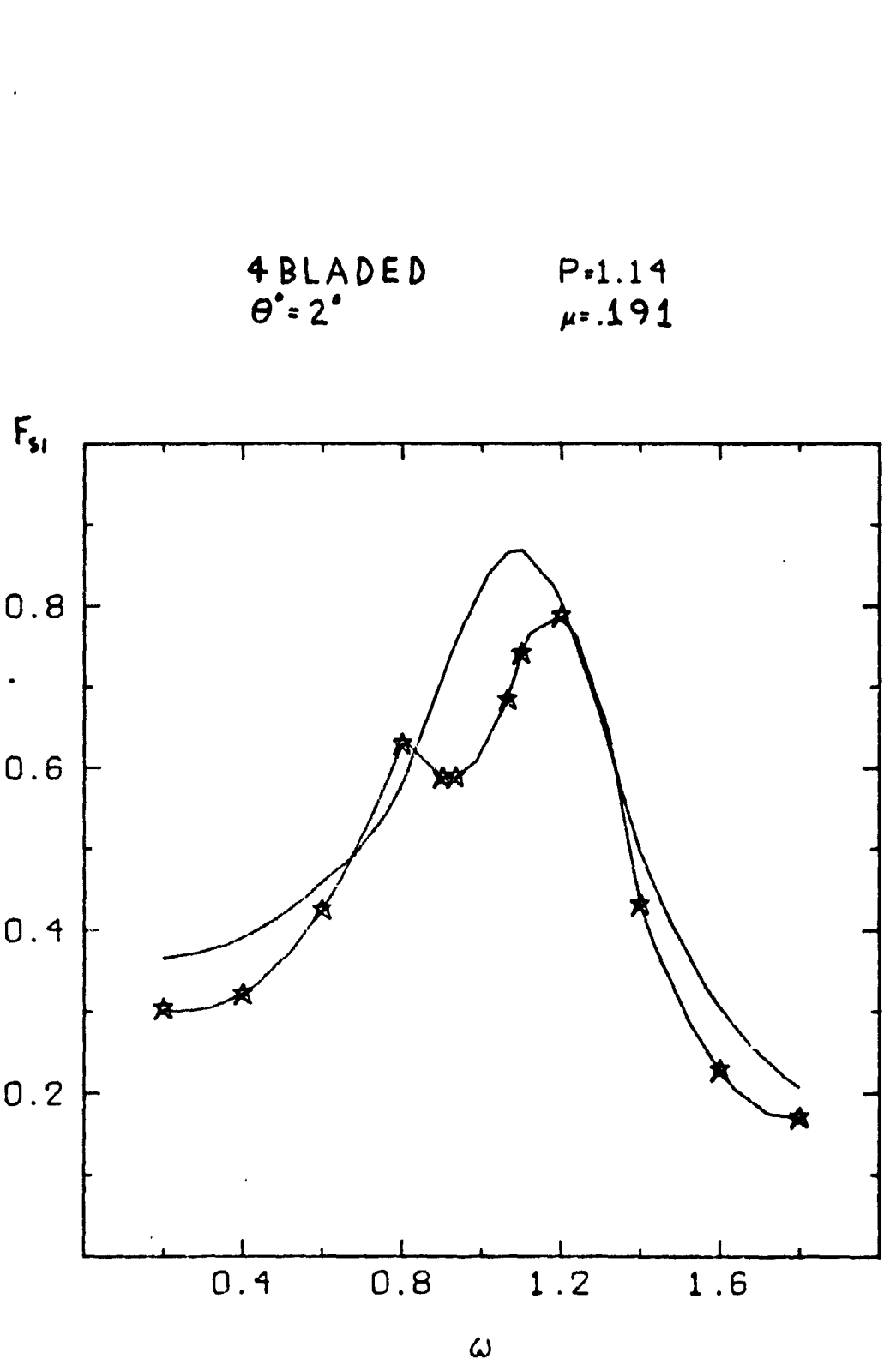

Figure 5d

4 BLADED $P=1.14$

$\theta_0 = 2°$ $\mu = .191$

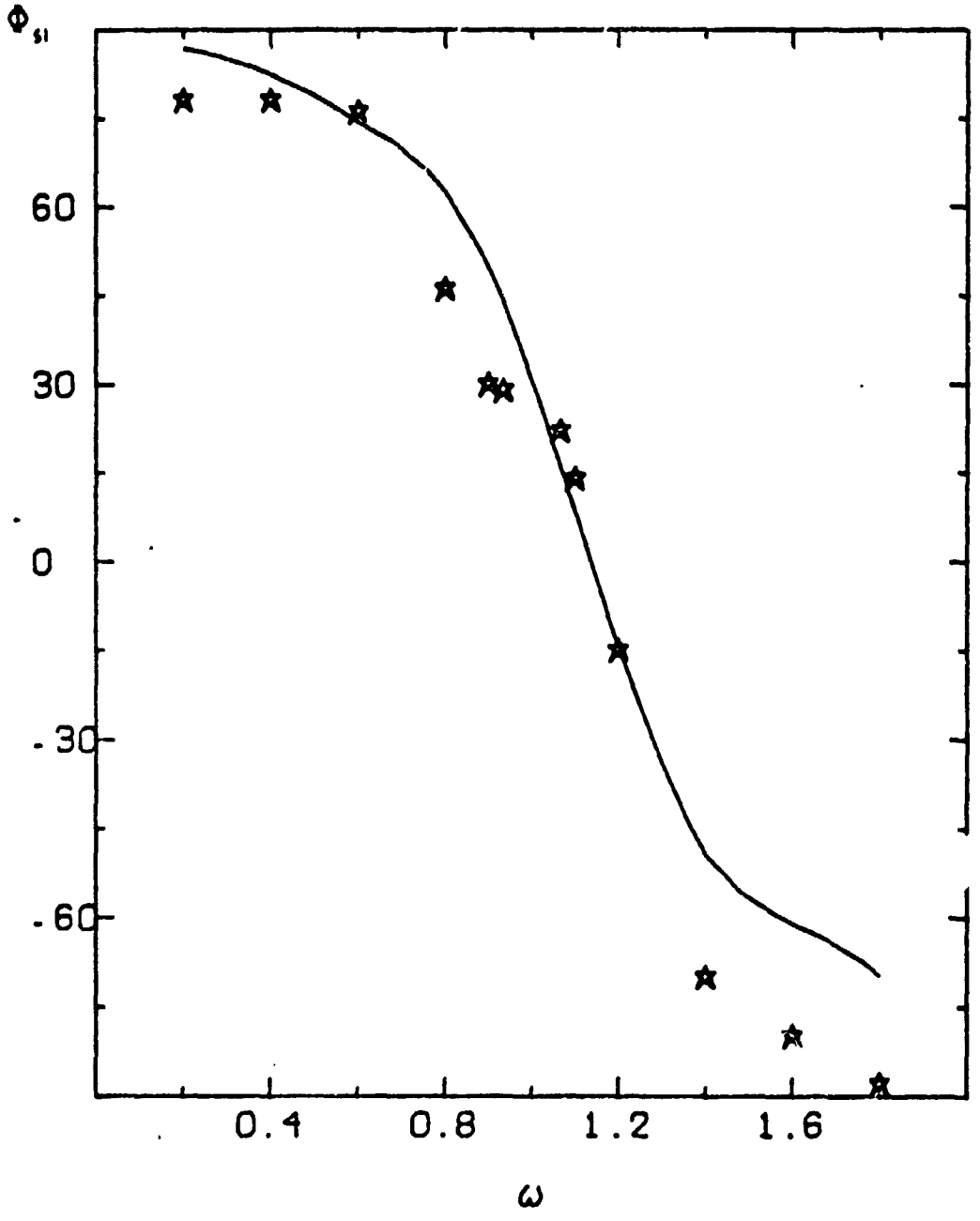

Figure 5e

4BLADED P=1.14
$\theta_o = 2°$ $\mu = .191$

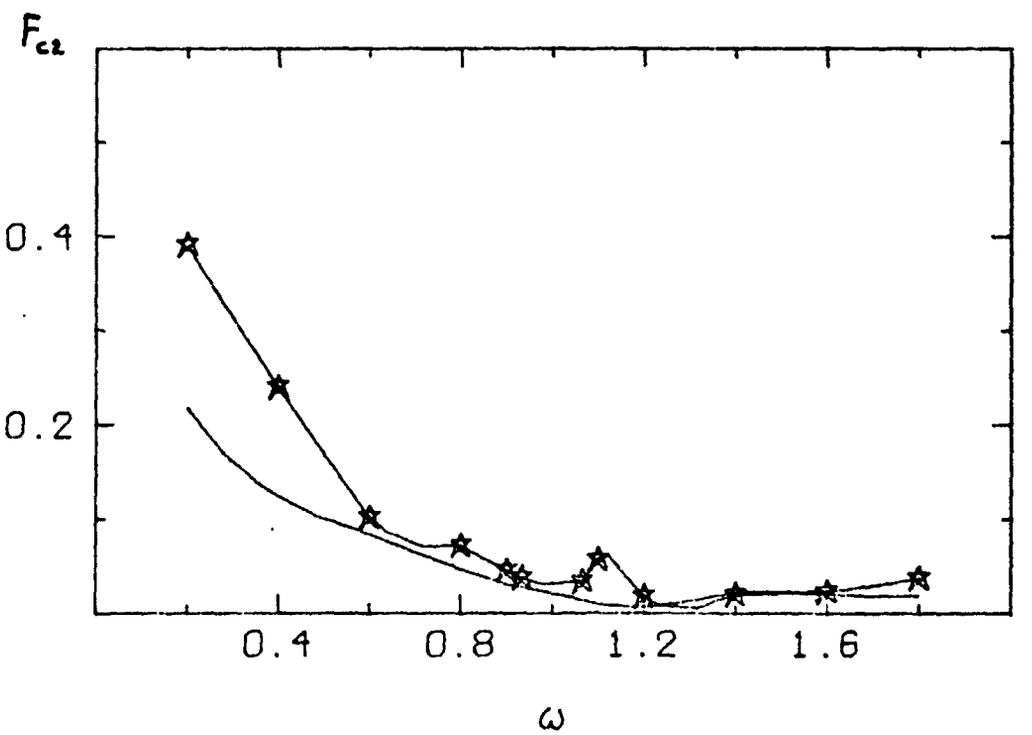

Figure 5f

4 BLADED $P=1.14$

$\theta_0 = 2^\circ$ $\mu=.191$

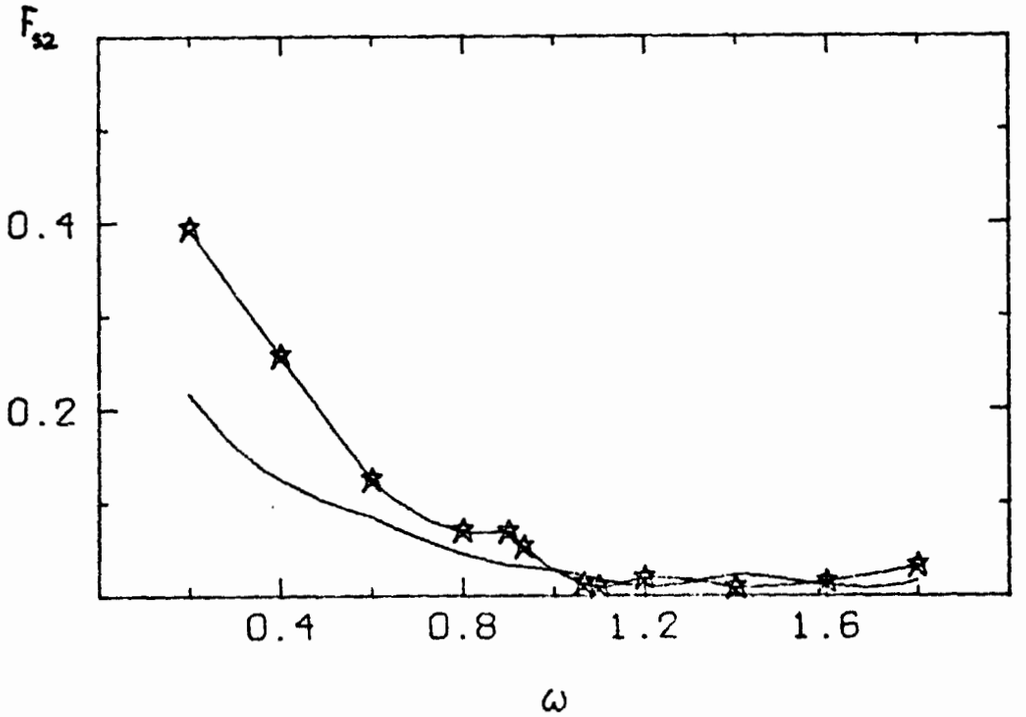

Figure 5g

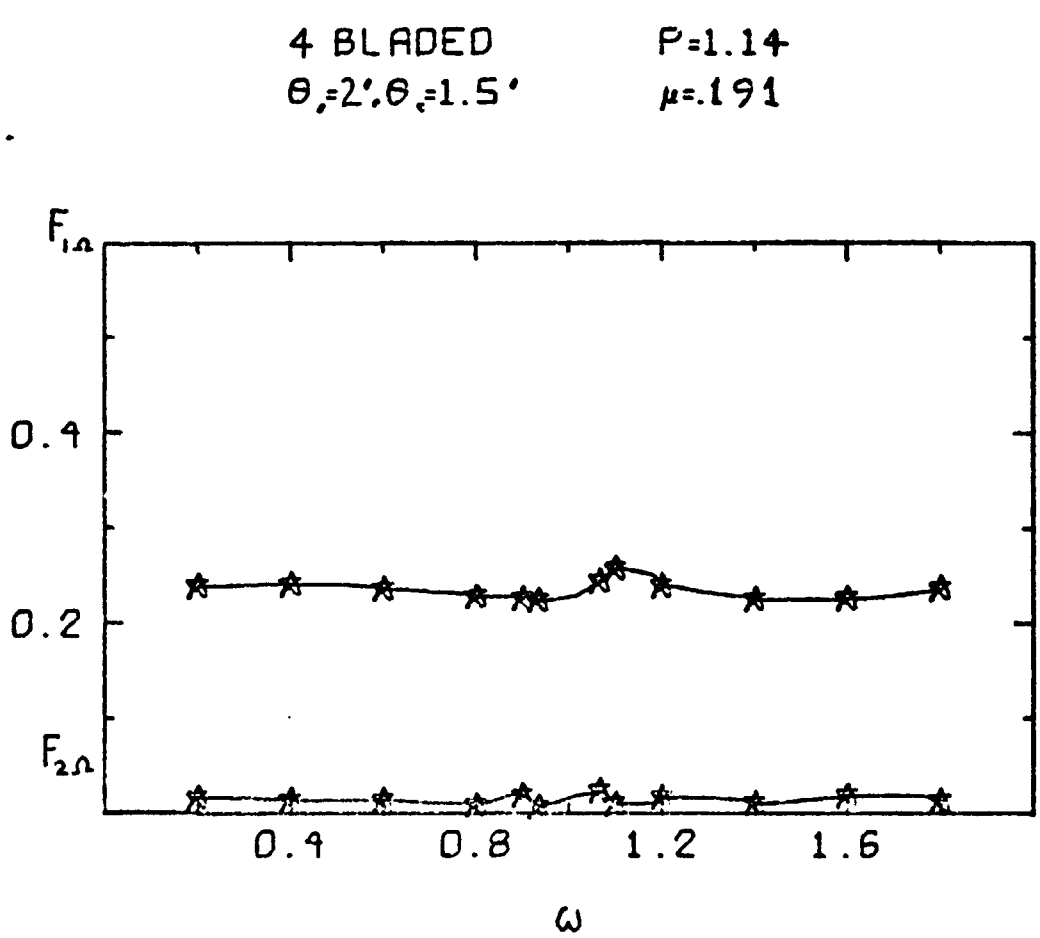

Figure 5h

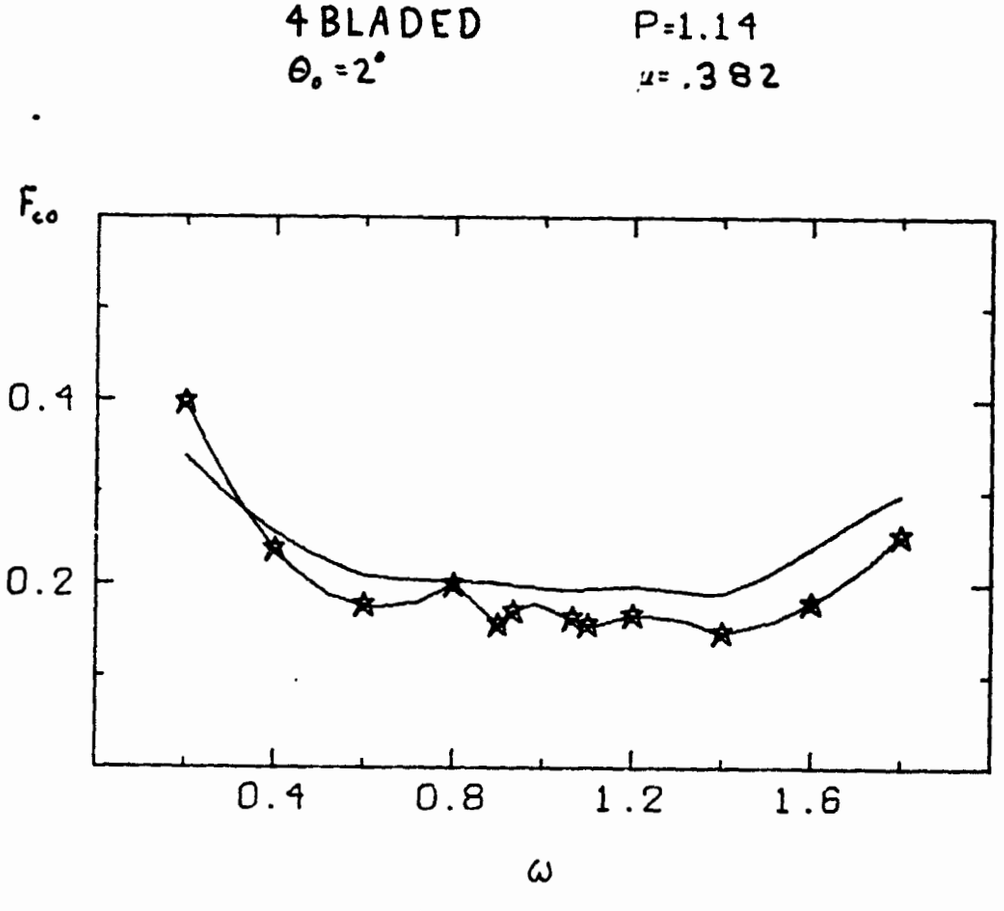

Figure 6a

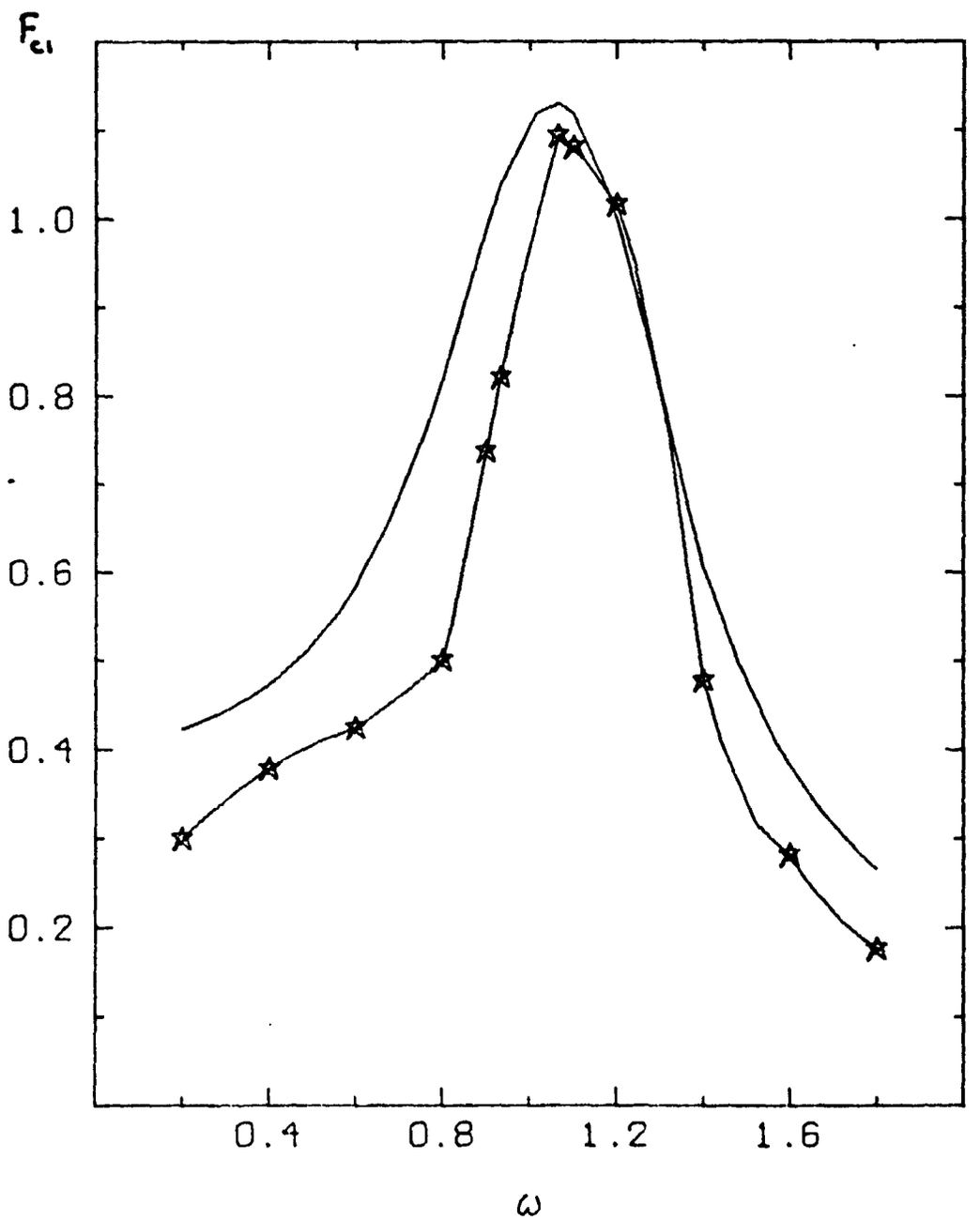

Figure 6b

4 BLADED $P=1.14$

$\theta_0 = 2°$ $\mu=.382$

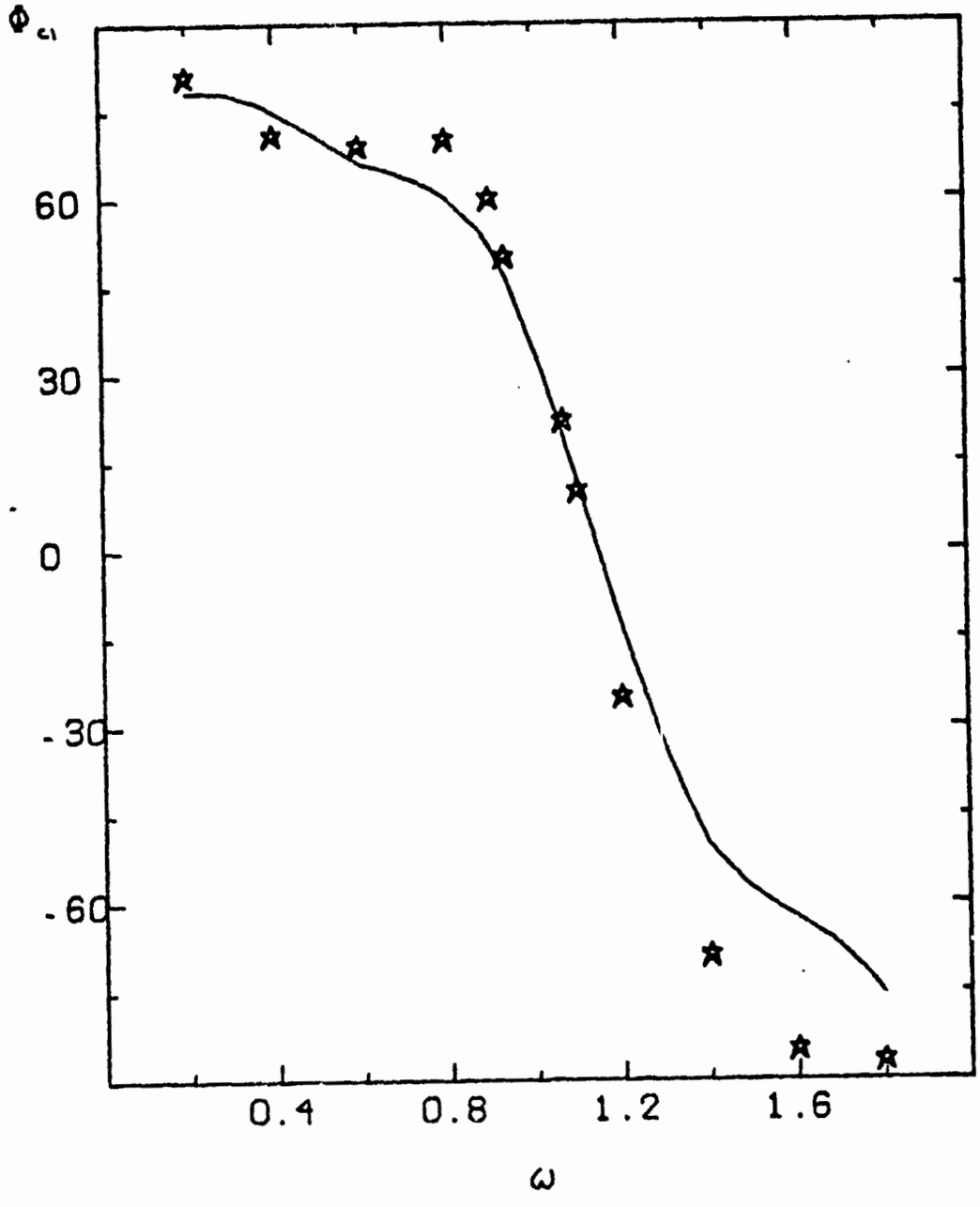

Figure 6c

4 BLADED $\theta_0 = 2°$ $P = 1.14$ $\mu = .382$

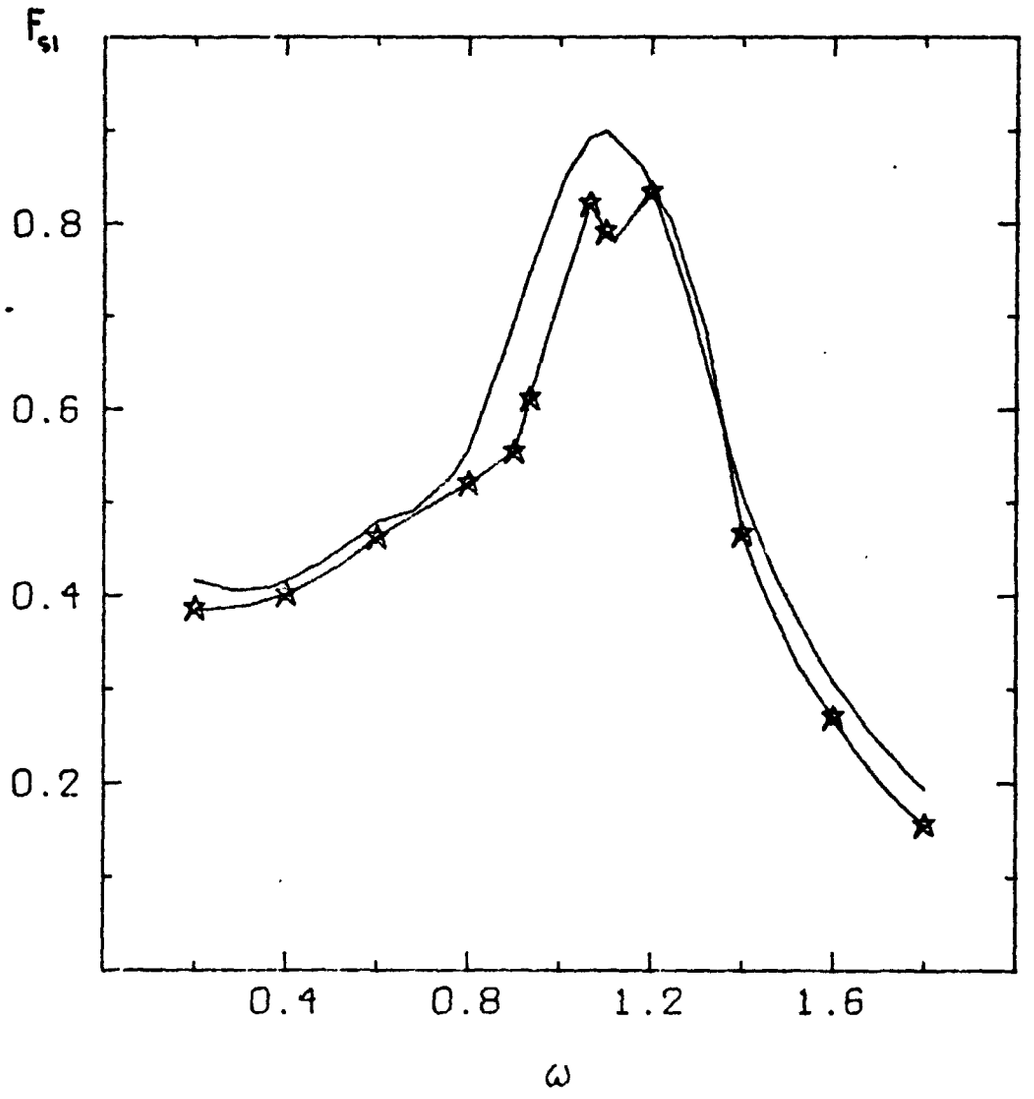

Figure 6d

4 BLADED $P=1.14$

$\theta_0 = 2°$ $\mu = .382$

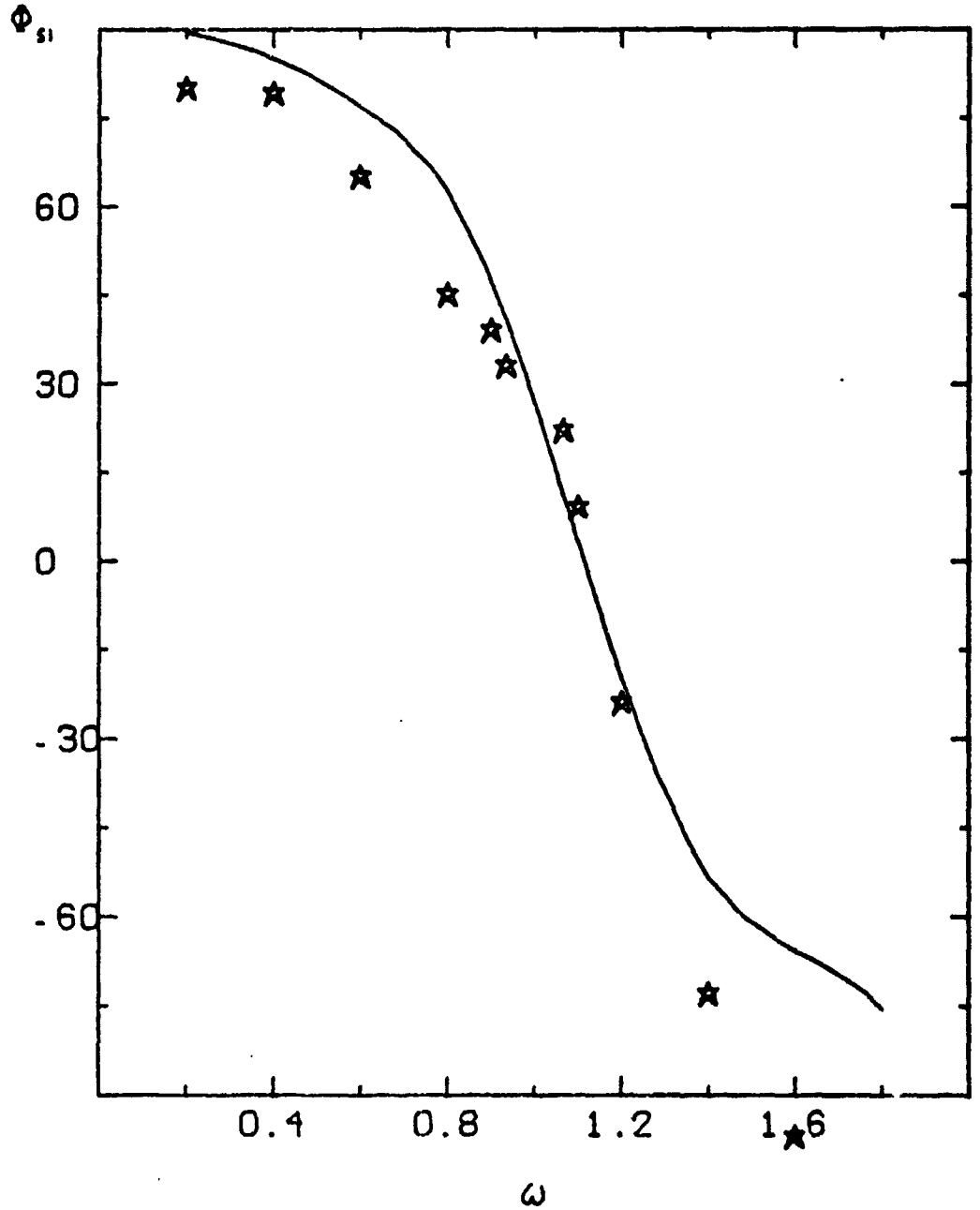

Figure 6e

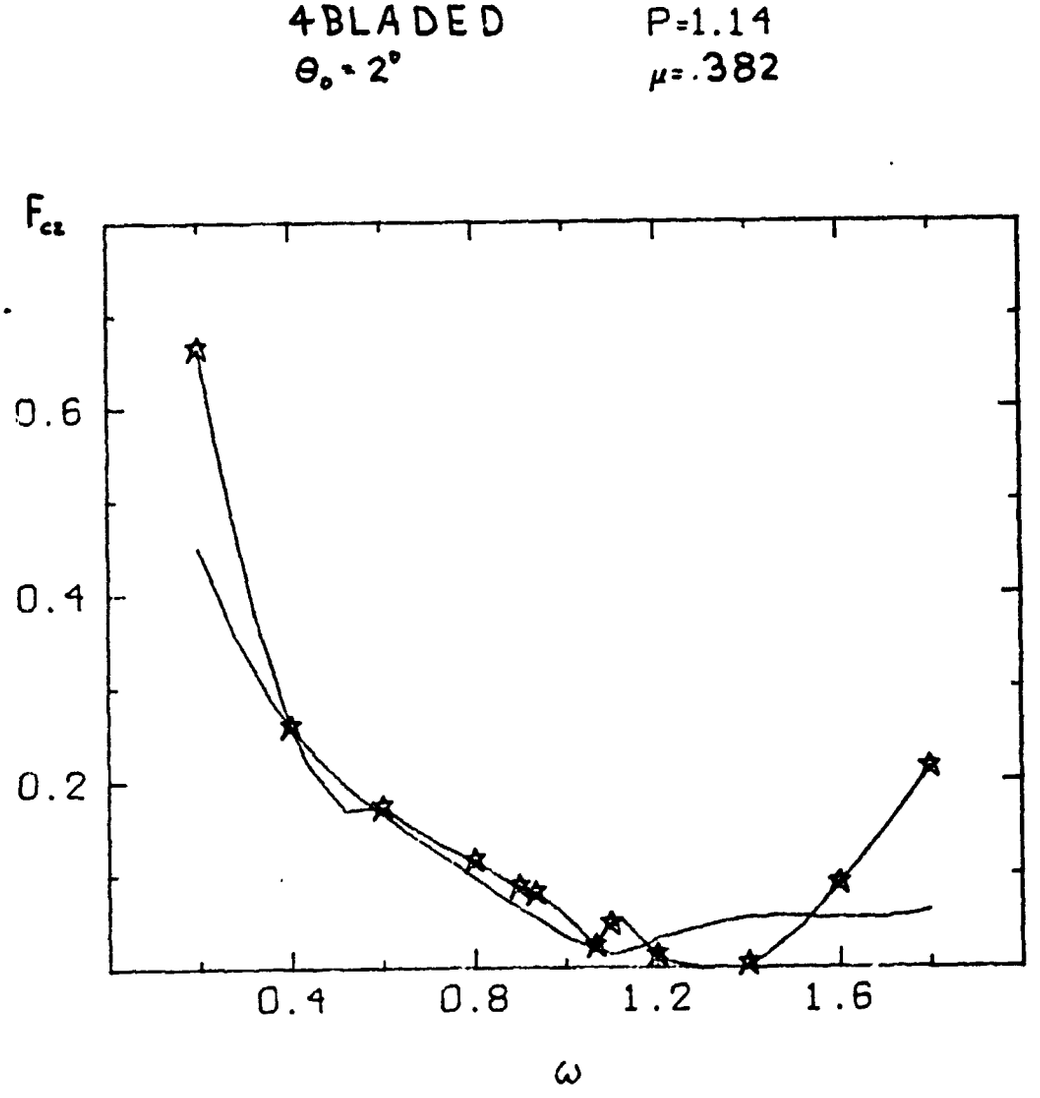

Figure 6f

4 BLADED P=1.14
$\theta_0 = 2°$ $\mu = .382$

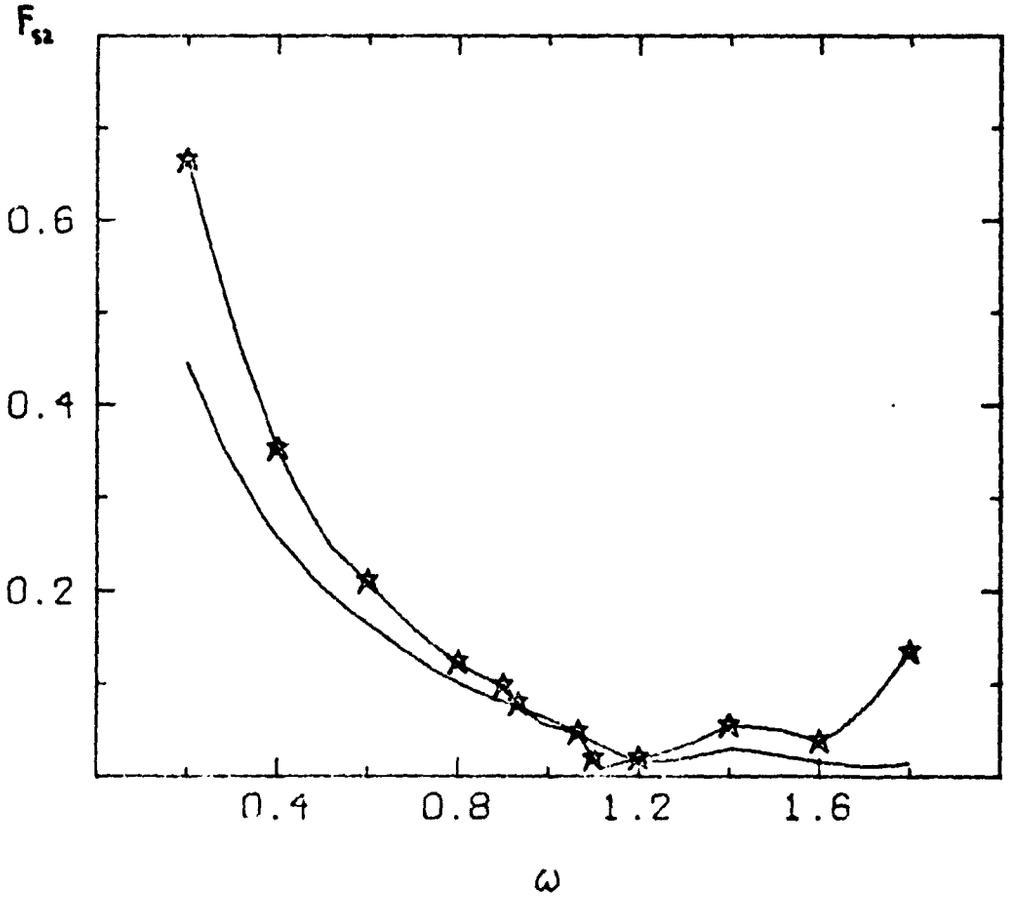

Figure 6g

4 BLADED P=1.14
θ_0=2°, θ_c=1.5° μ=.382

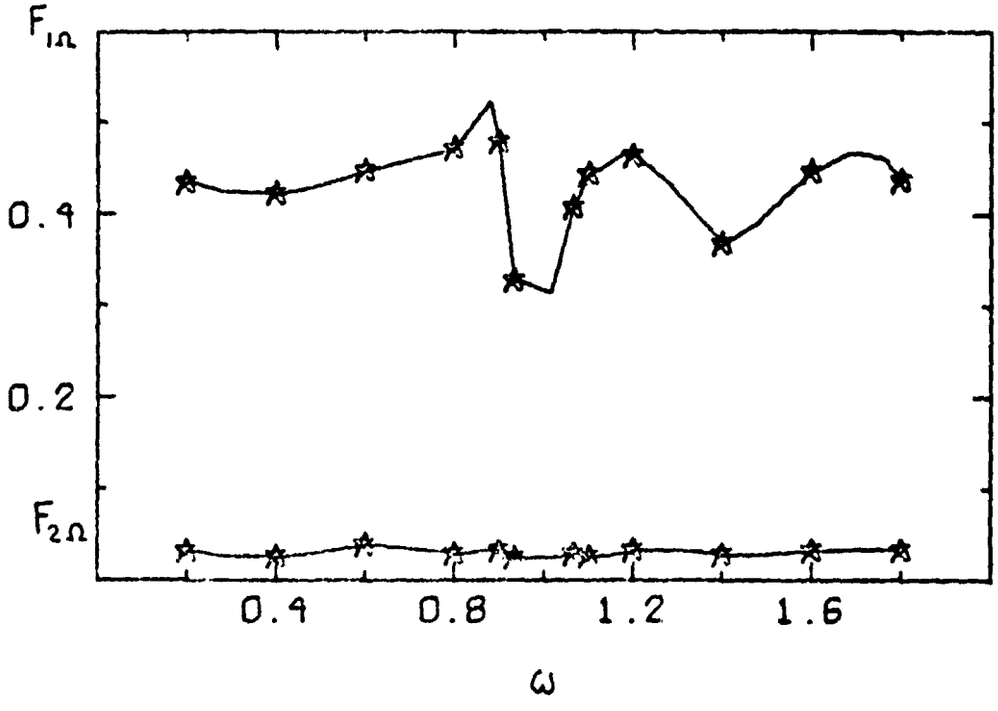

Figure 6h

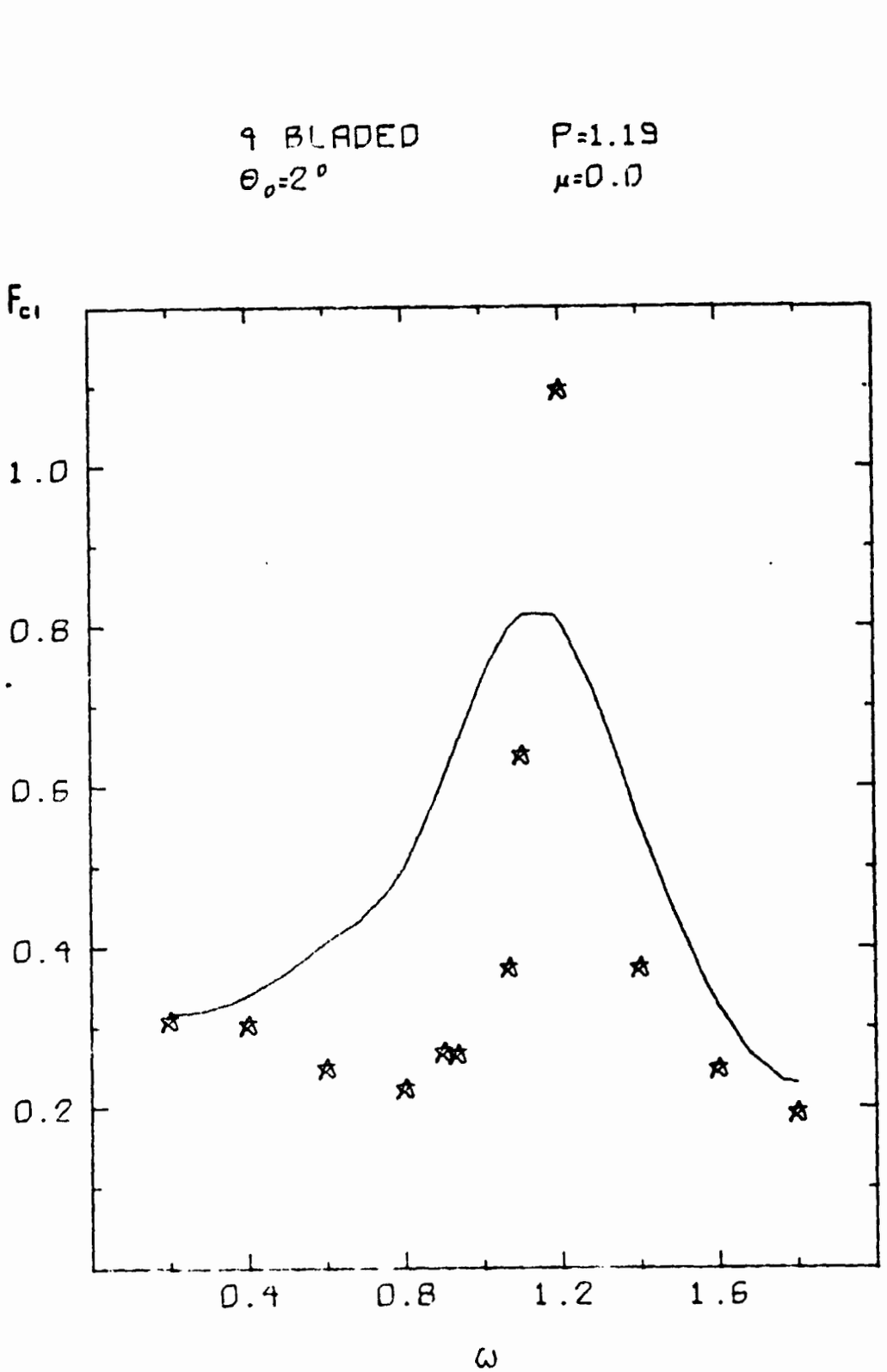

Figure 7a

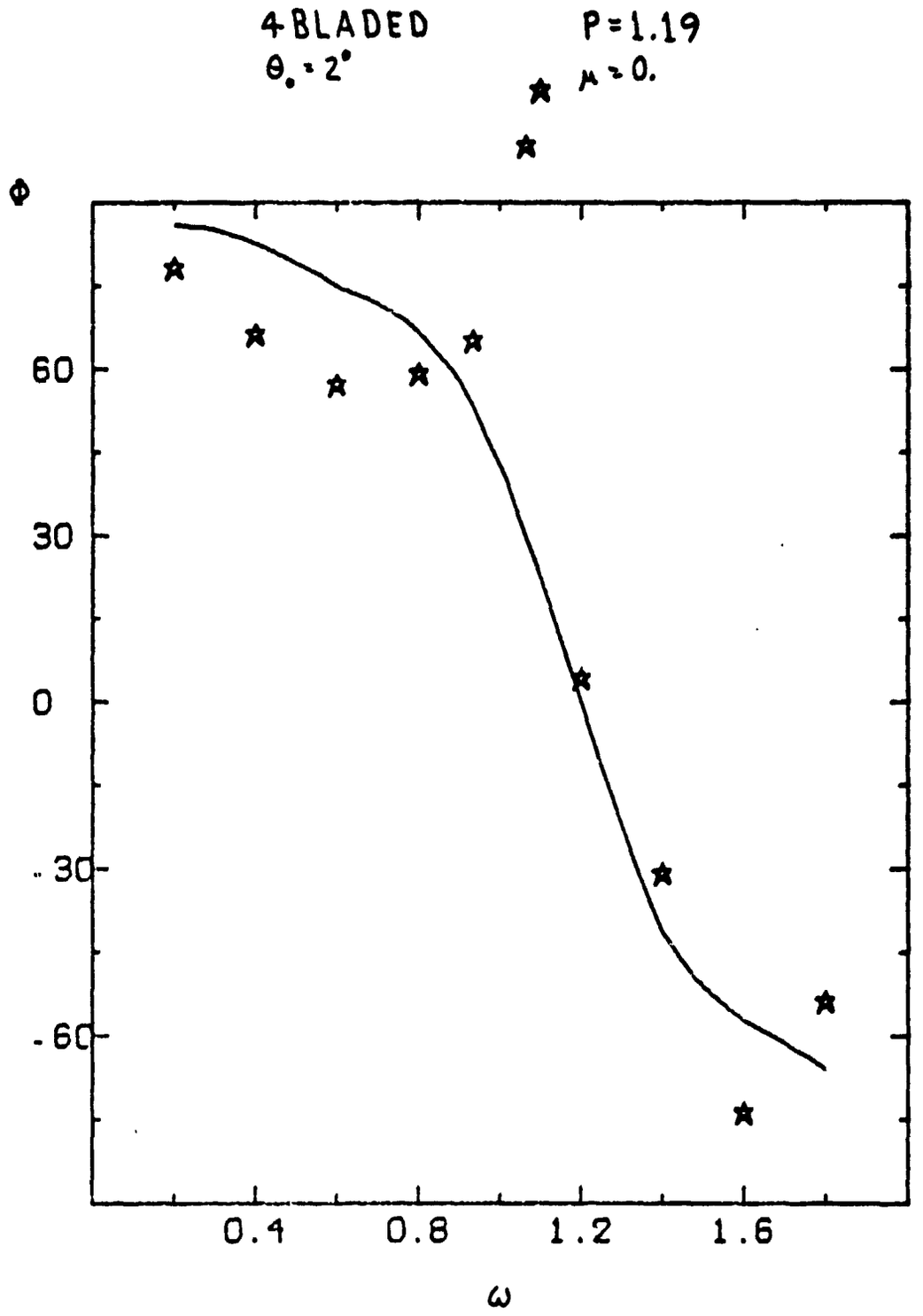

Figure 7b

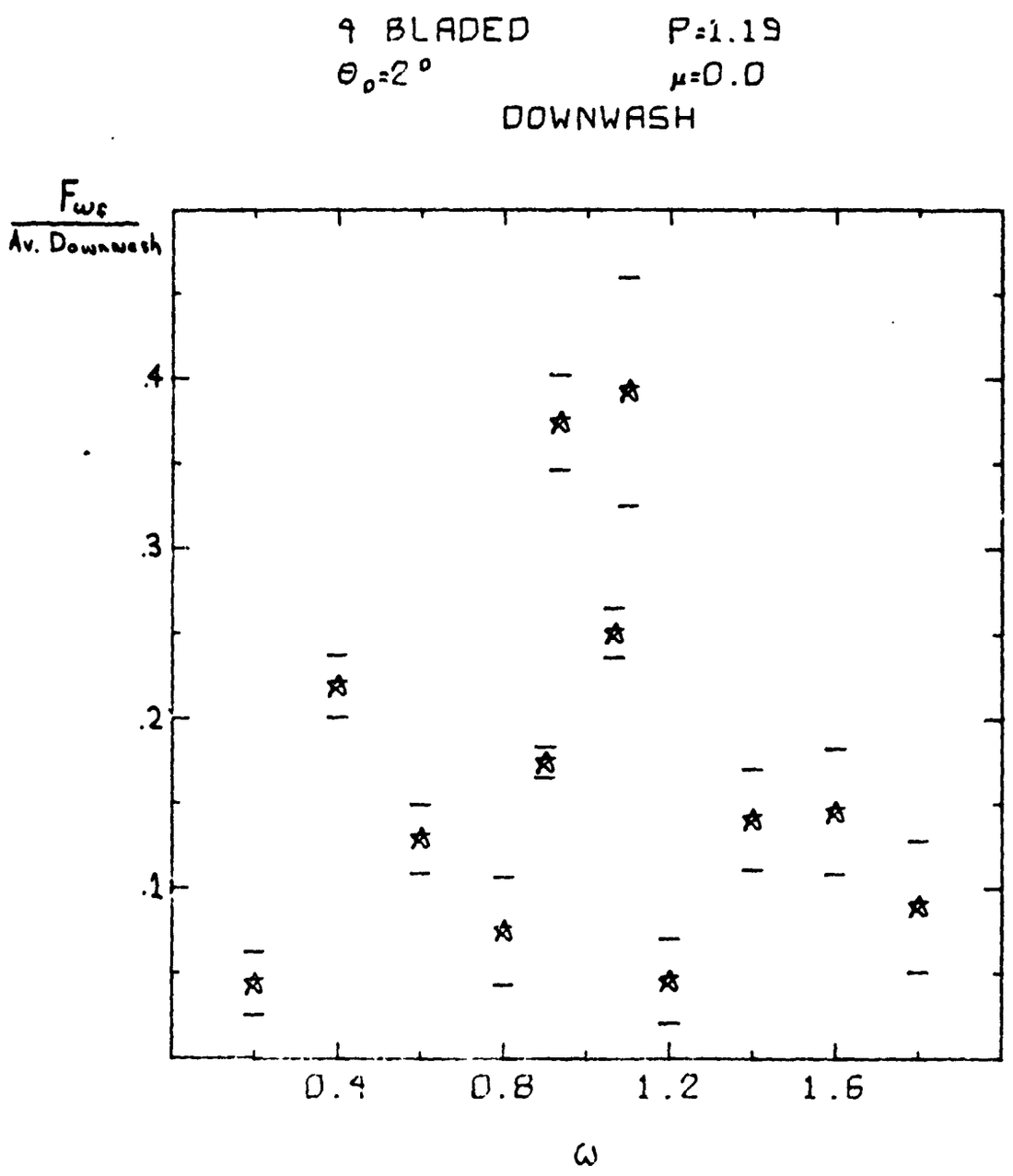
9 BLADED
P=1.19
θ_0=2°
μ=0.0
DOWNWASH
$\frac{F_{\omega c}}{\text{Av. Downwash}}$
.4
.3
.2
.1
0.4
0.8
1.2
1.6
ω

Figure 7c

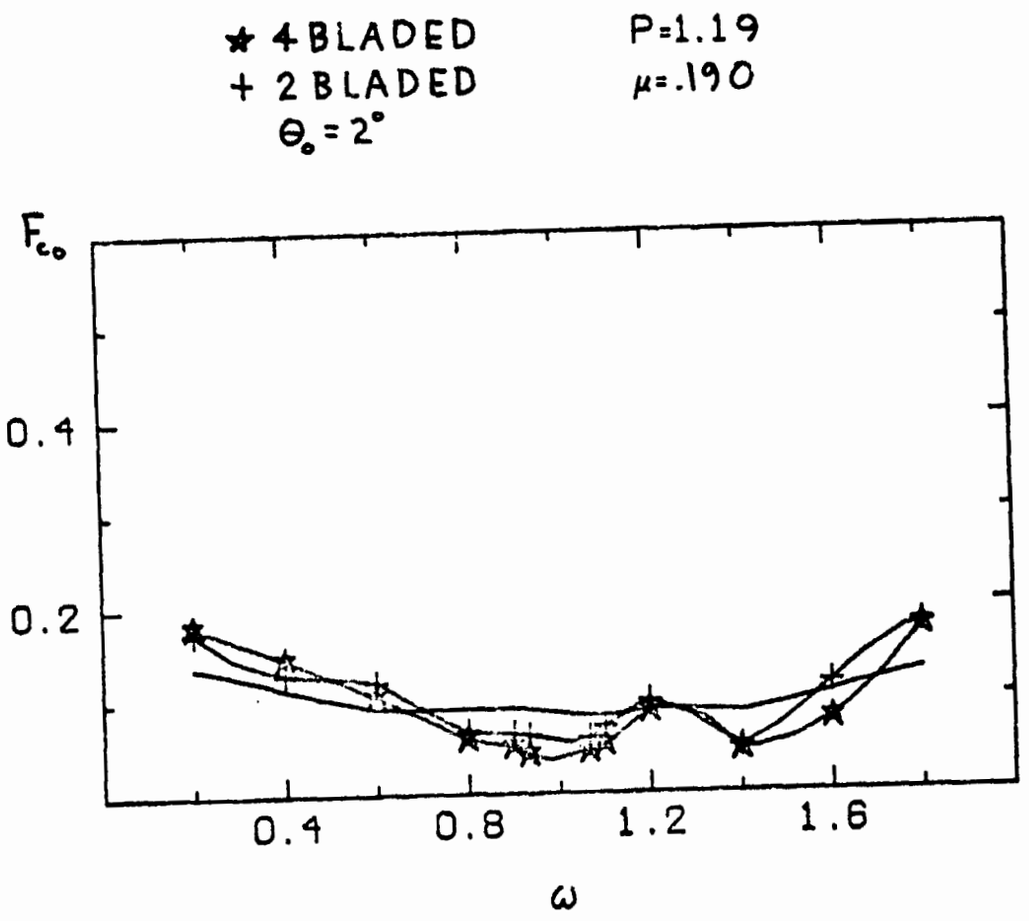
★ 4 BLADED
+ 2 BLADED
$\theta_o = 2°$
P=1.19
μ=.190
F_{c_o}
0.4
0.2
0.4
0.8
1.2
1.6
ω

Figure 8a

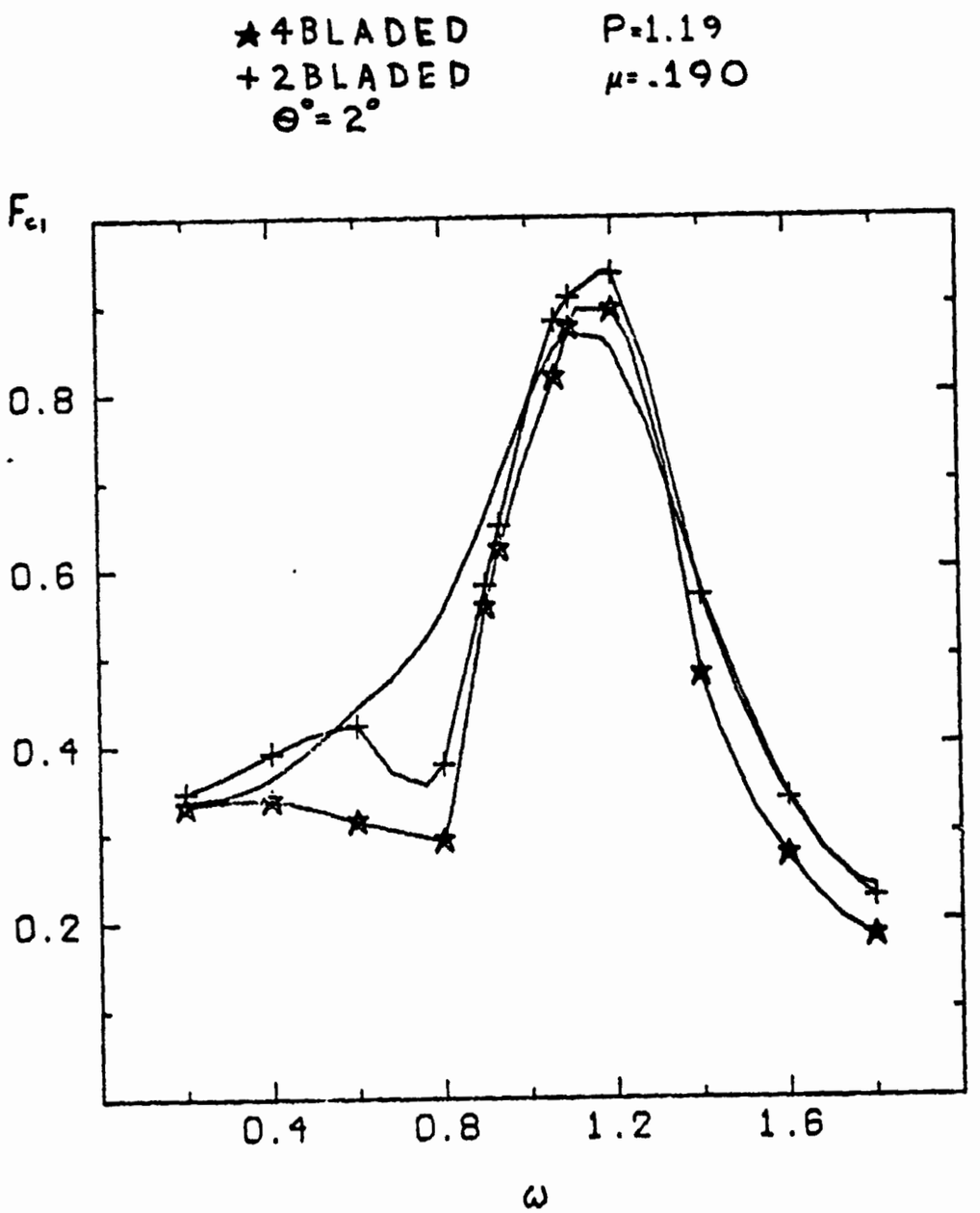

Figure 8b

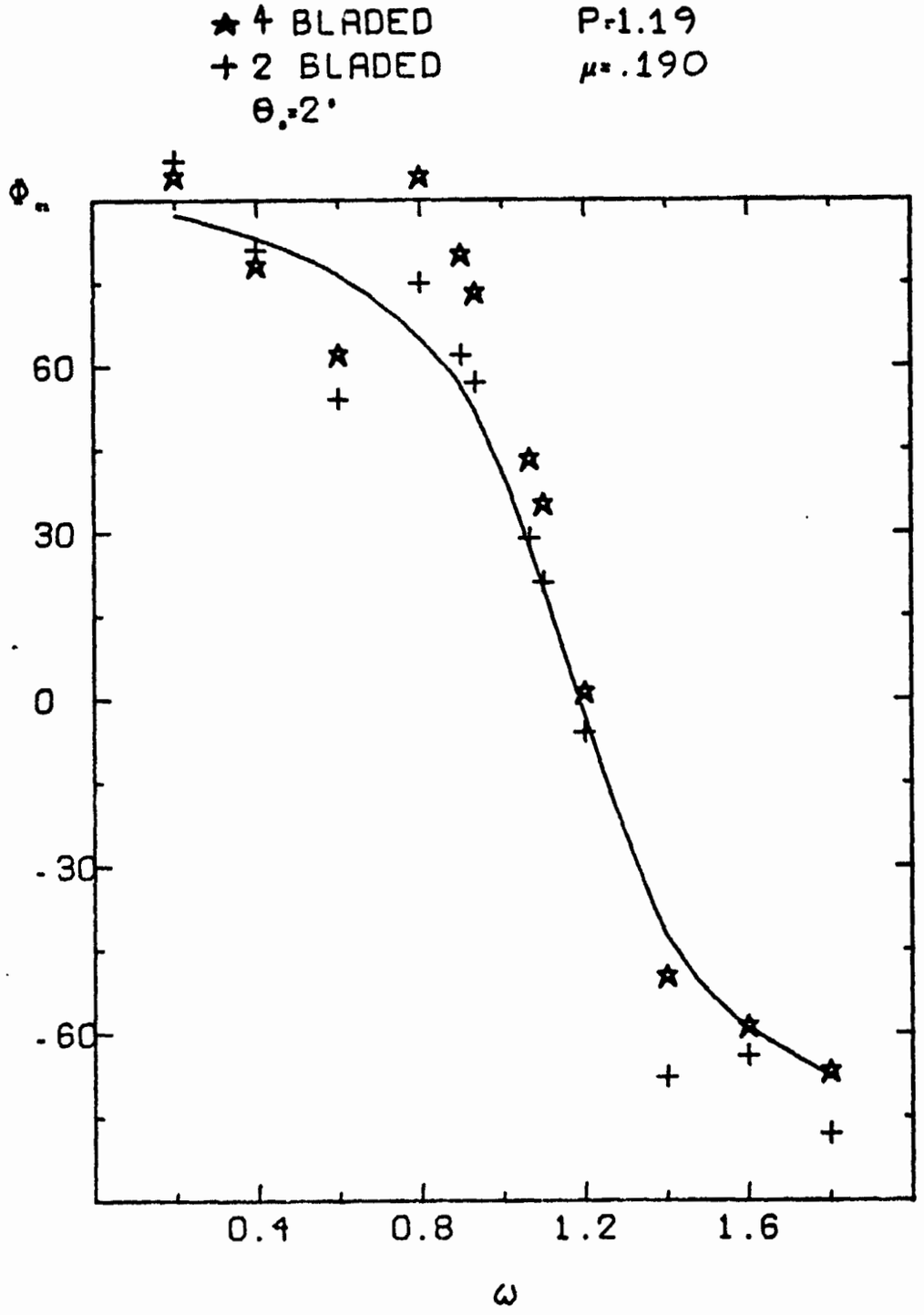

Figure 8c

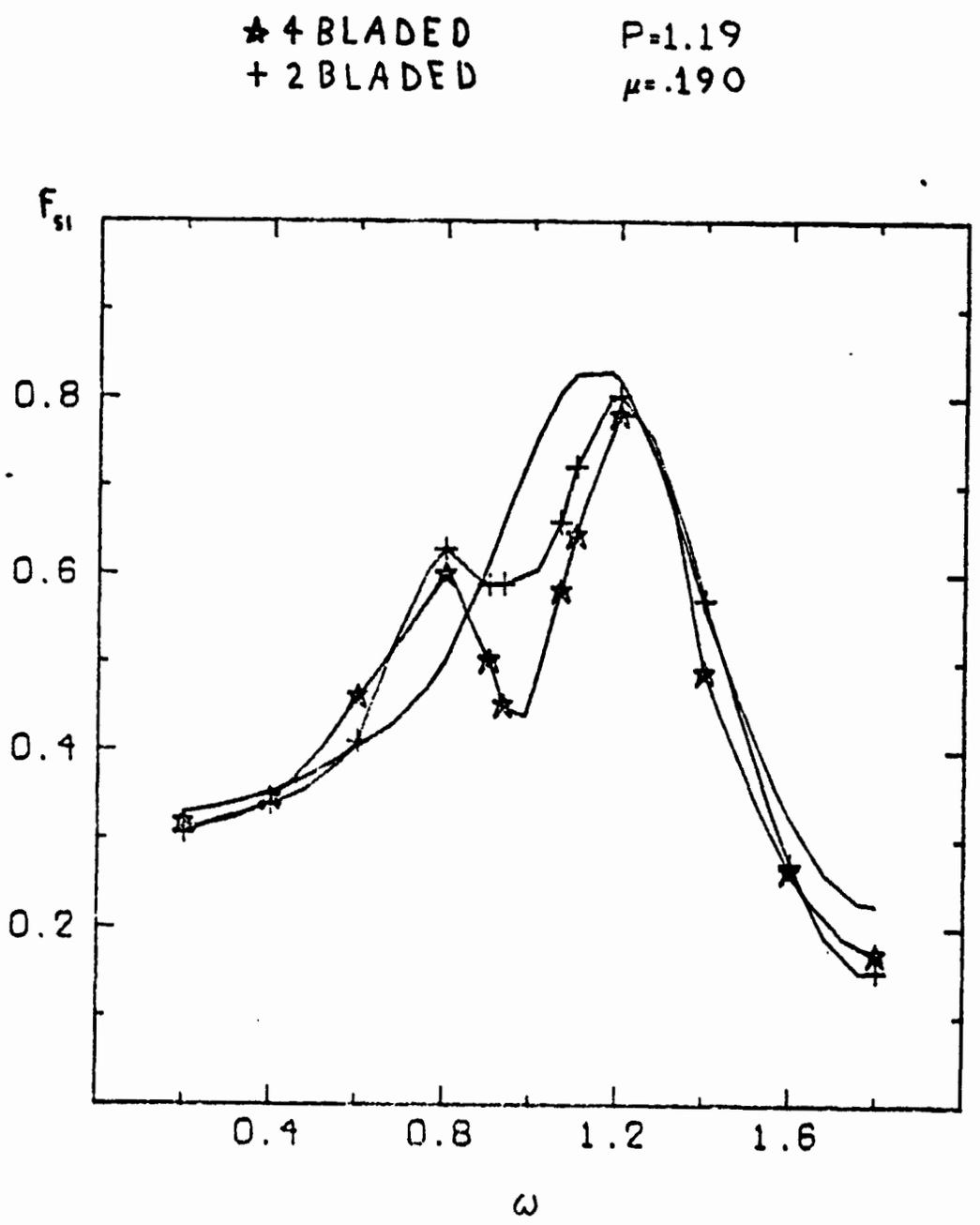

Figure 8d

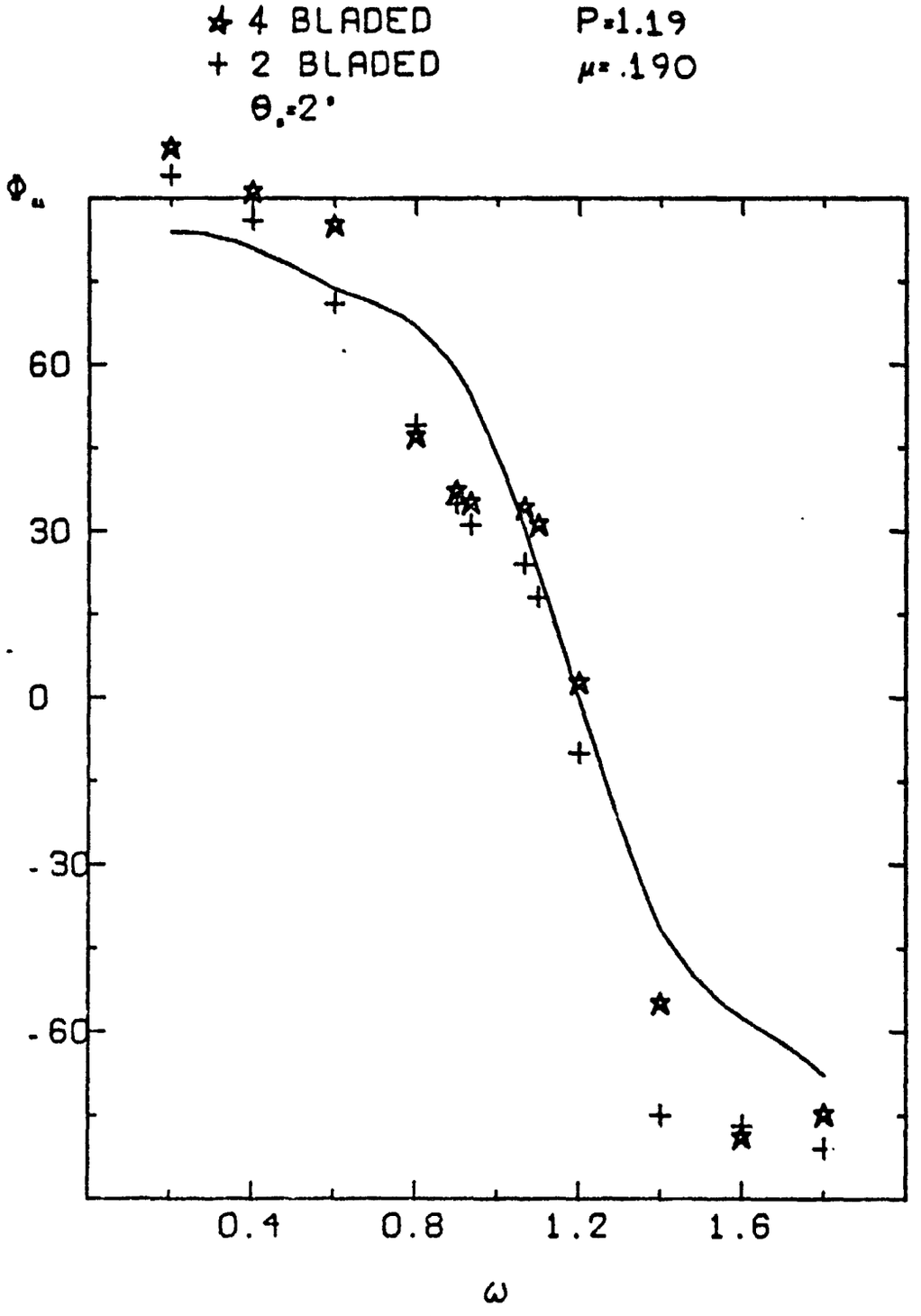

Figure 8e

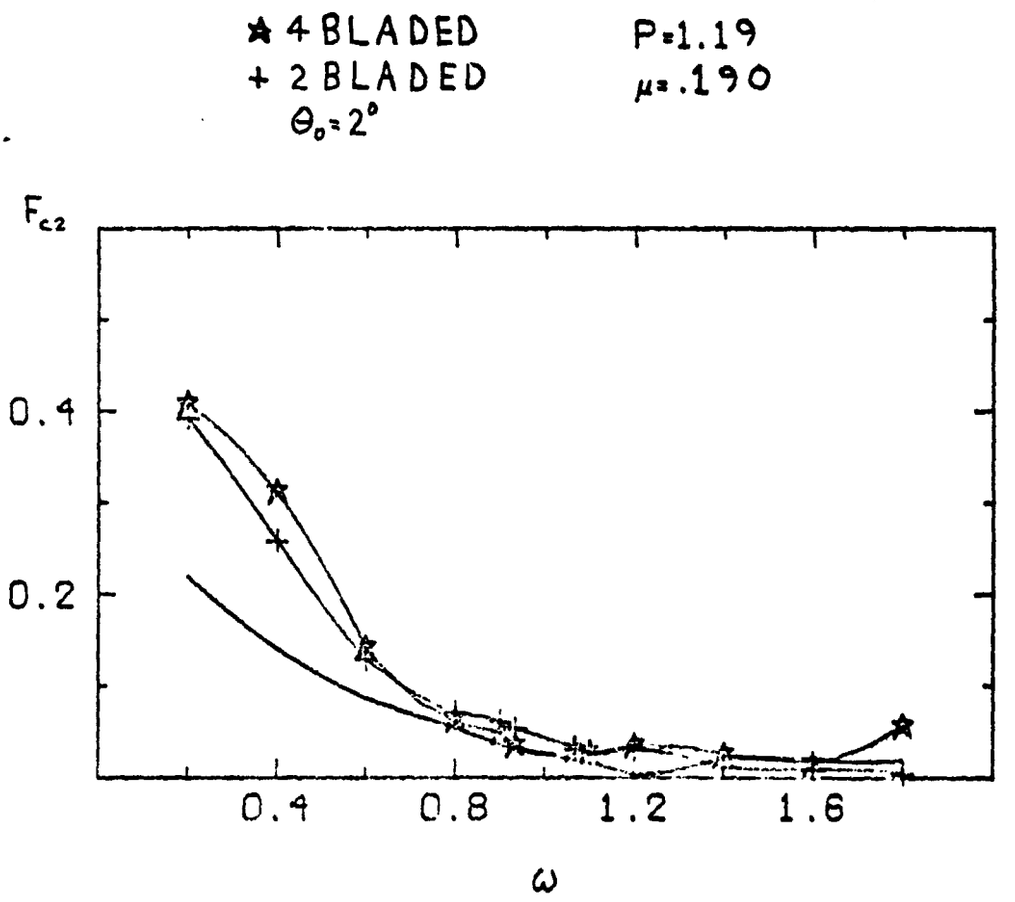

Figure 8f

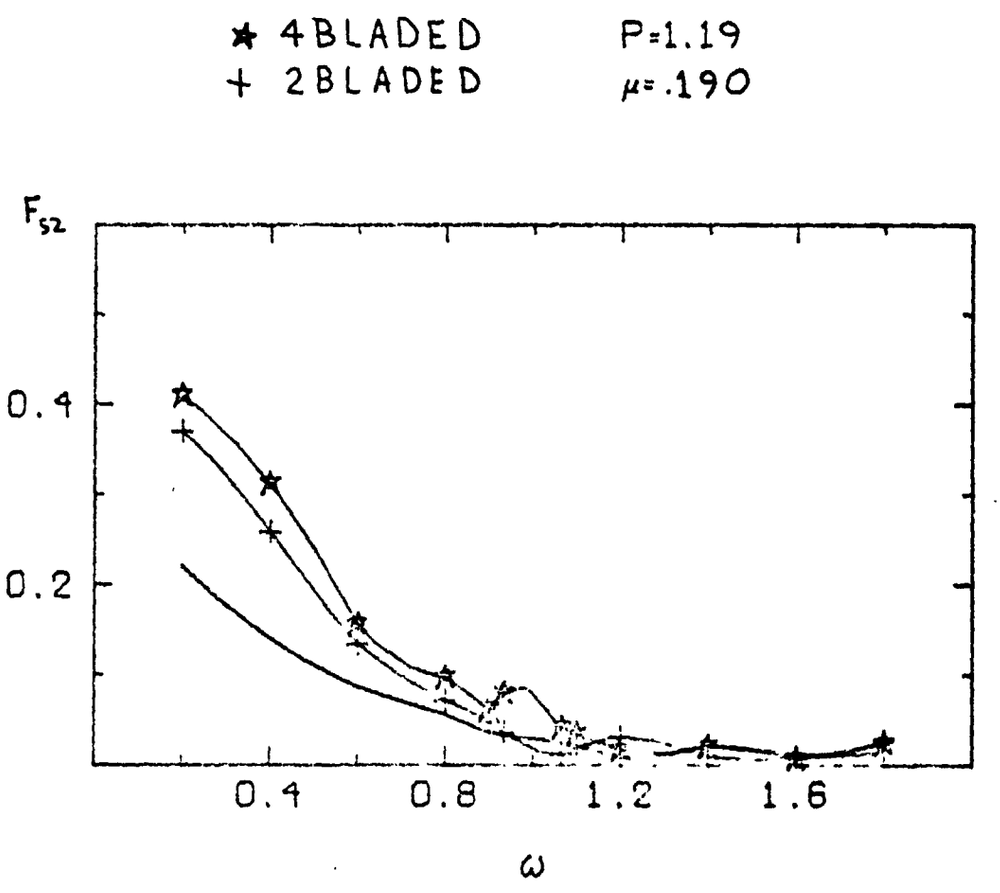

Figure 8g

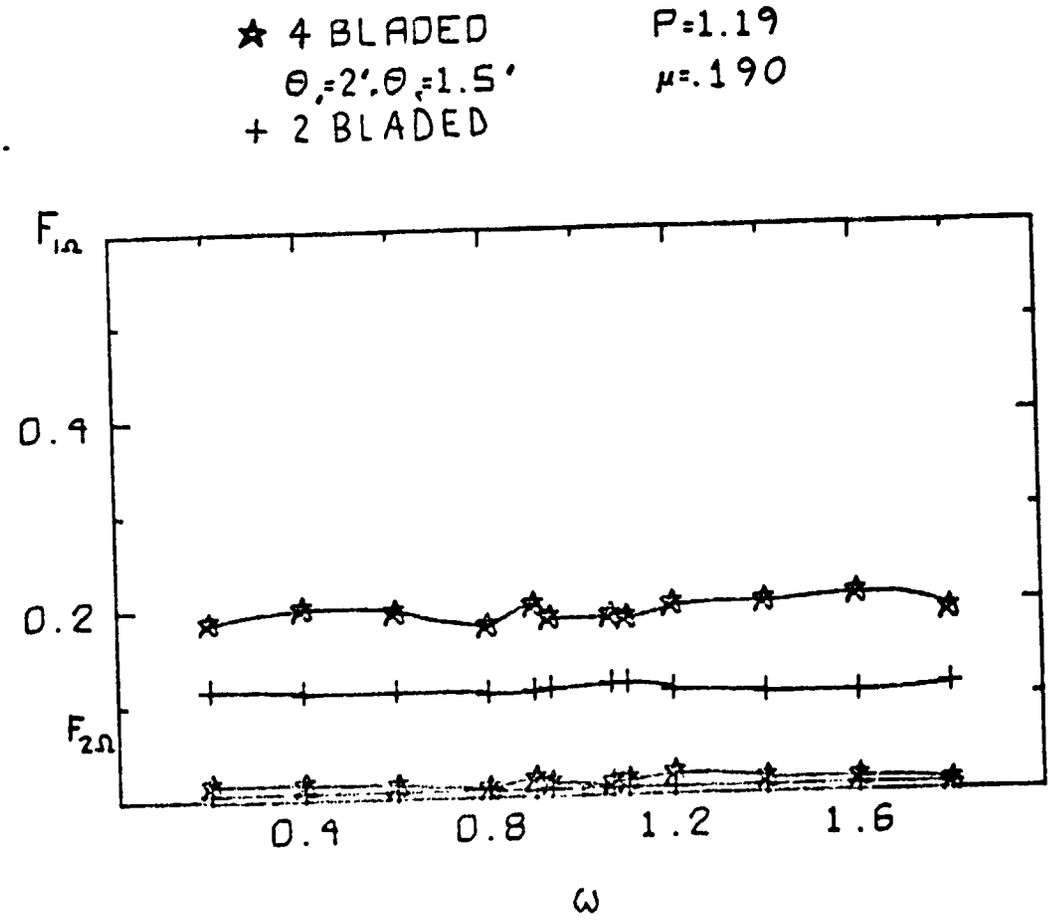
★ 4 BLADED
θ_0=2°, θ_c=1.5°
+ 2 BLADED
P=1.19
μ=.190
$F_{1\Omega}$
0.9
0.2
$F_{2\Omega}$
0.4
0.8
1.2
1.6
ω

Figure 8h

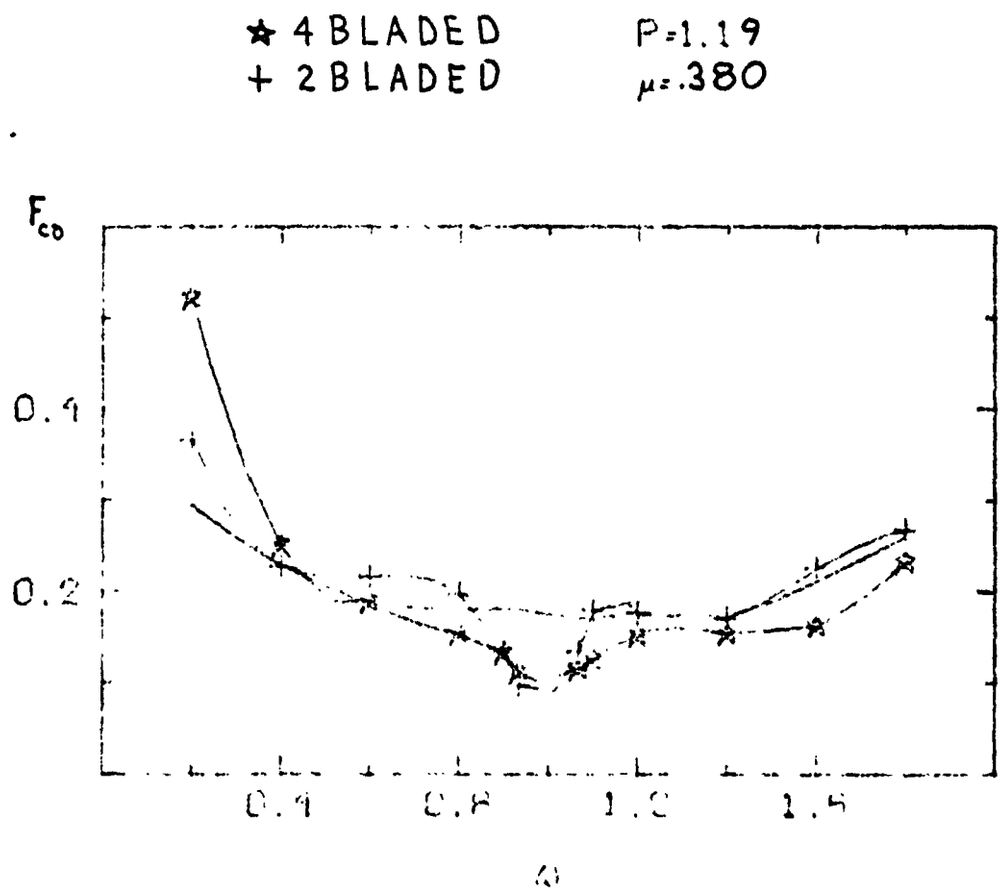

Figure 9a

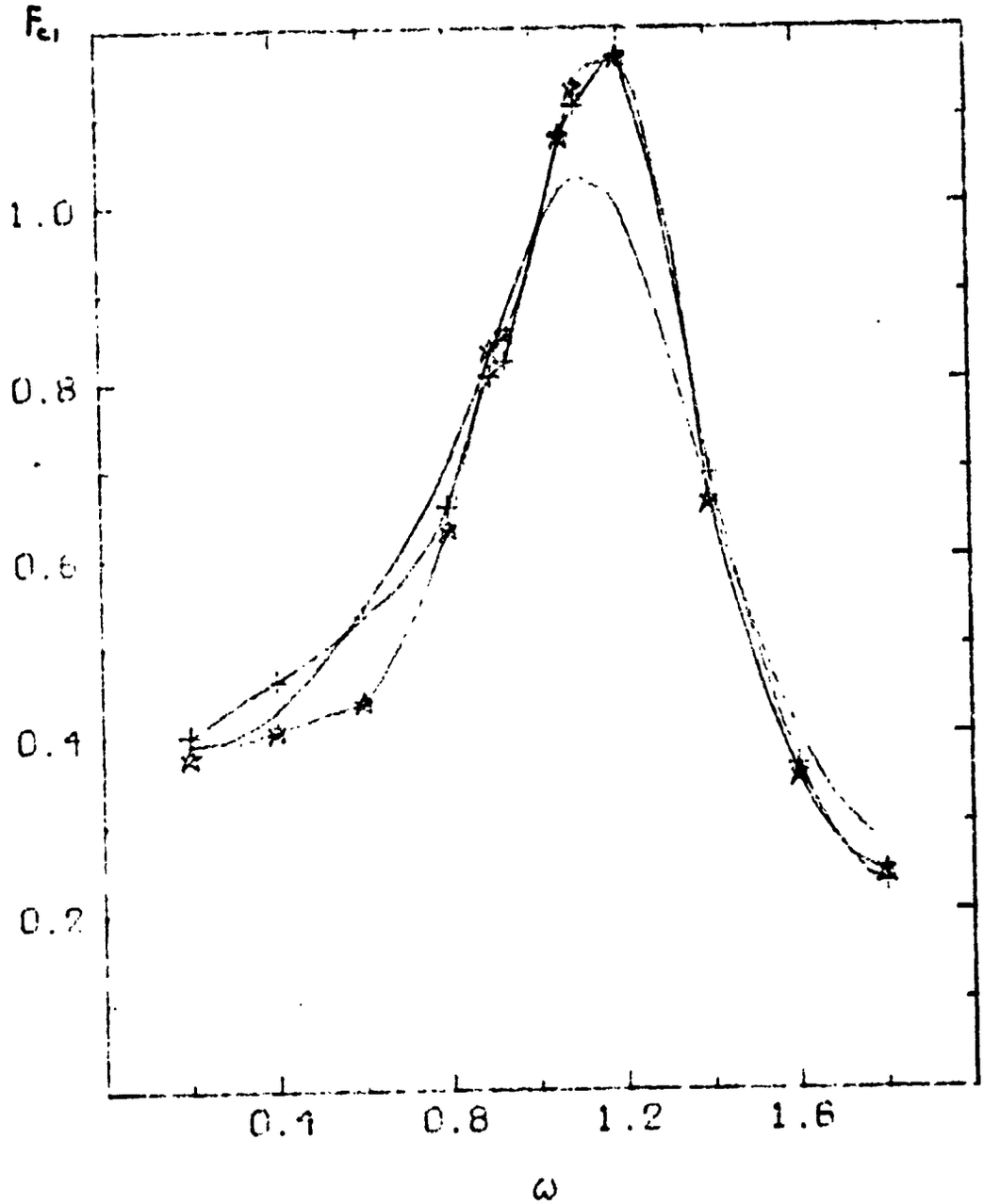
★ 4 BLADED
+ 2 BLADED
$\theta_0 = 2°$
P=1.19
μ=.380
F_{c_1}
1.0
0.8
0.6
0.4
0.2
0.4
0.8
1.2
1.6
ω

Figure 9b

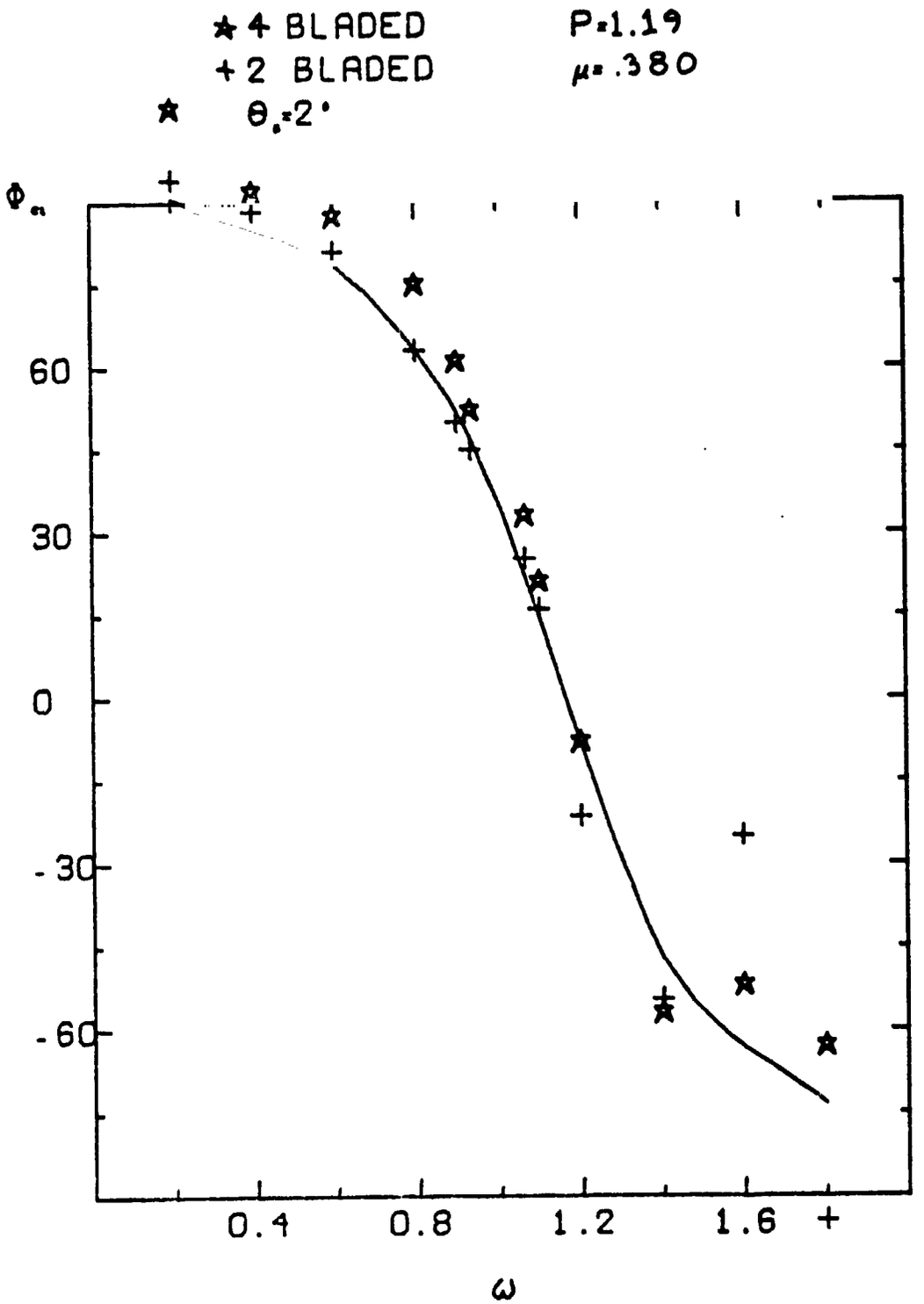

Figure 9c

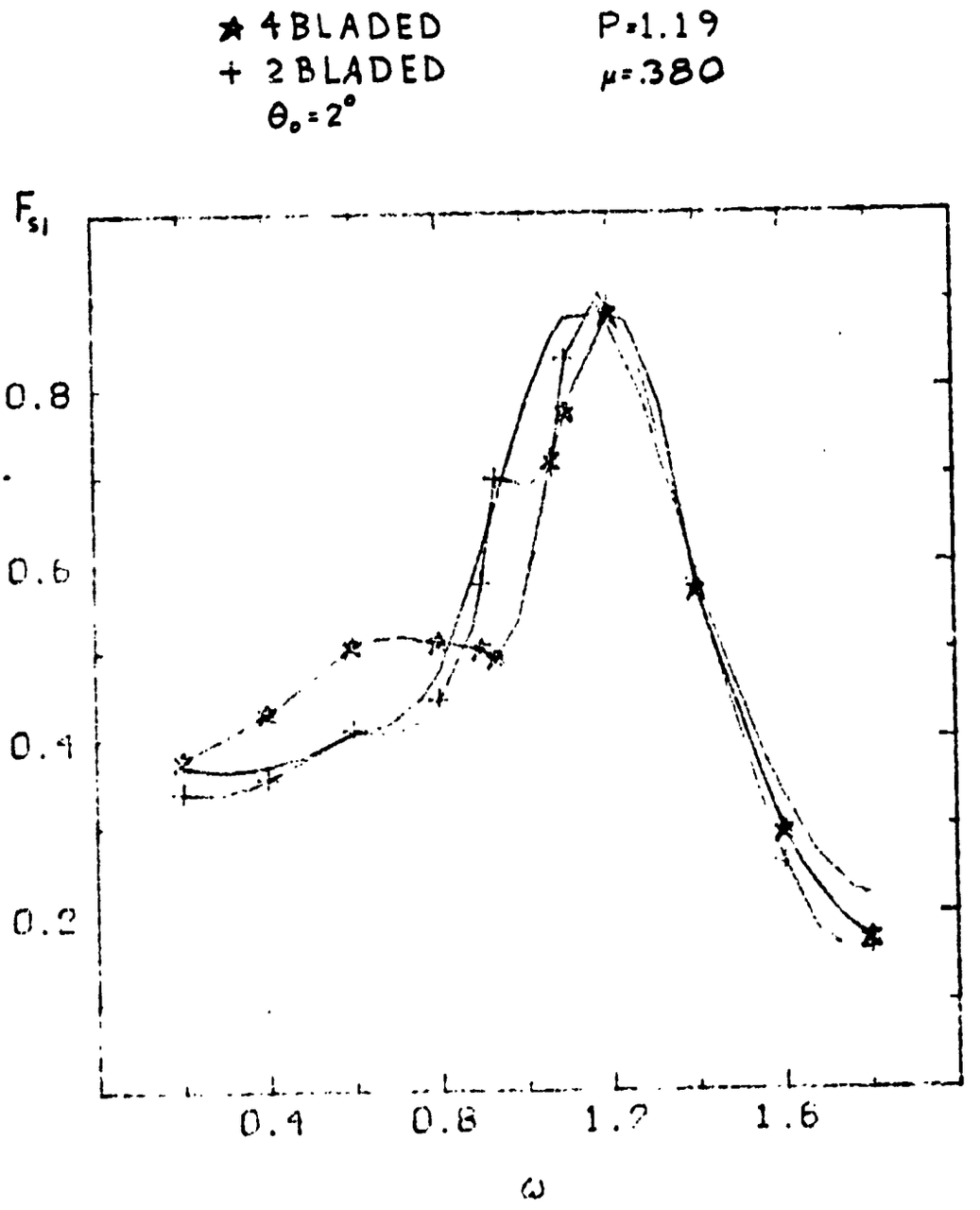
★ 4 BLADED
+ 2 BLADED
$\theta_0 = 2°$
P=1.19
μ=.380
F_{s1}
0.8
0.6
0.4
0.2
0.4
0.8
1.2
1.6
ω

Figure 9d

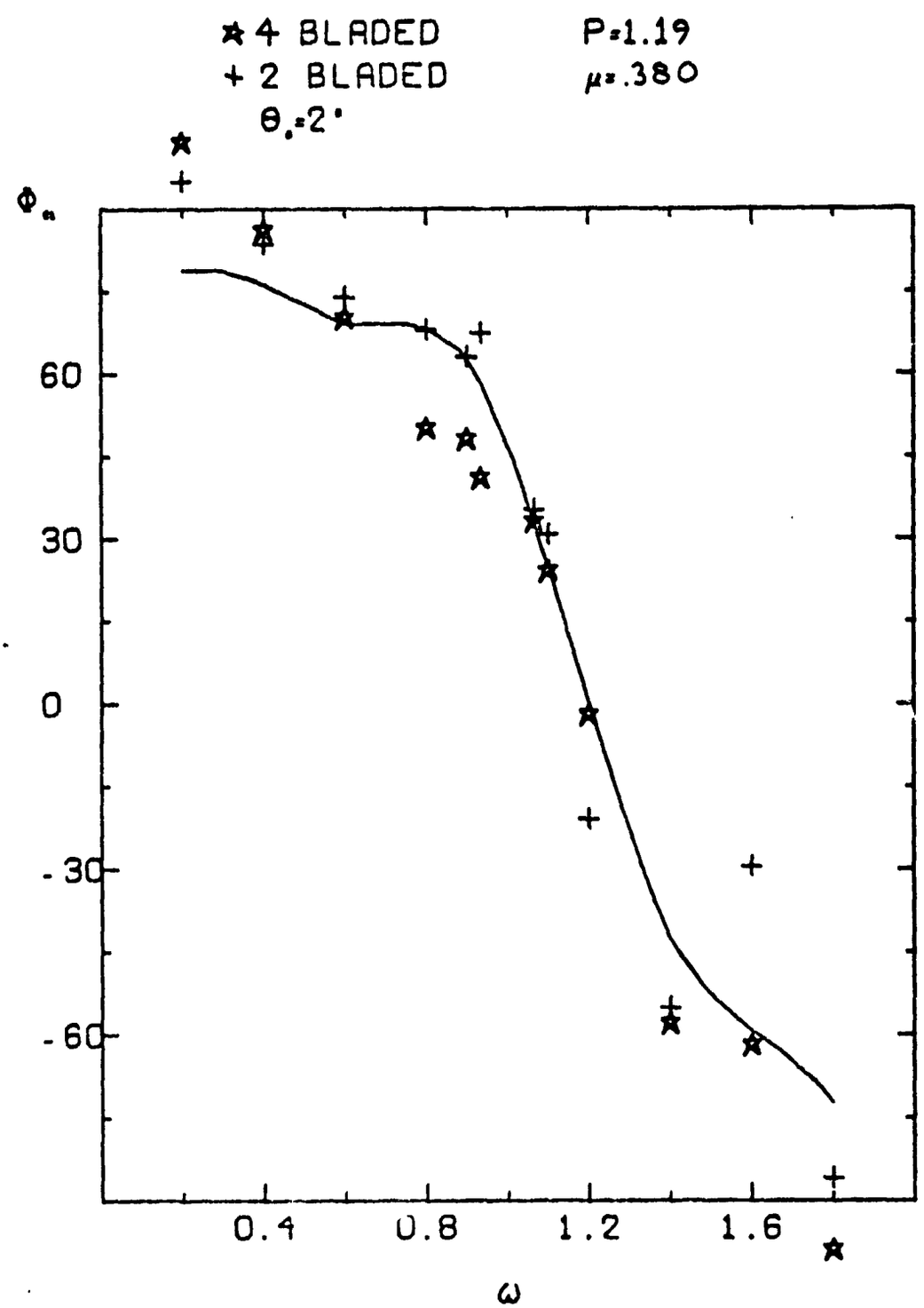

Figure 9e

★ 4 BLADED P=1.19
\+ 2 BLADED μ=.380
$\theta_o = 2°$

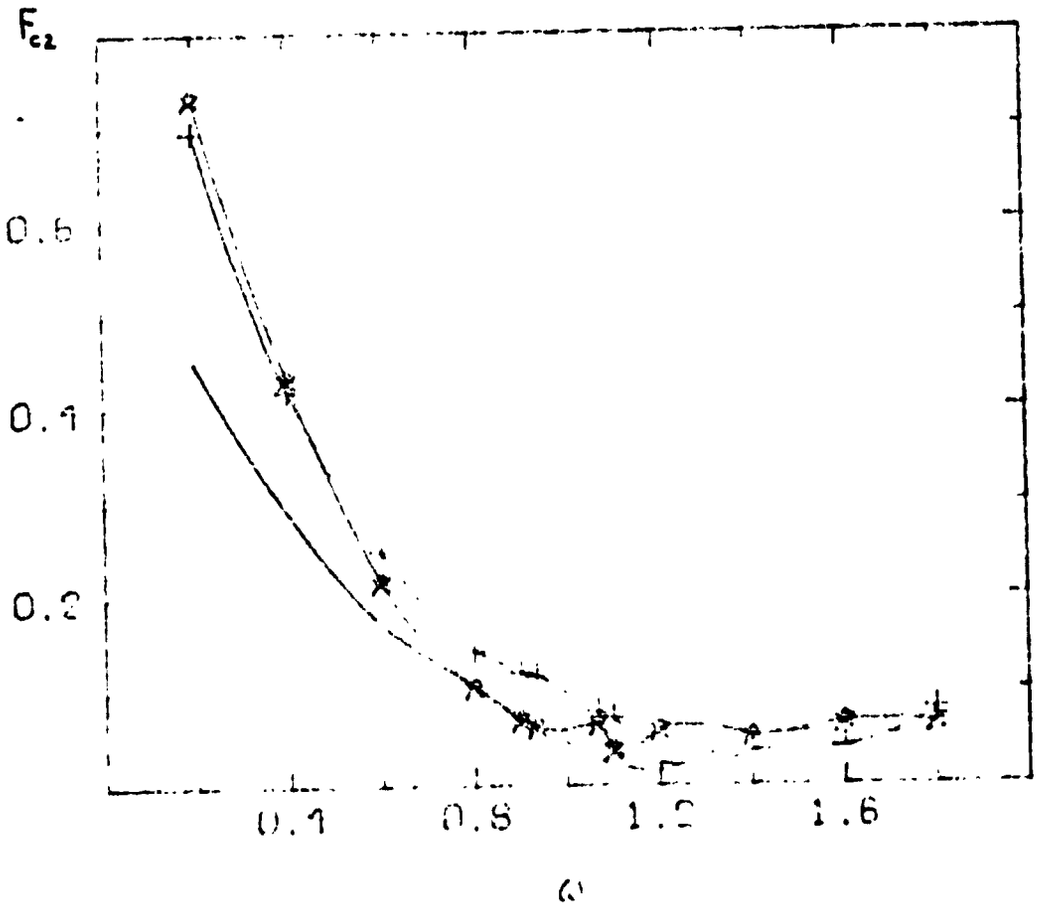

Figure 9f

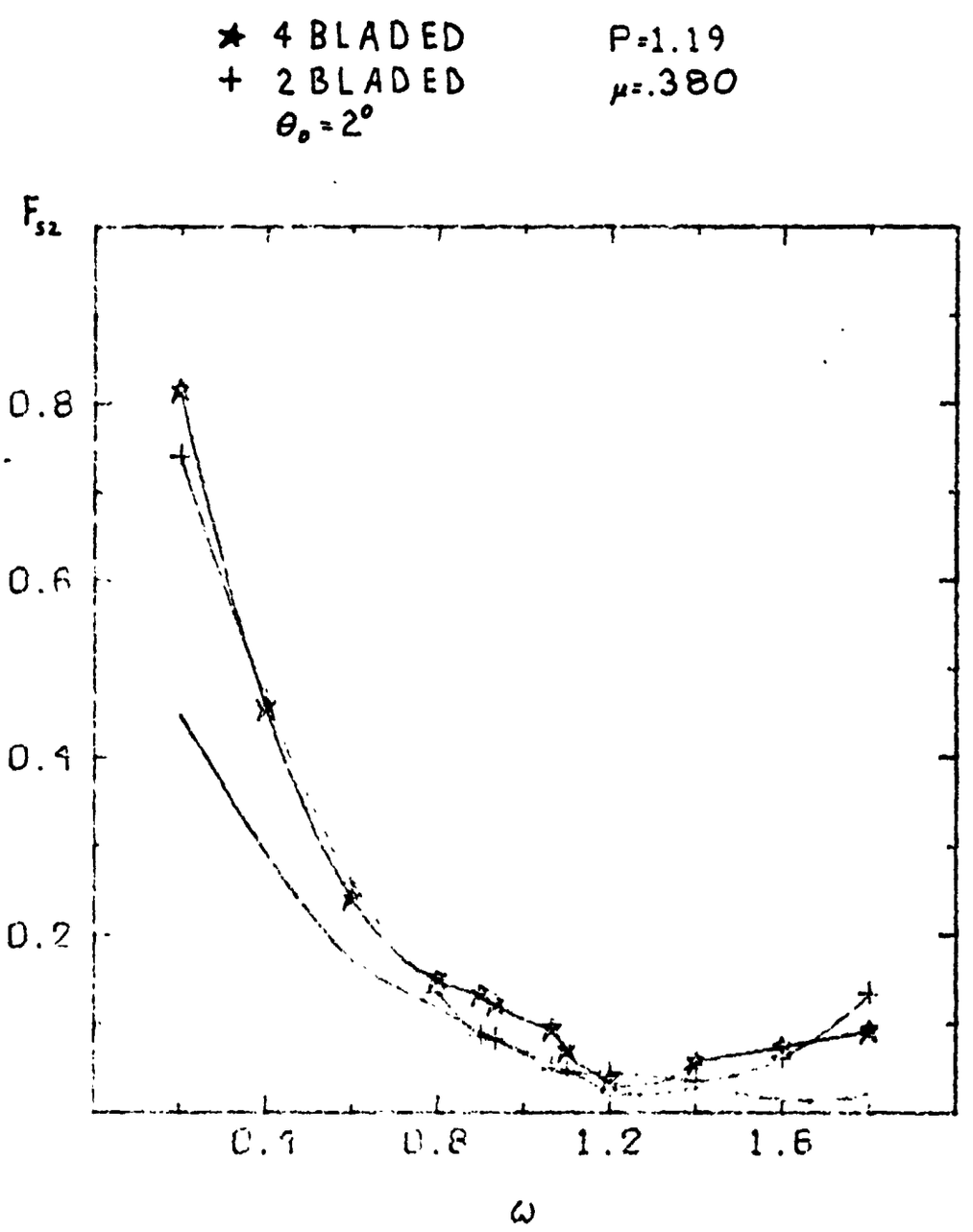
★ 4 BLADED
+ 2 BLADED
$\theta_0 = 2^\circ$
P=1.19
μ=.380
F_{s2}
0.8
0.6
0.4
0.2
0.4
0.8
1.2
1.6
ω

Figure 9g

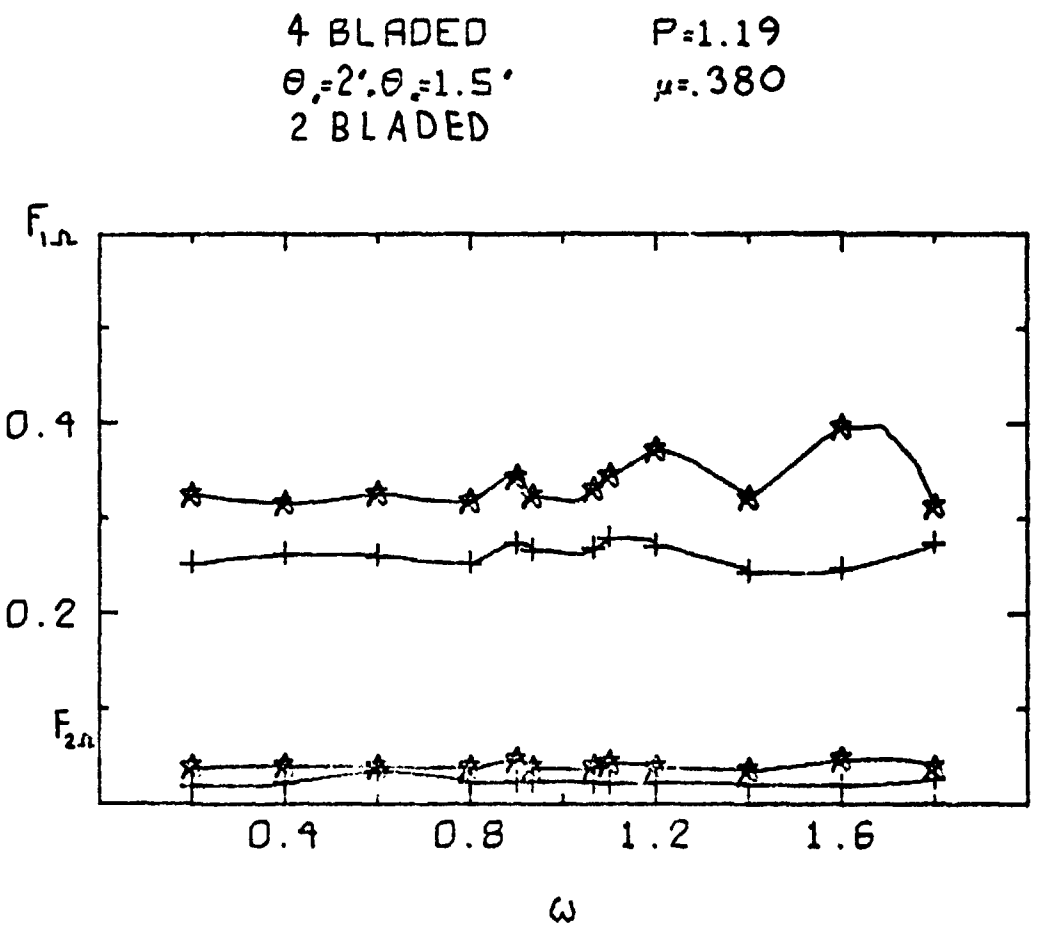

Figure 9h

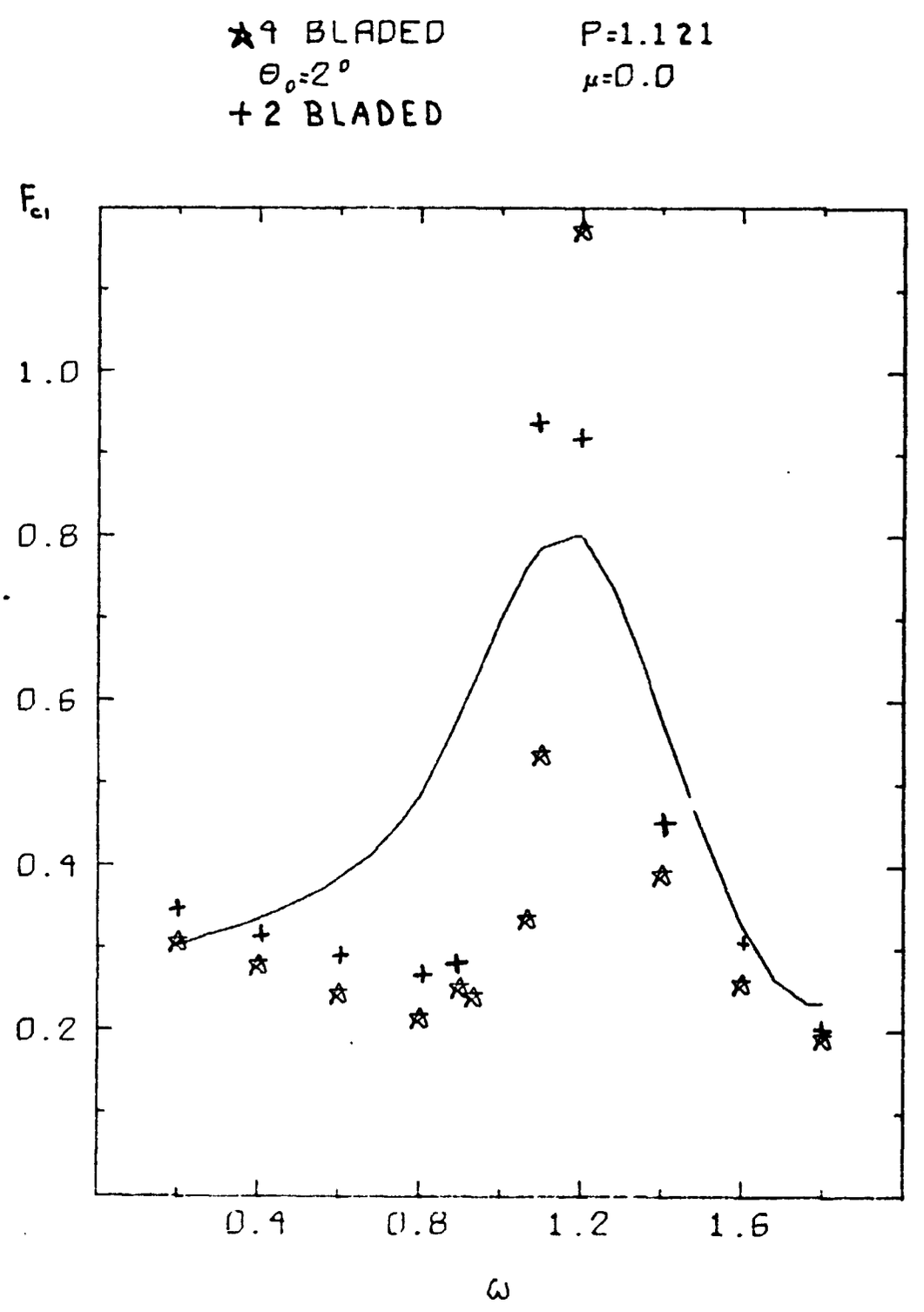
★9 BLADED
θ_0=2°
+2 BLADED
P=1.121
μ=0.0
F_{c_1}
1.0
0.8
0.6
0.4
0.2
0.4
0.8
1.2
1.6
ω

Figure 10a

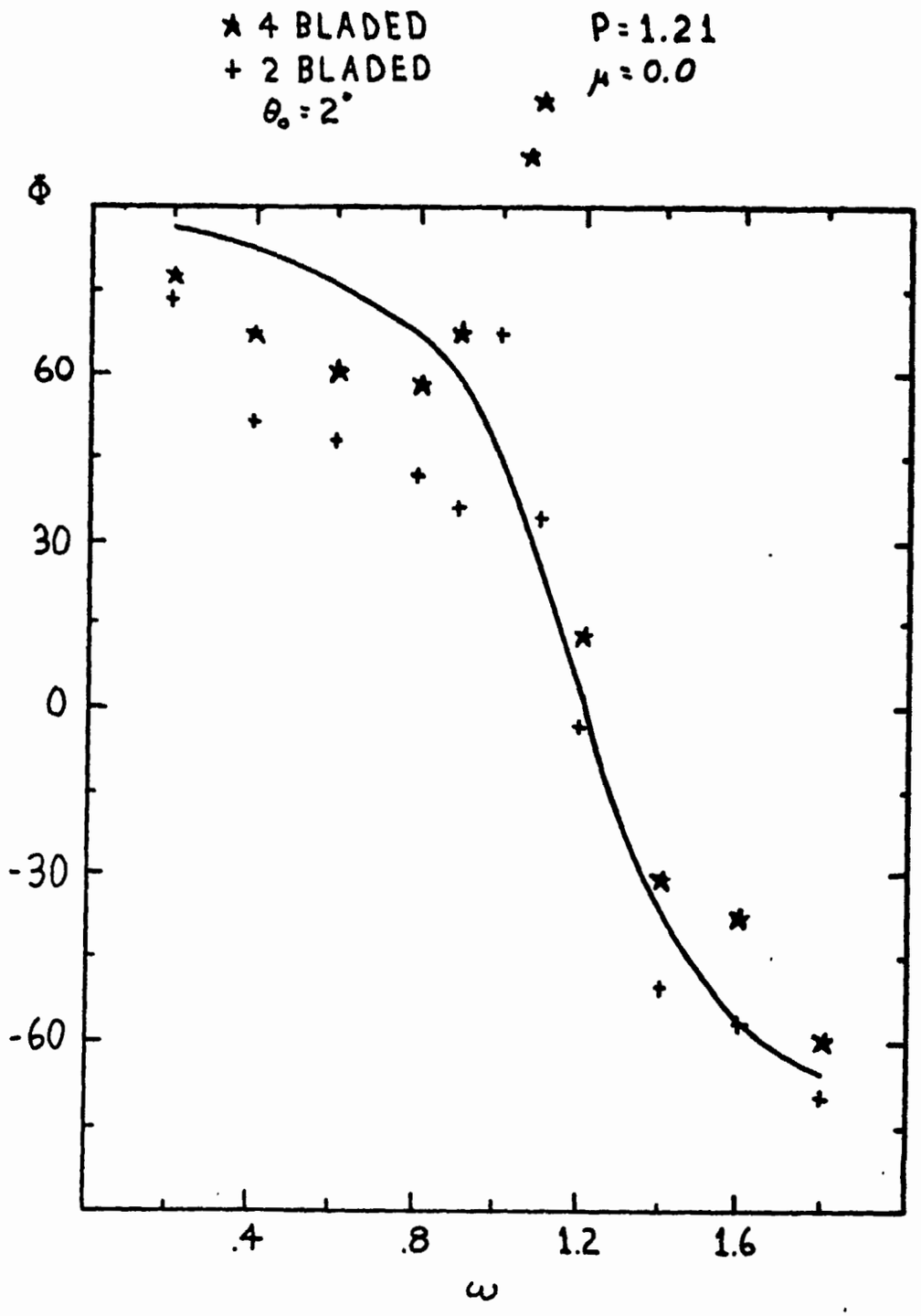

Figure 10b

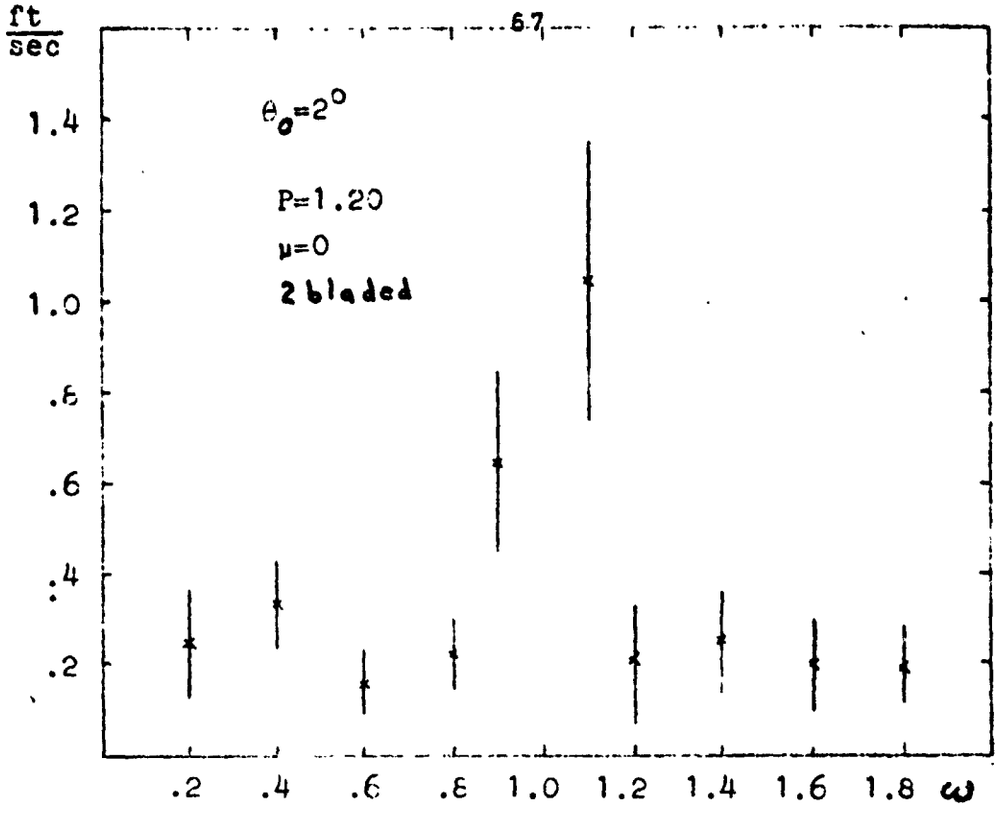

4 BLADED P=1.121
$\theta_0=2^\circ$ μ=0.0
DOWNWASH

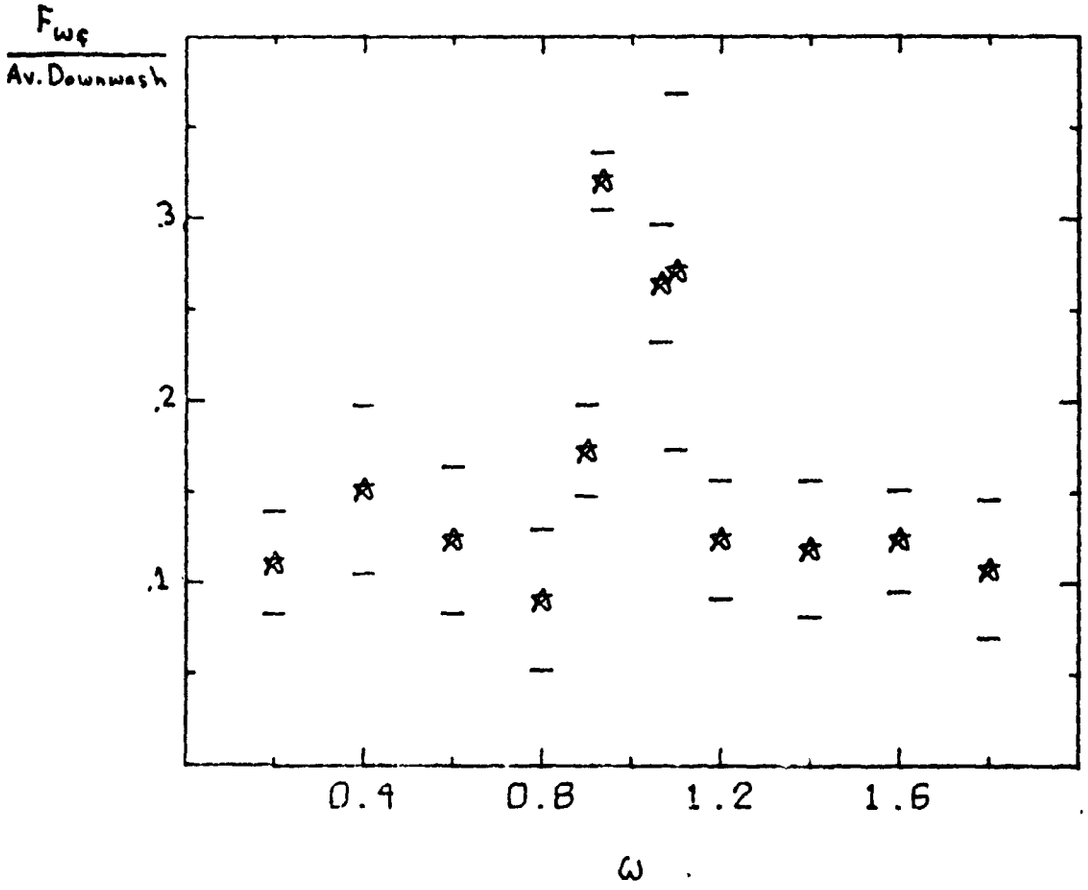

2 BLADED P=1.105
θ_o=5° μ=.192

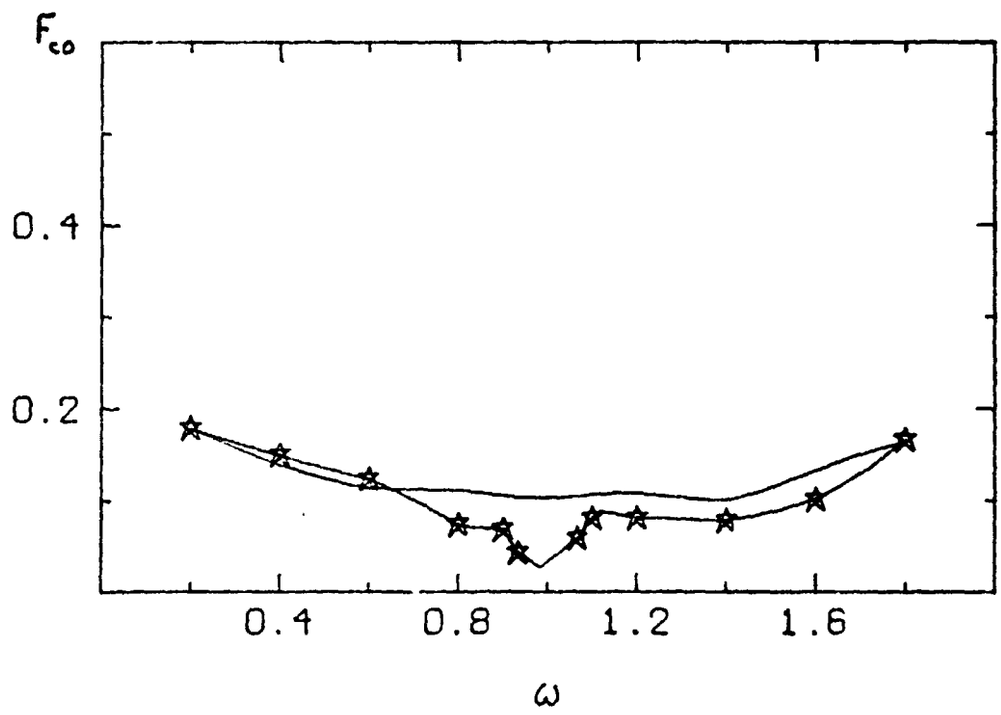

Figure 11a

2 BLADED P=1.105
θ_0=5° μ=.192

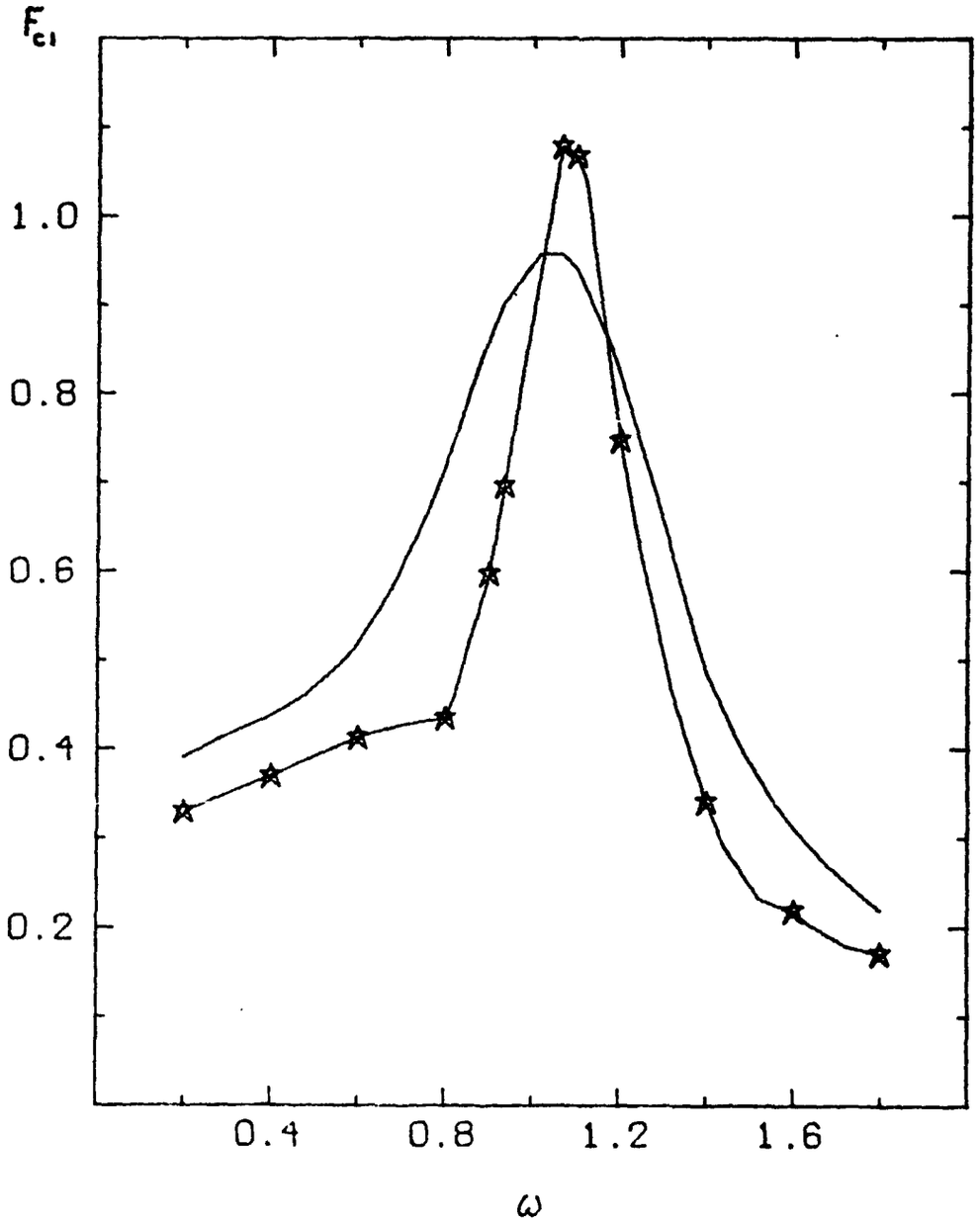

Figure 11b

2 BLADED $\theta_0 = 5^\circ$ $P = 1.105$ $\mu = .192$

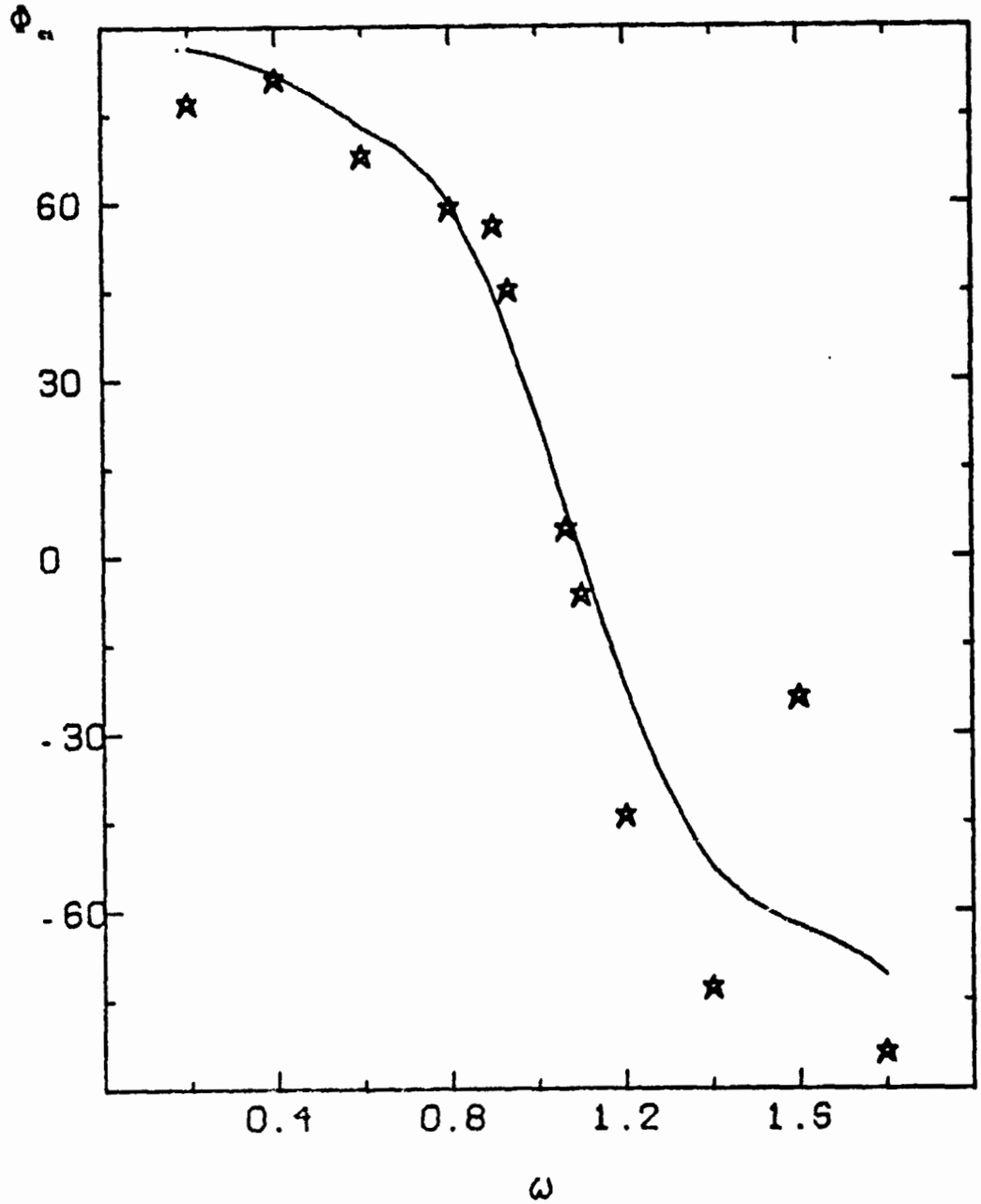

Figure 11c

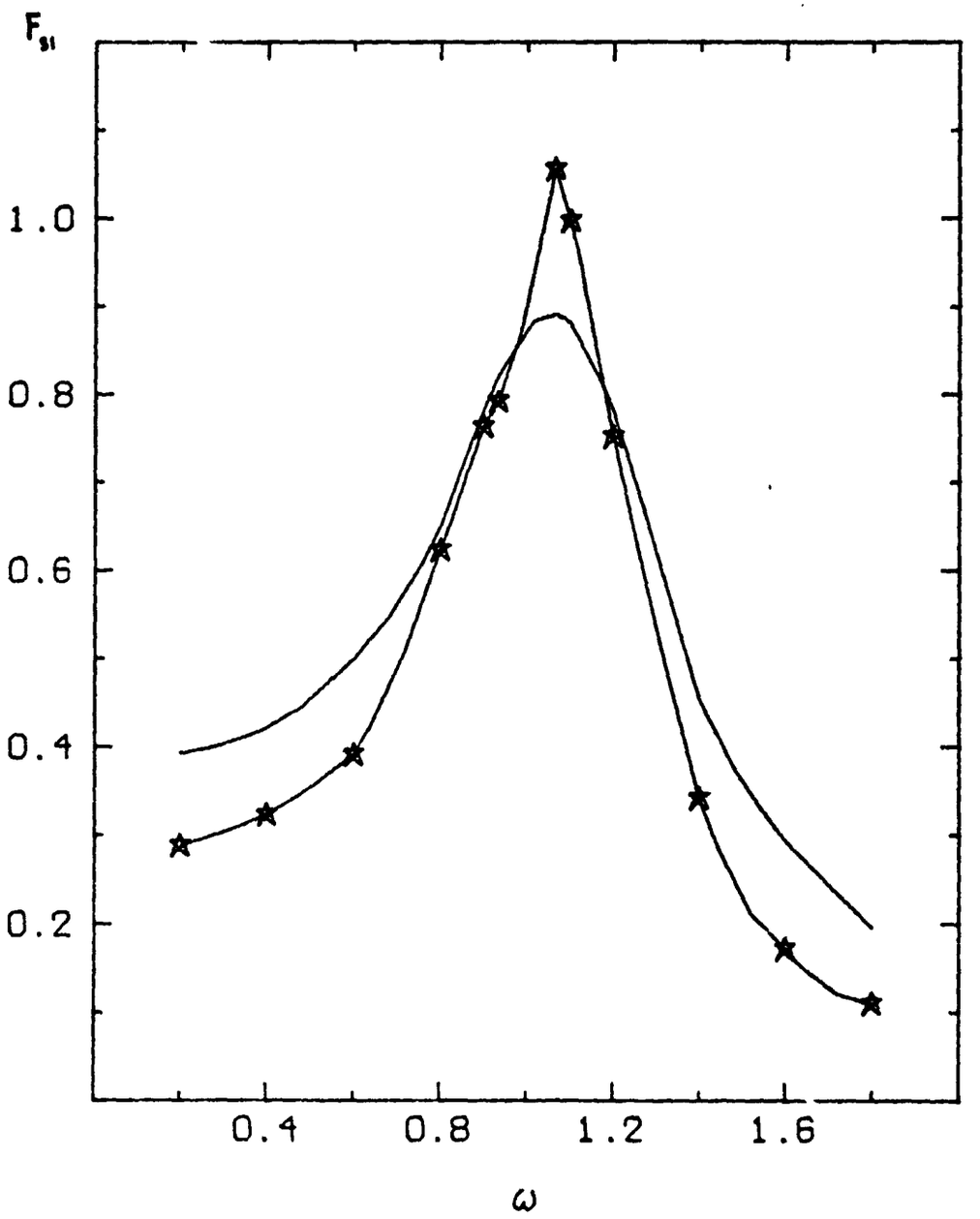

Figure 11d

2 BLADED $\theta_0 = 5°$ $P = 1.105$ $\mu = .192$

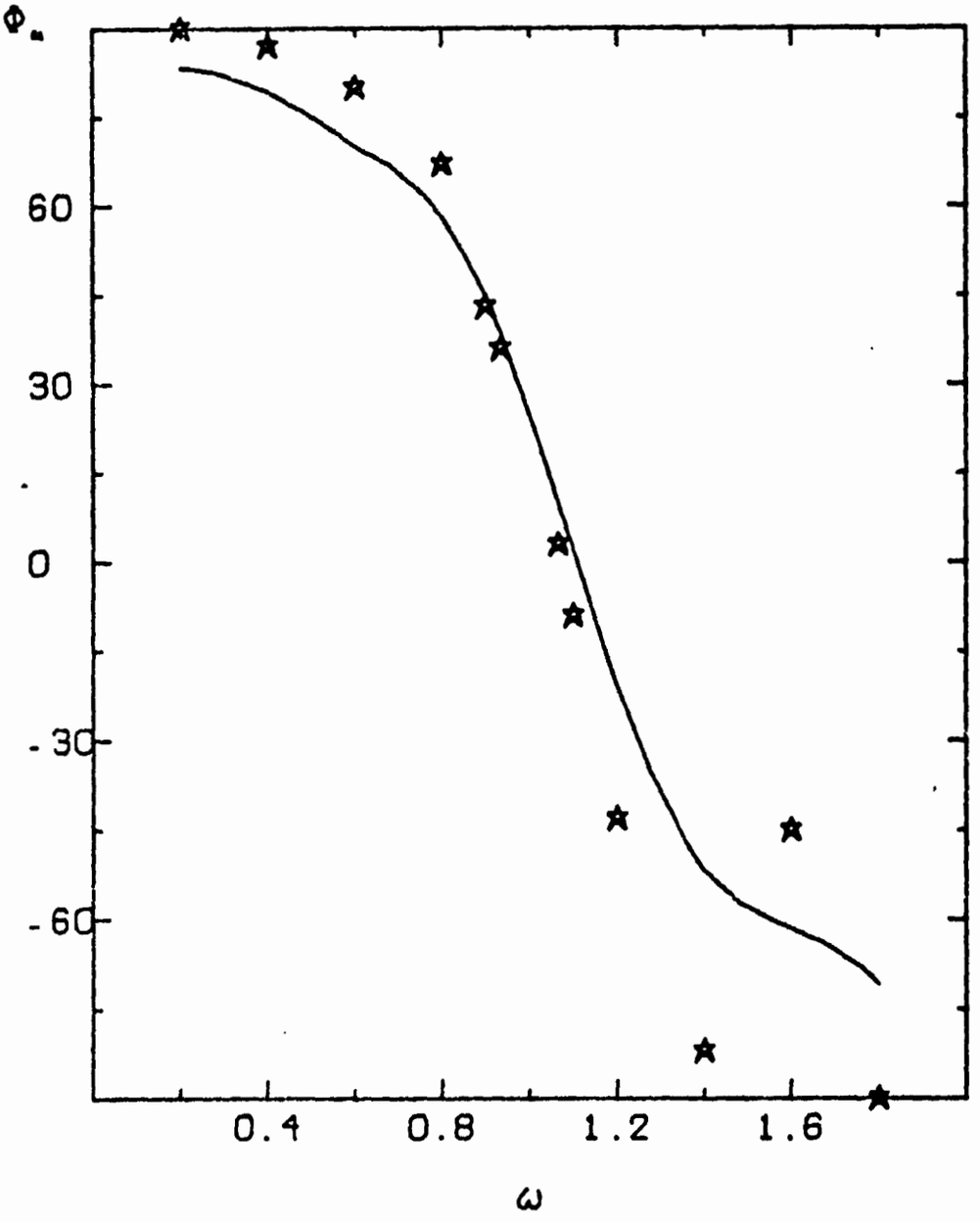

Figure 11e

2 BLADED P=1.105
θ_o=5° μ=.192

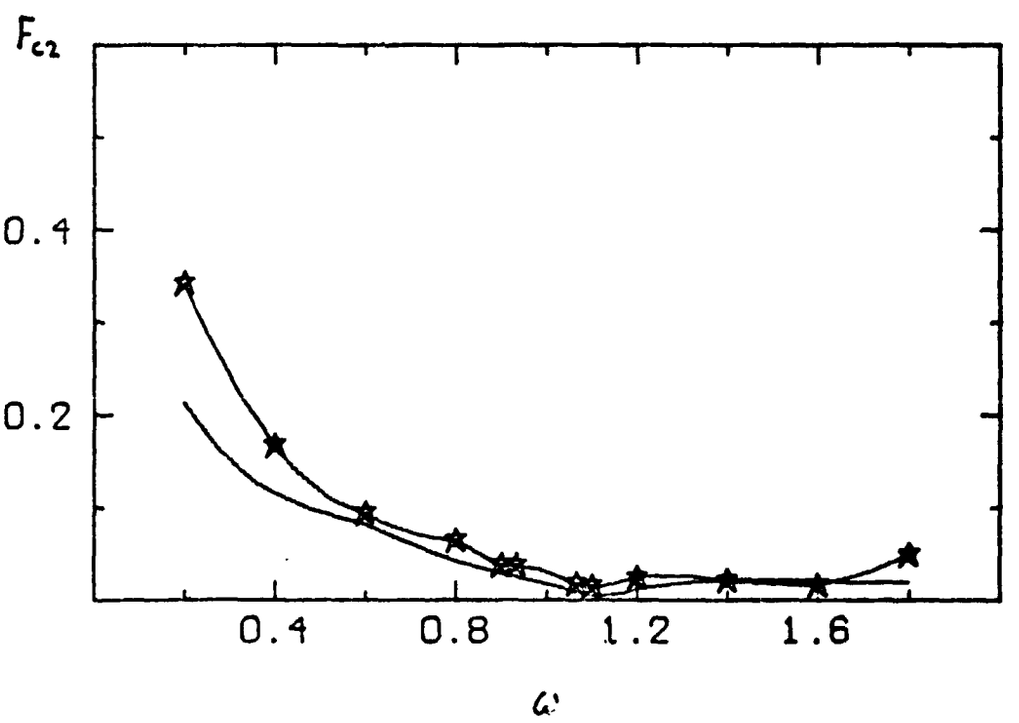

Figure 11f

2 BLADED P=1.10S
θ_0=5° μ=.192

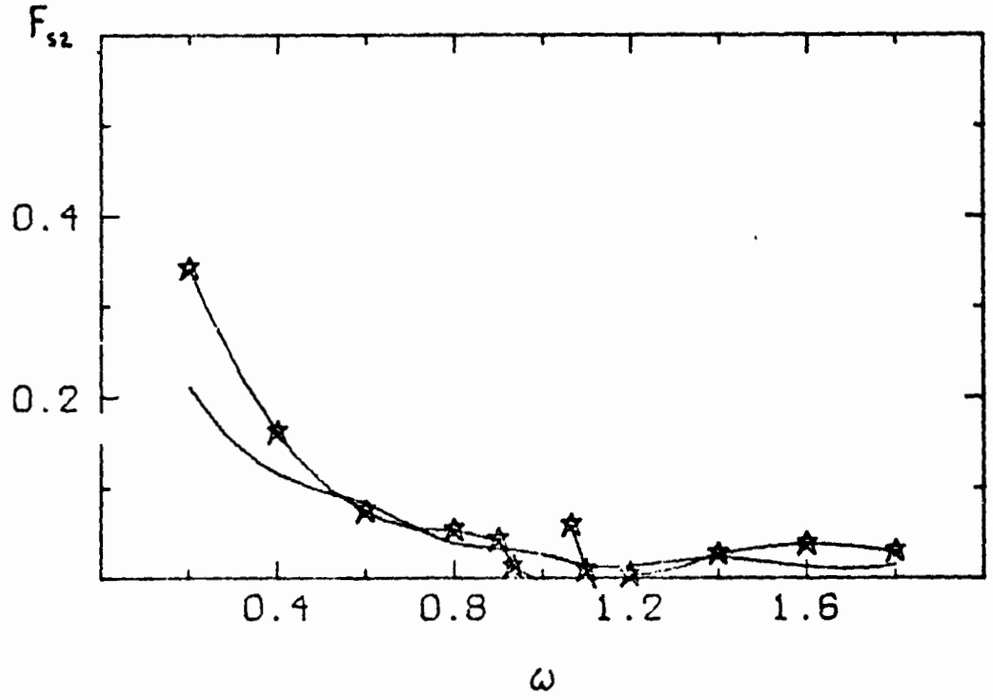

Figure 11g

2 BLADED $\theta_{.5}$=5°, $\theta_{1.5}$=1.5°

P=1.105

μ=.192

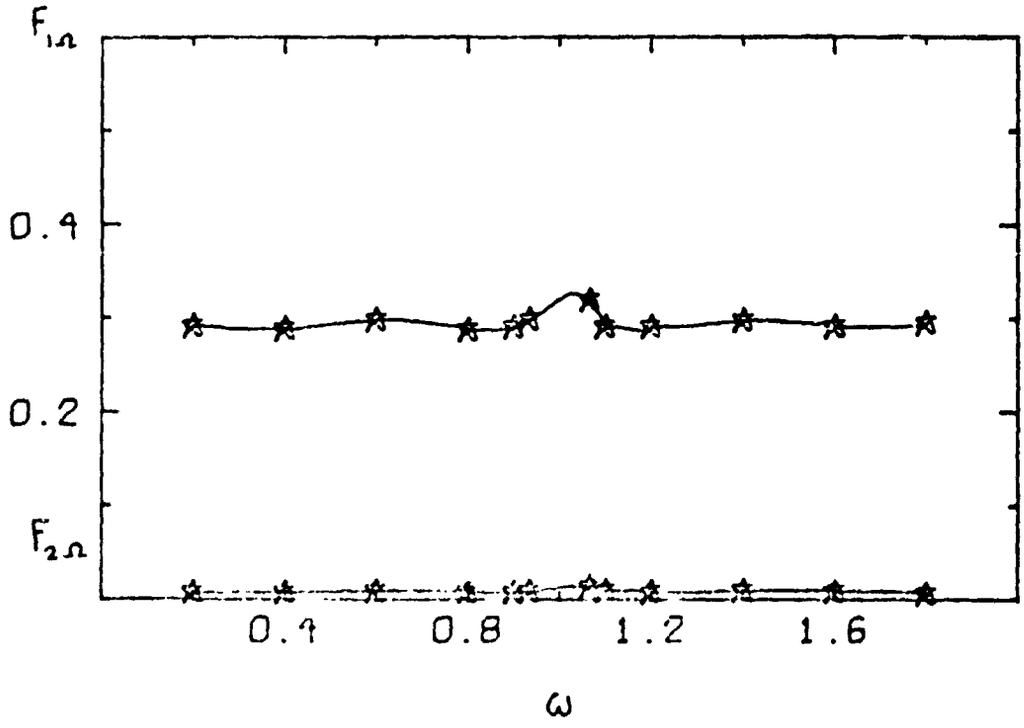

Figure 11h

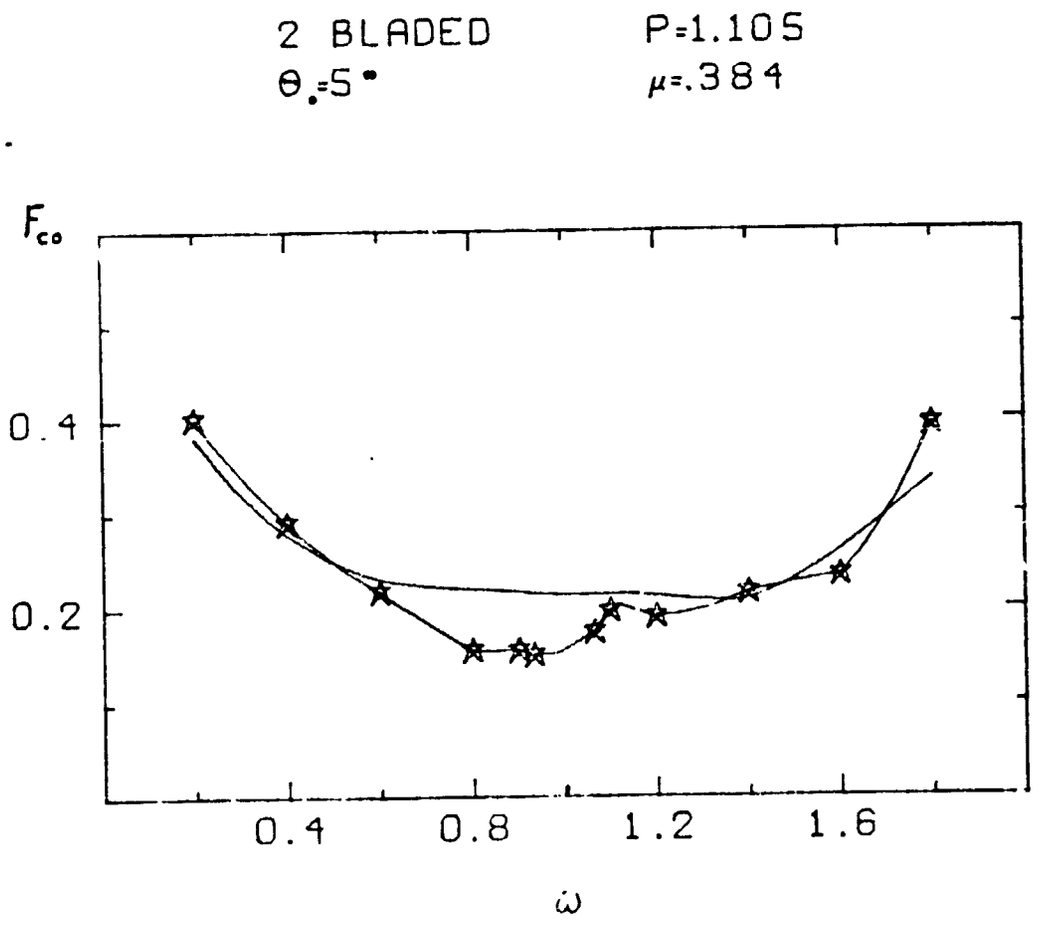

Figure 12a

2 BLADED P=1.105
$\theta_{.75}$=5° μ=.384

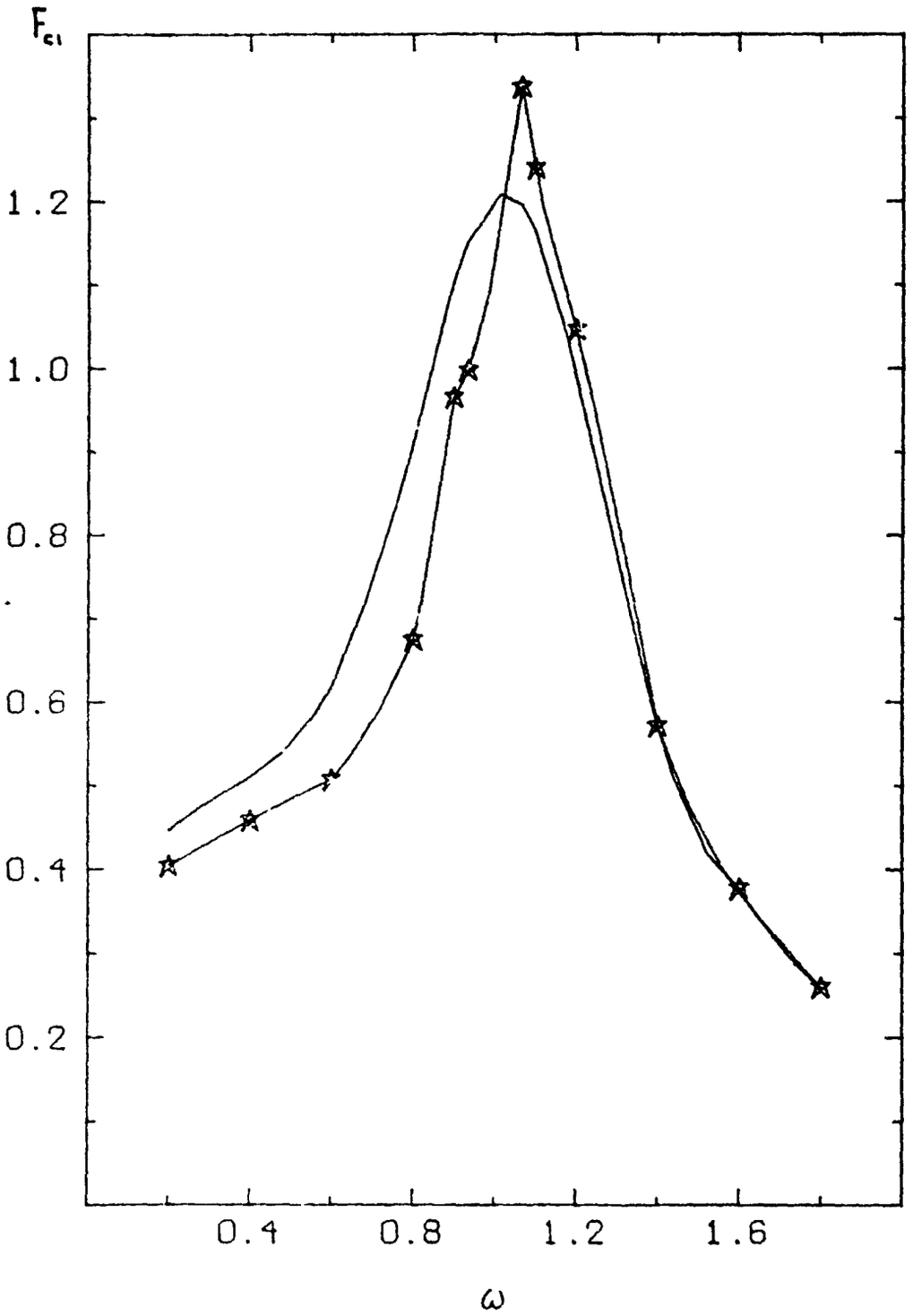

Figure 12b

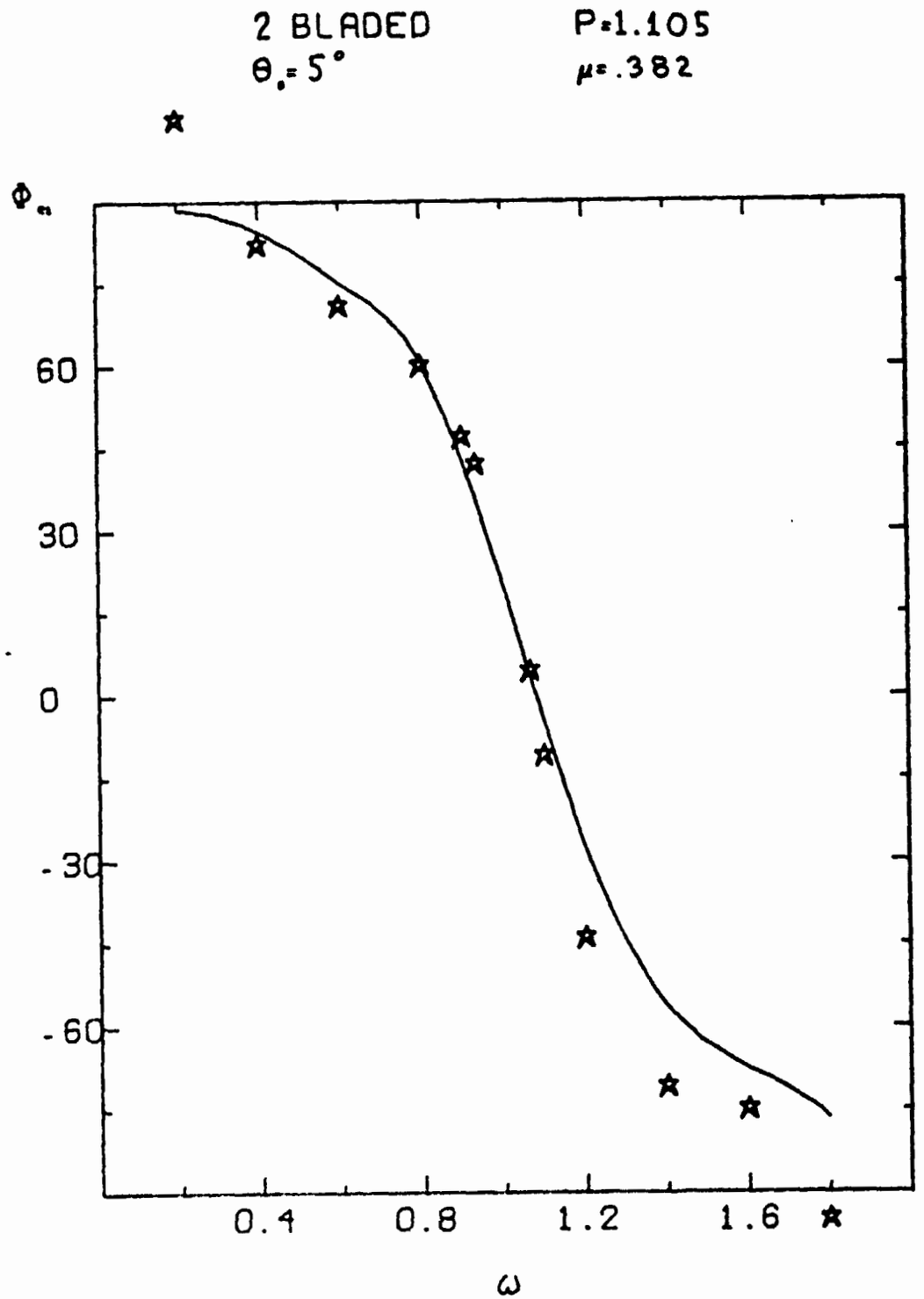
2 BLADED
$\theta_0 = 5°$
P=1.105
μ=.382
Φ_n
60
30
0
-30
-60
0.4
0.8
1.2
1.6
ω

Figure 12c

2 BLADED P=1.105
θ_0=5° μ=.384

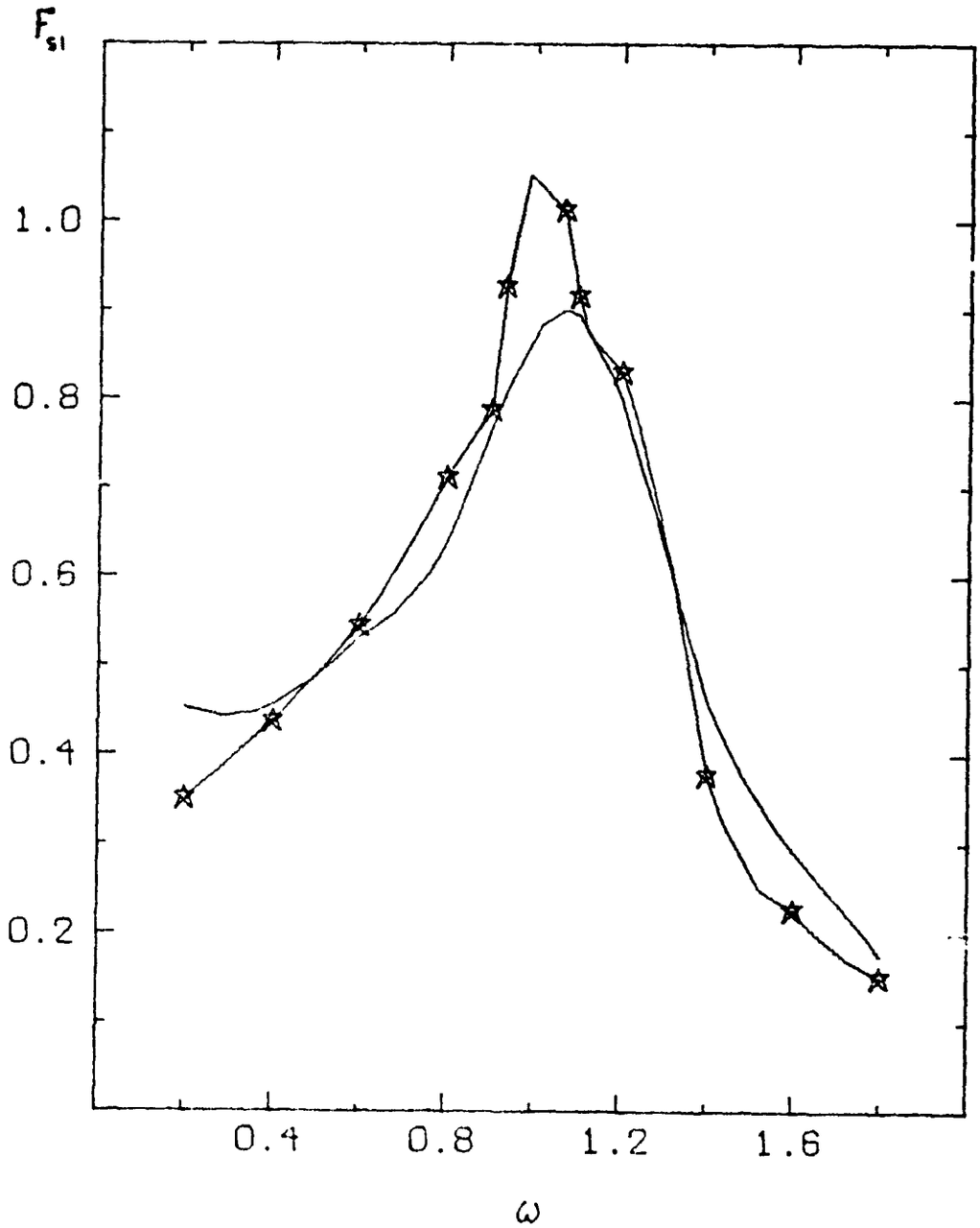

Figure 12d

2 BLADED $\theta_1 = 5°$ $P = 1.105$ $\mu = .382$

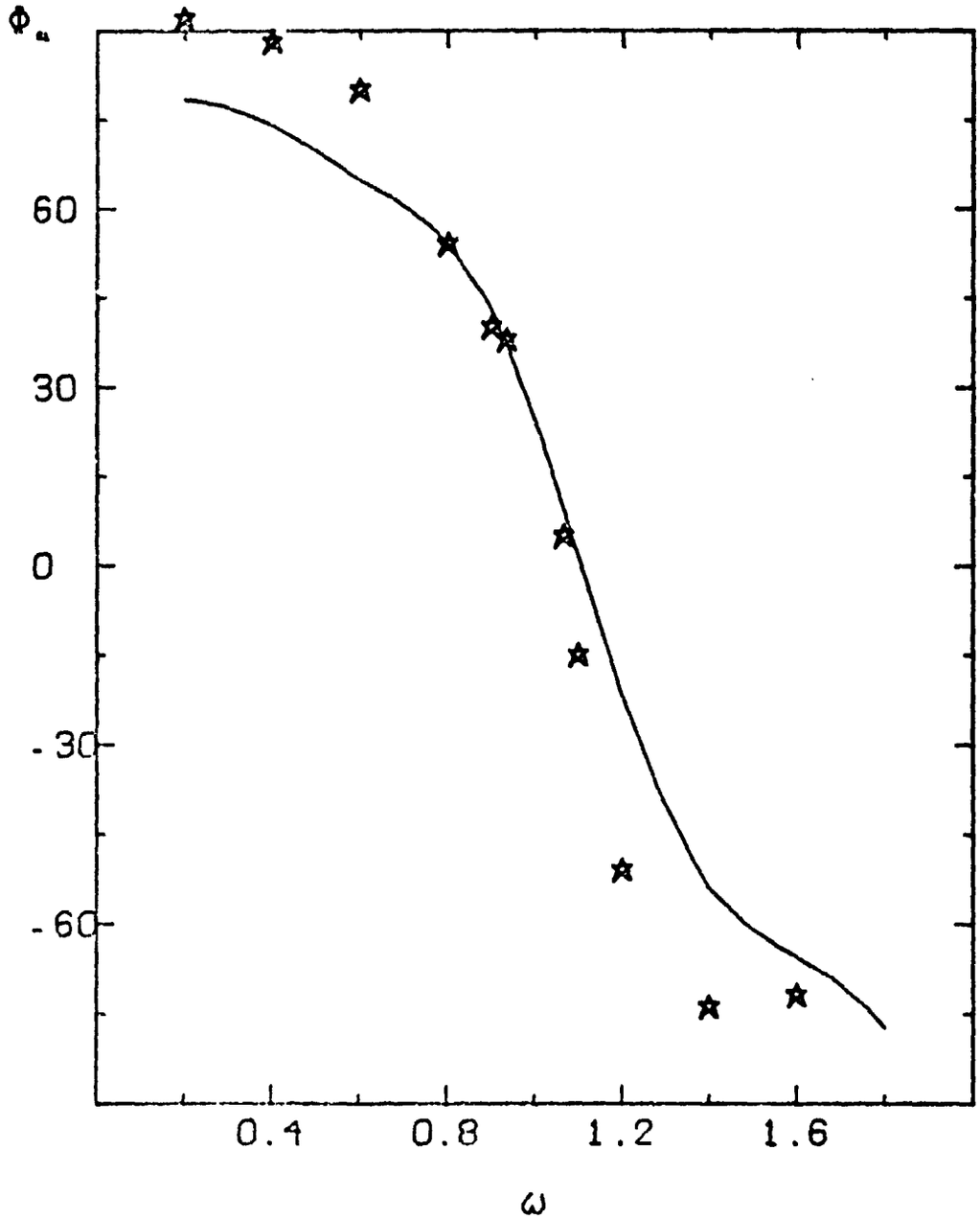

Figure 12e

2 BLADED P=1.10S
$\theta_{.75}$=5° μ=.384

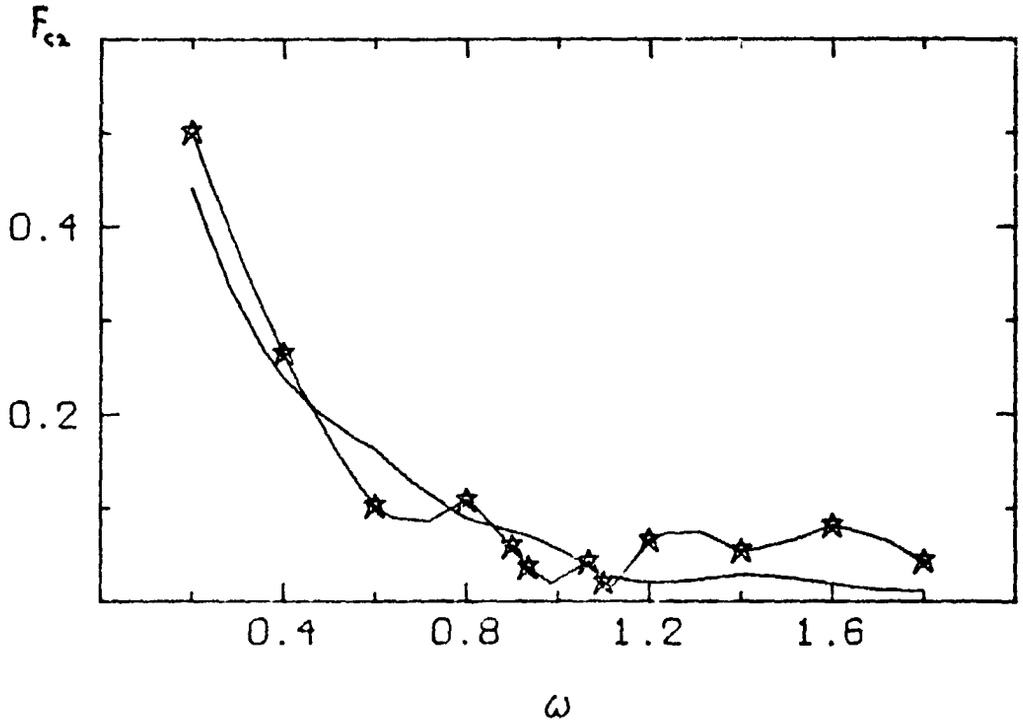

Figure 12f

2 BLADED P=1.105
θ_o=5° μ=.384

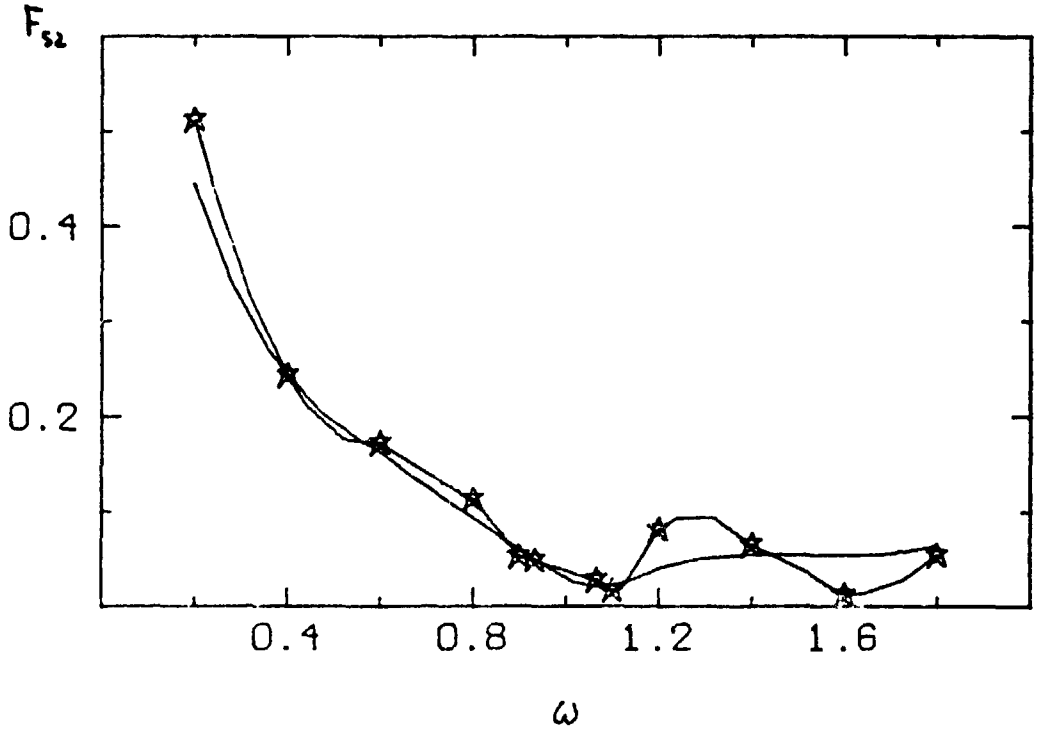

Figure 12g

2 BLADED P=1.105
θ_1=5°, θ_2=1.5° μ=.384

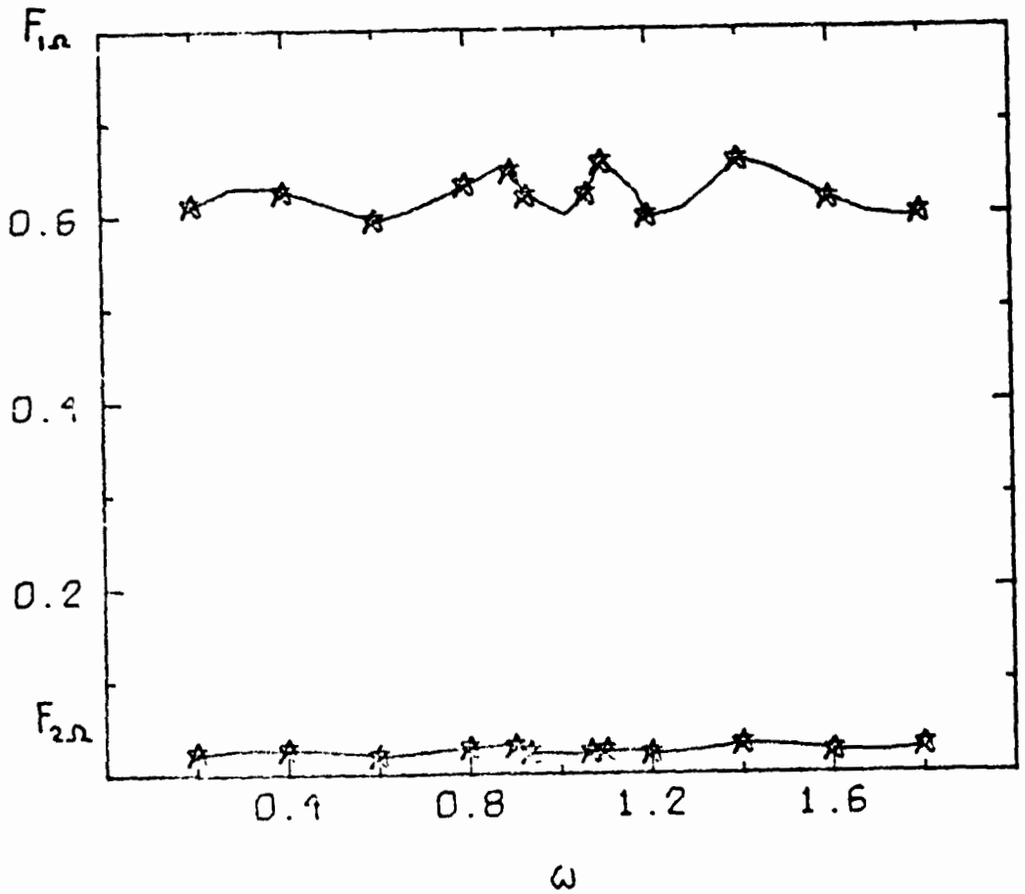

Figure 12h

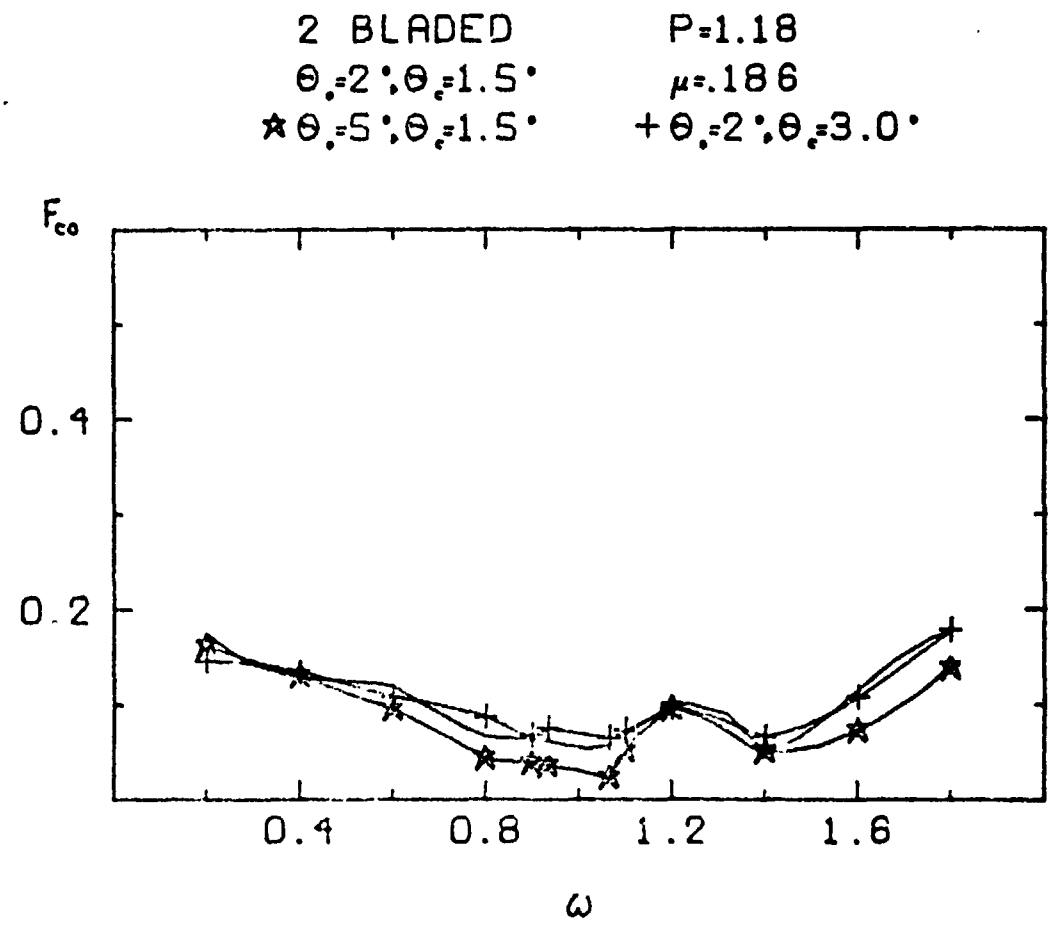

Figure 13a

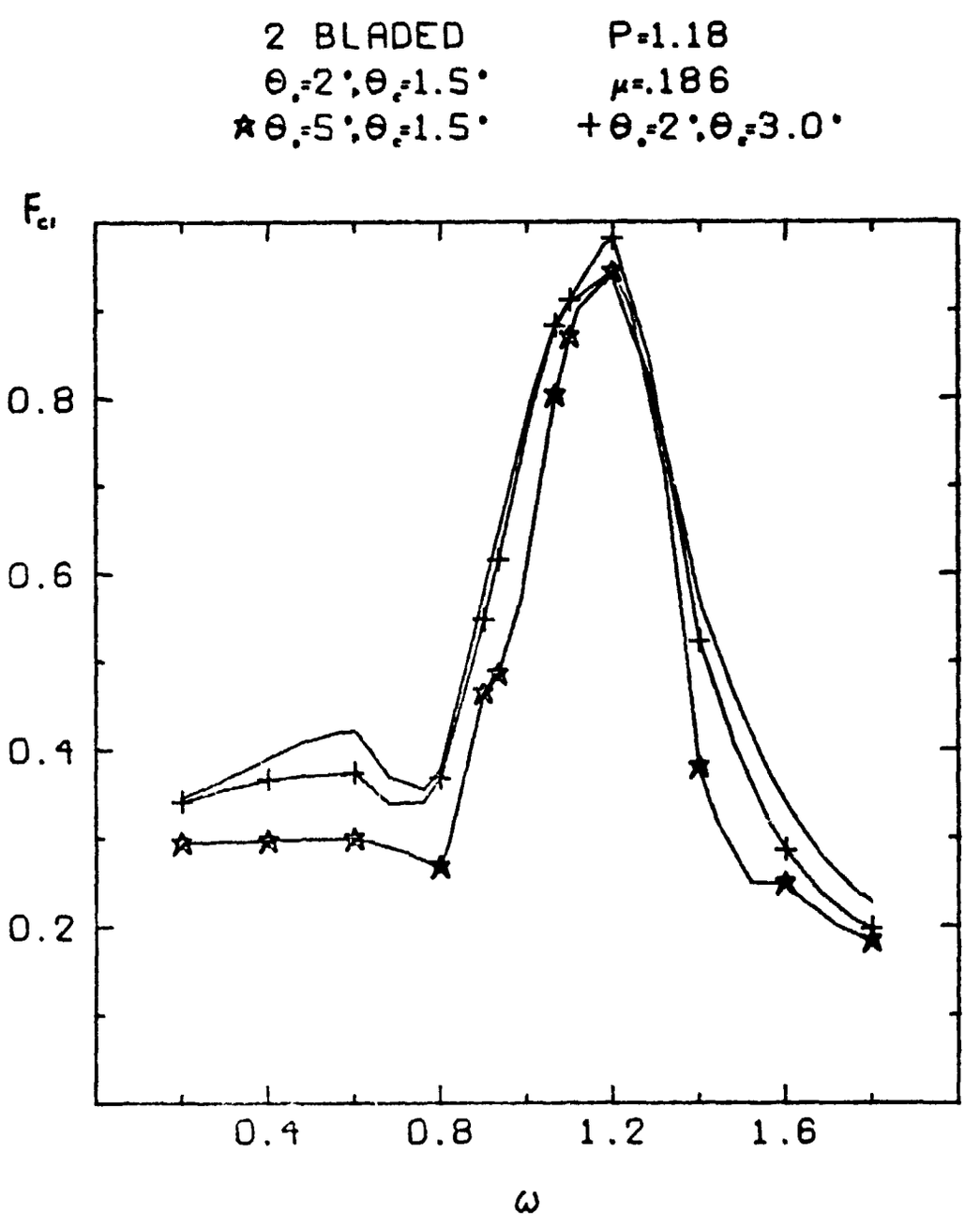
2 BLADED
θ_o=2°,θ_c=1.5°
★ θ_o=5°,θ_c=1.5°
P=1.18
μ=.186
+ θ_o=2°,θ_c=3.0°
F_{c_1}
0.8
0.6
0.4
0.2
0.4
0.8
1.2
1.6
ω

Figure 13b

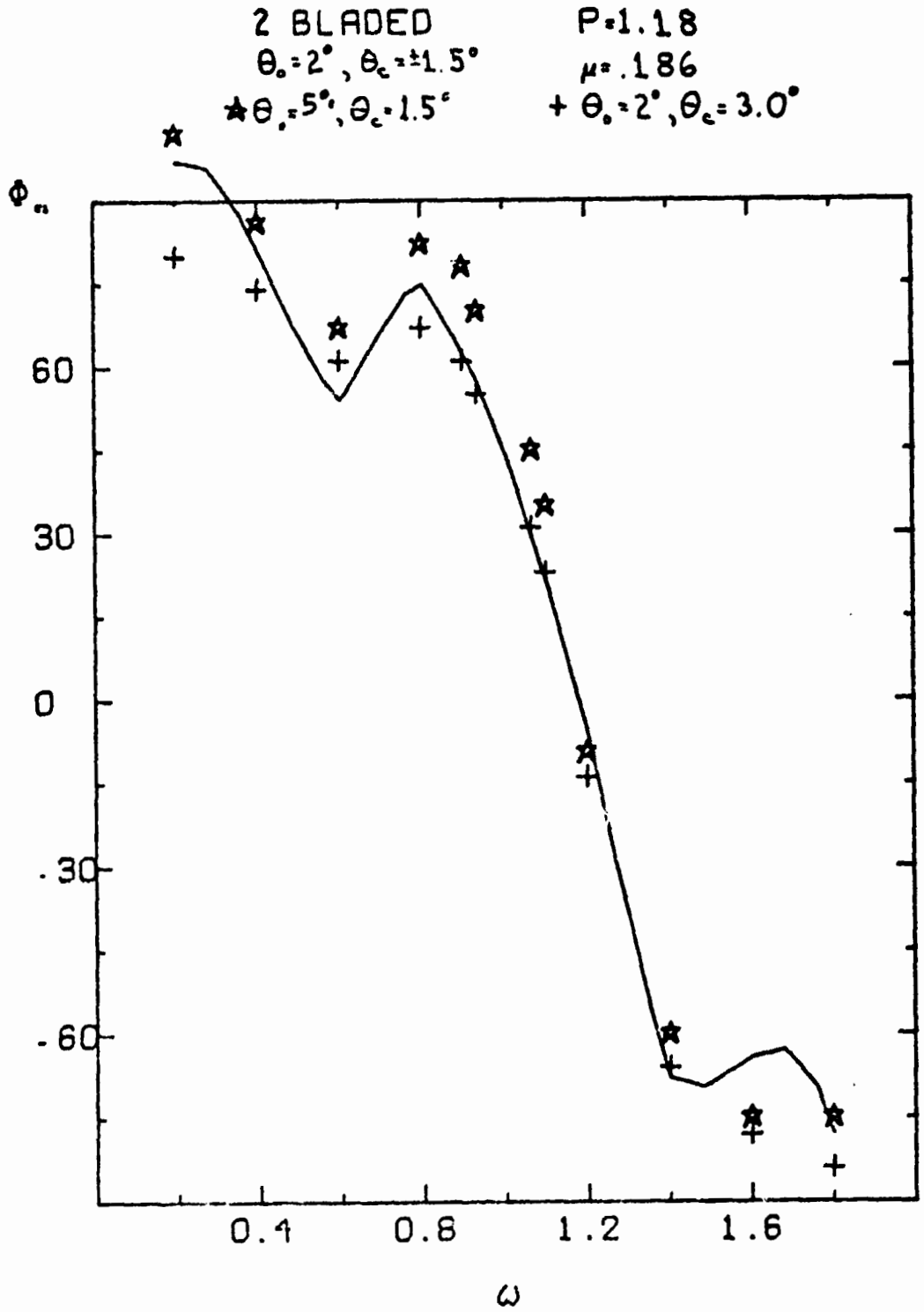
2 BLADED
$\theta_o = 2°, \theta_c = \pm 1.5°$
$\star\ \theta_o = 5°, \theta_c = 1.5°$
P=1.18
$\mu = .186$
$+\ \theta_o = 2°, \theta_c = 3.0°$
Φ_n
60
30
0
-30
-60
0.4
0.8
1.2
1.6
ω

Figure 13c

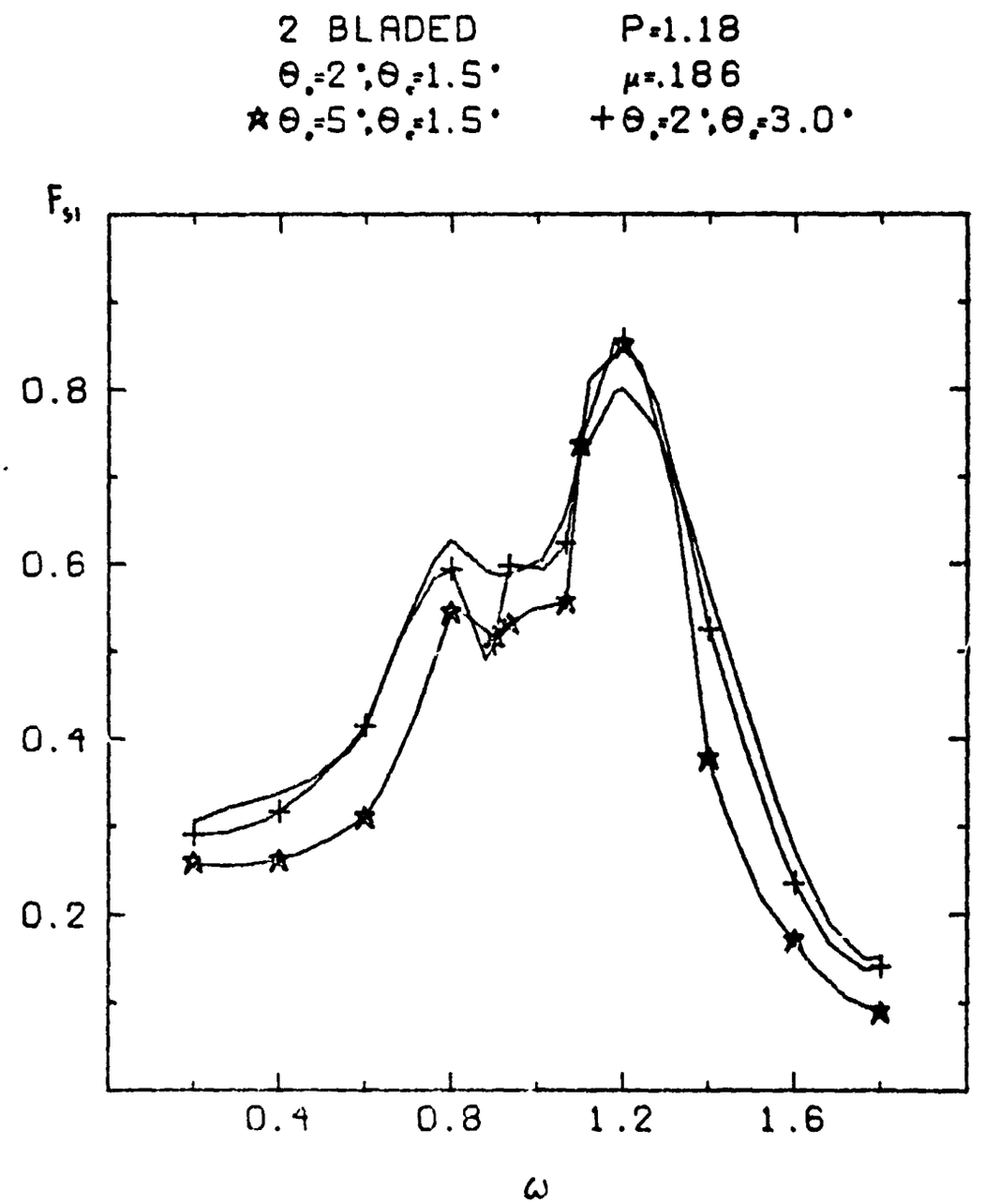
2 BLADED
P=1.18
θ.=2°,θ₁=1.5°
μ=.186
★θ.=5°,θ₁=1.5°
+θ.=2°,θ₁=3.0°
F₅₁
0.8
0.6
0.4
0.2
0.4
0.8
1.2
1.6
ω

Figure 13d

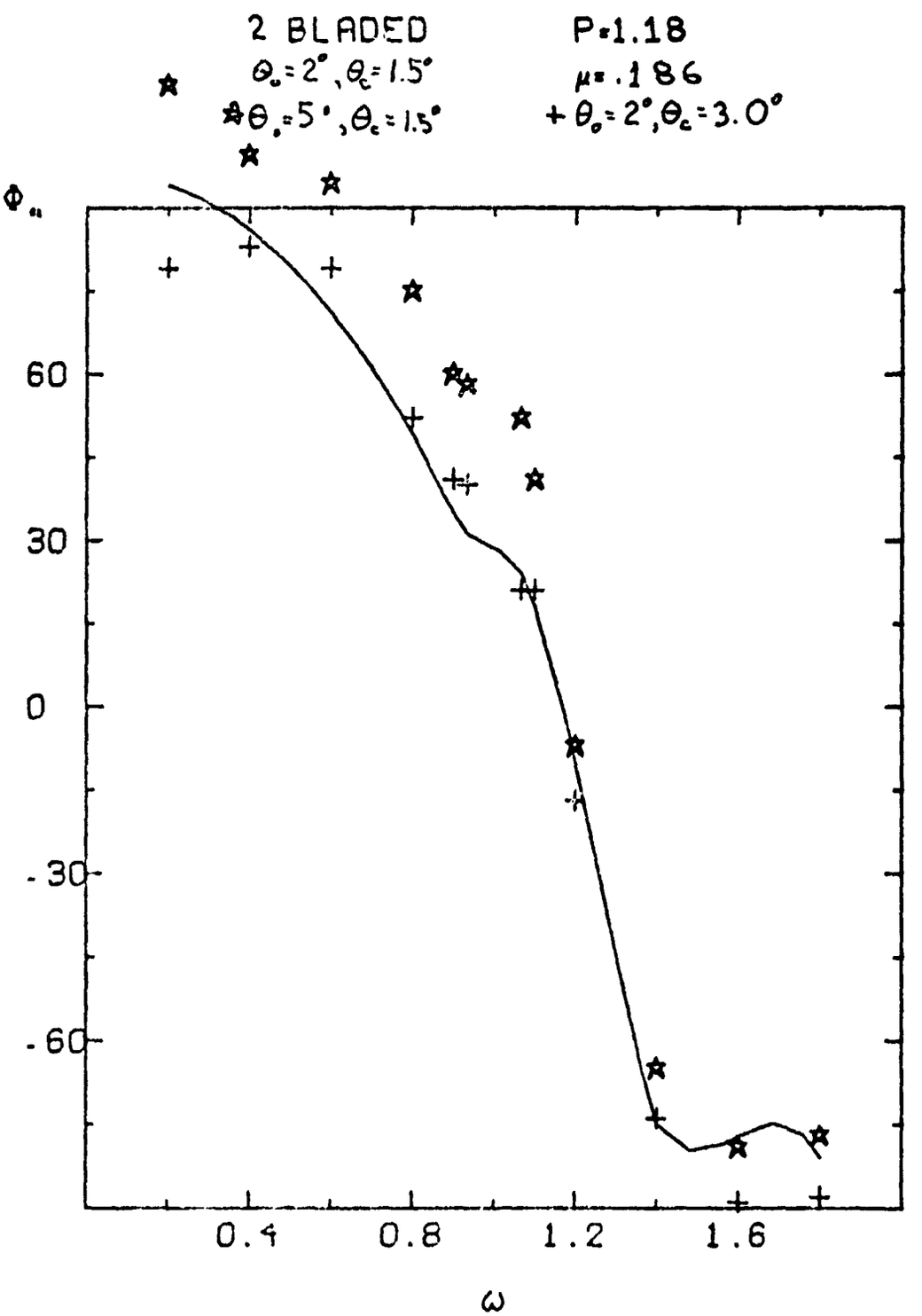
2 BLADED
$\theta_o = 2°, \theta_c = 1.5°$
$\theta_o = 5°, \theta_c = 1.5°$
P=1.18
$\mu = .186$
$\theta_o = 2°, \theta_c = 3.0°$
Φ_{1s}
60
30
0
-30
-60
0.4
0.8
1.2
1.6
ω

Figure 13e

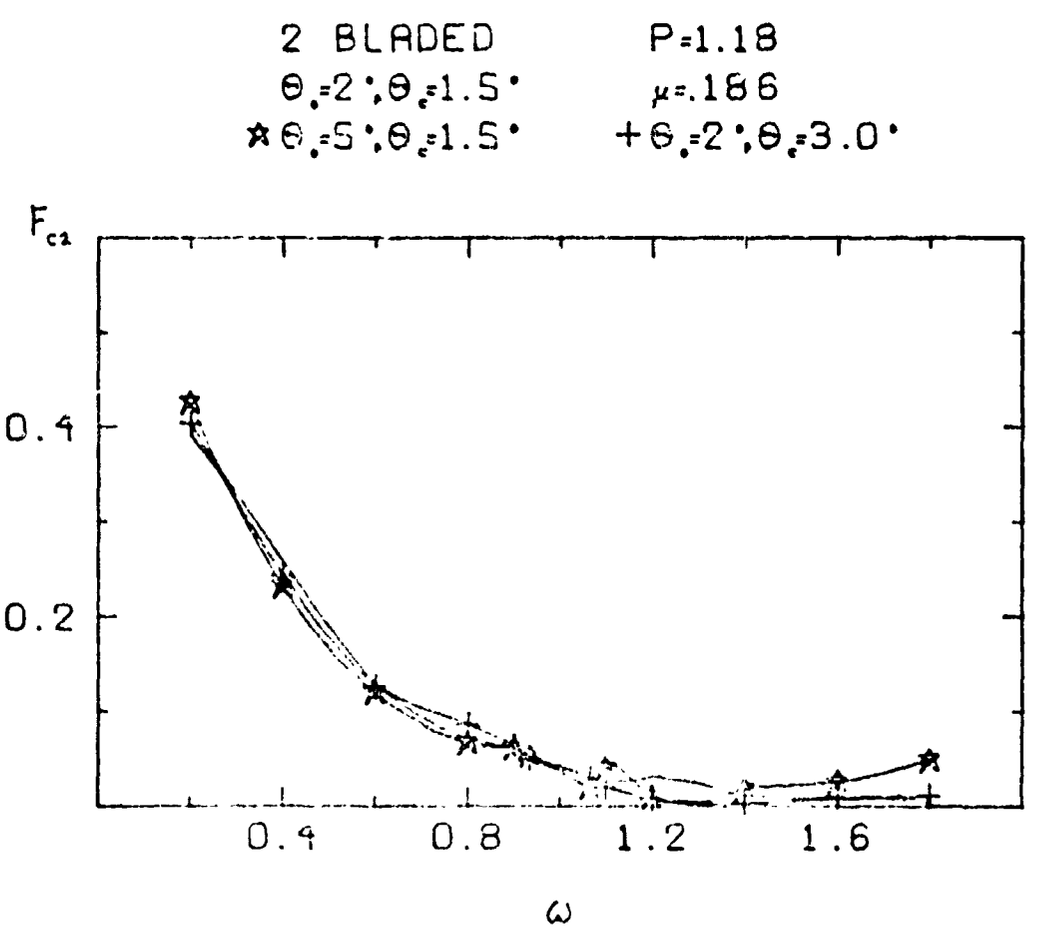
2 BLADED
θ_0=2°,θ_c=1.5°
☆θ_0=5°,θ_c=1.5°
P=1.18
μ=.186
+θ_0=2°,θ_c=3.0°
F_{c_2}
0.4
0.2
0.4
0.8
1.2
1.6
ω

Figure 13f

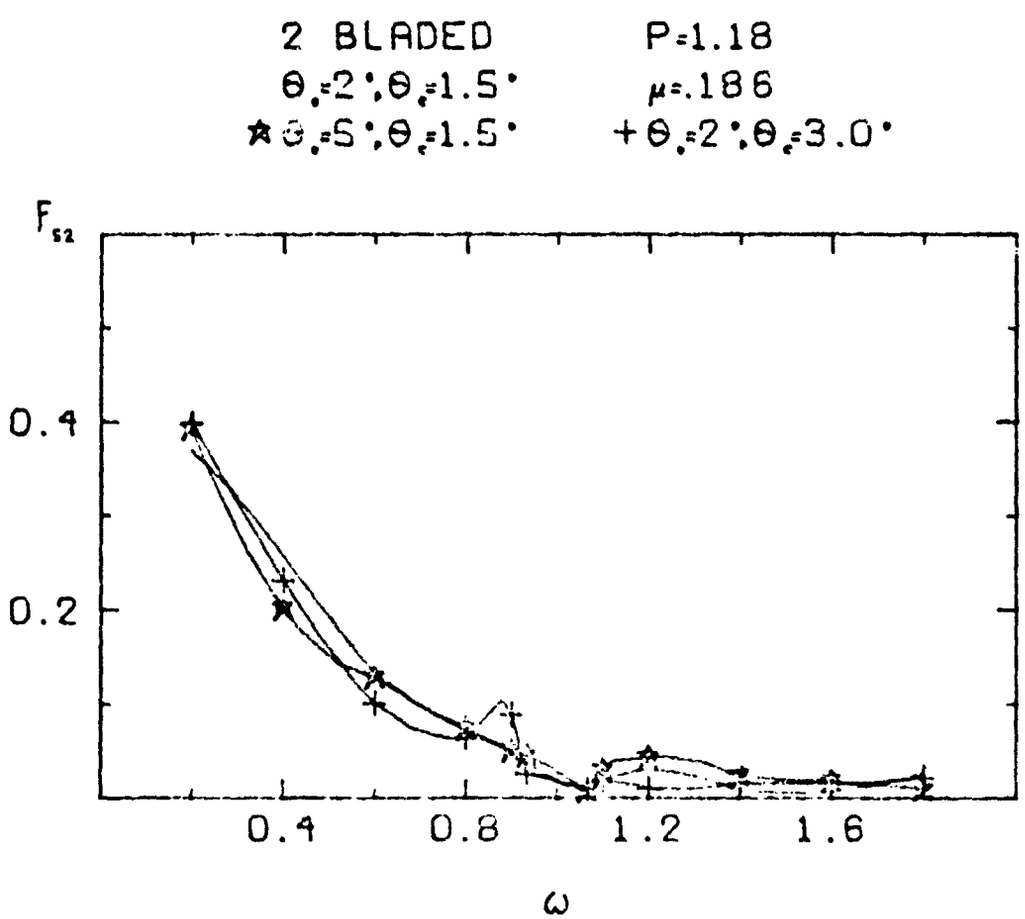
2 BLADED
P=1.18
θ₀=2°, θ₁=1.5°
μ=.186
★ θ₀=5°, θ₁=1.5°
+ θ₀=2°, θ₁=3.0°
F_s2
0.4
0.2
0.4
0.8
1.2
1.6
ω

Figure 13g

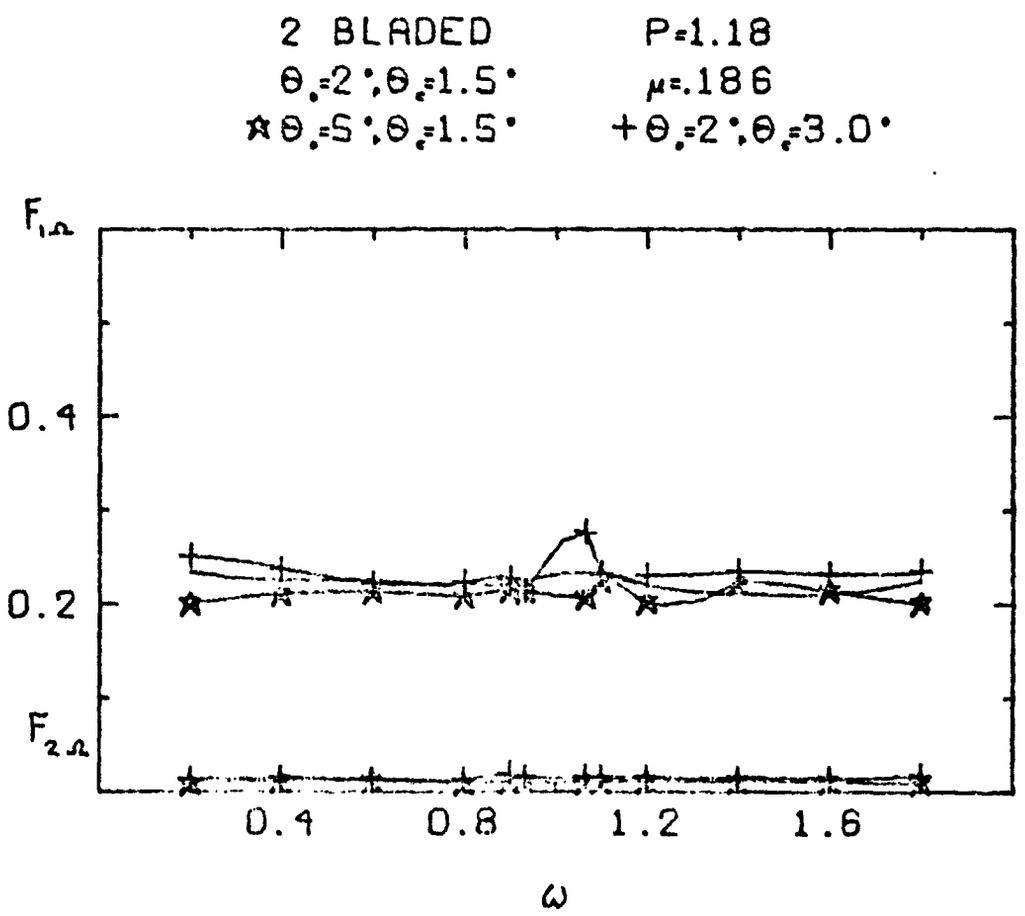

Figure 13h

C-2

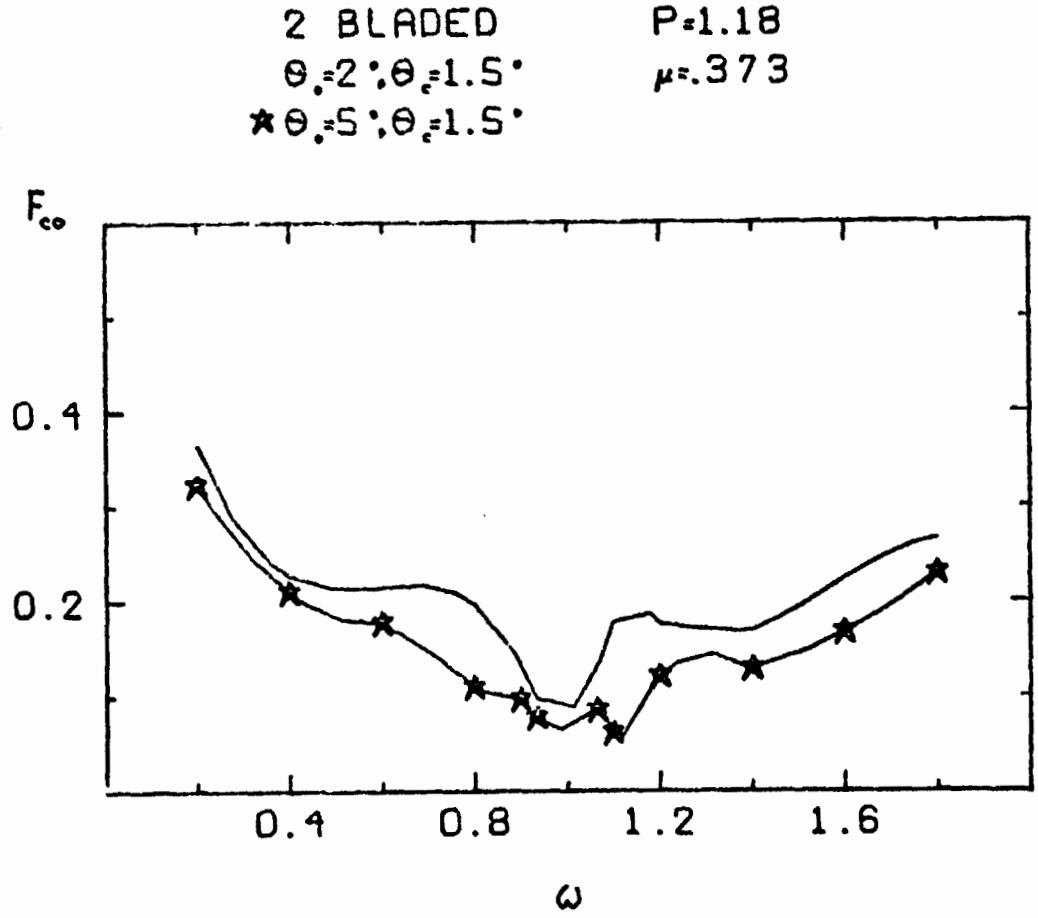

Figure 14a

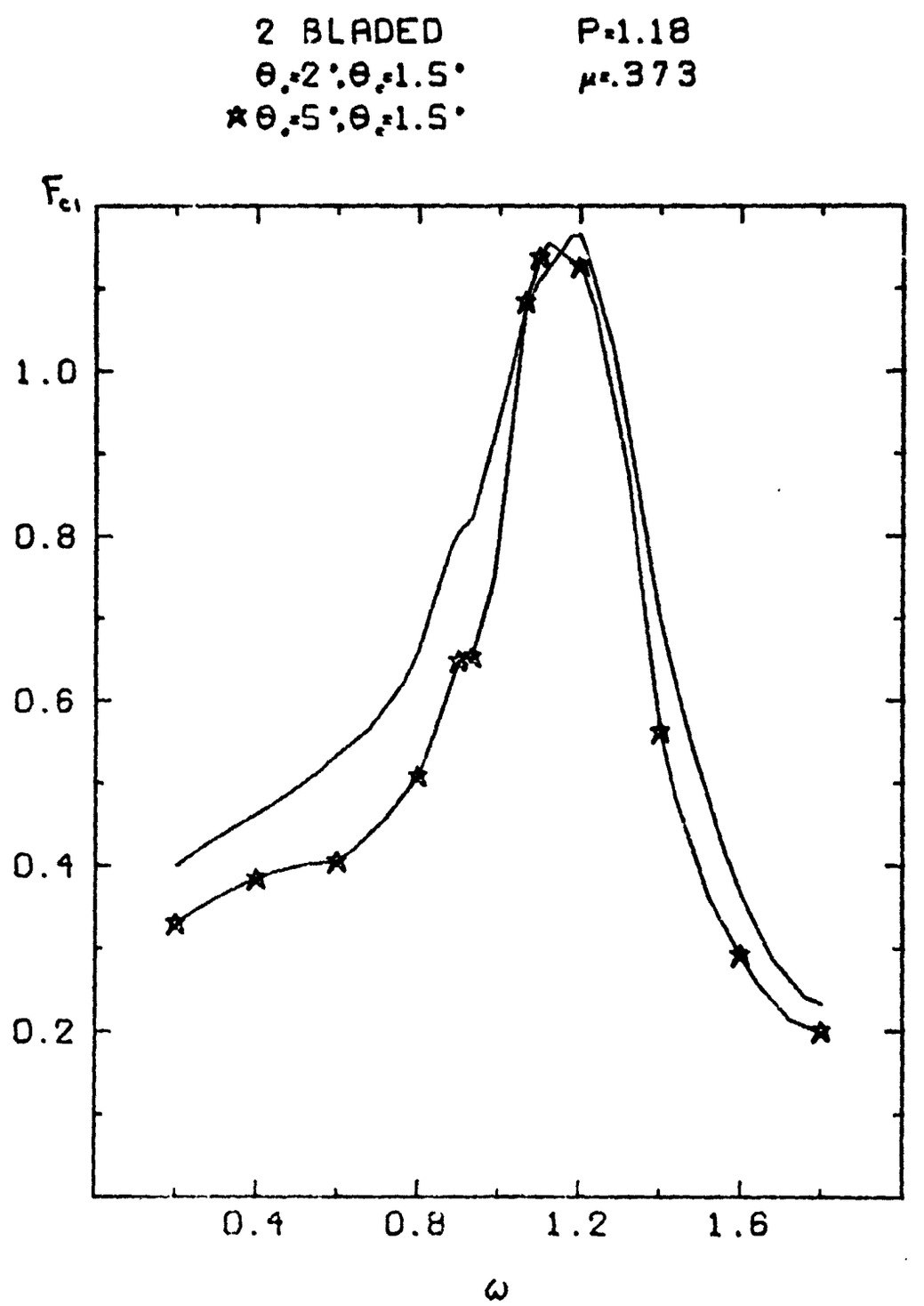
2 BLADED
P=1.18
θ₀=2°, θ₁=1.5°
μ=.373
★ θ₀=5°, θ₁=1.5°
F_c1
1.0
0.8
0.6
0.4
0.2
0.4
0.8
1.2
1.6
ω

Figure 14b

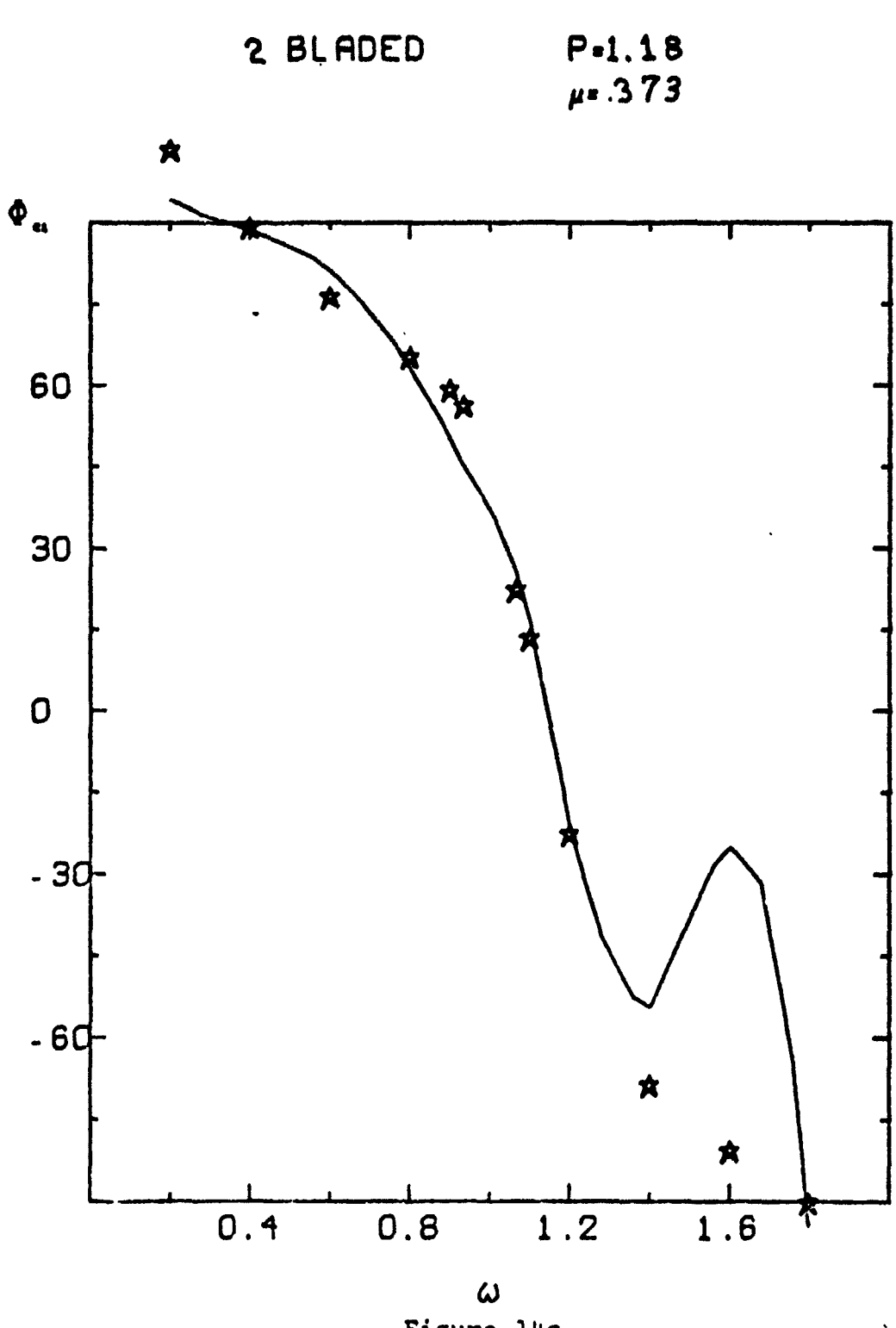

Figure 14c

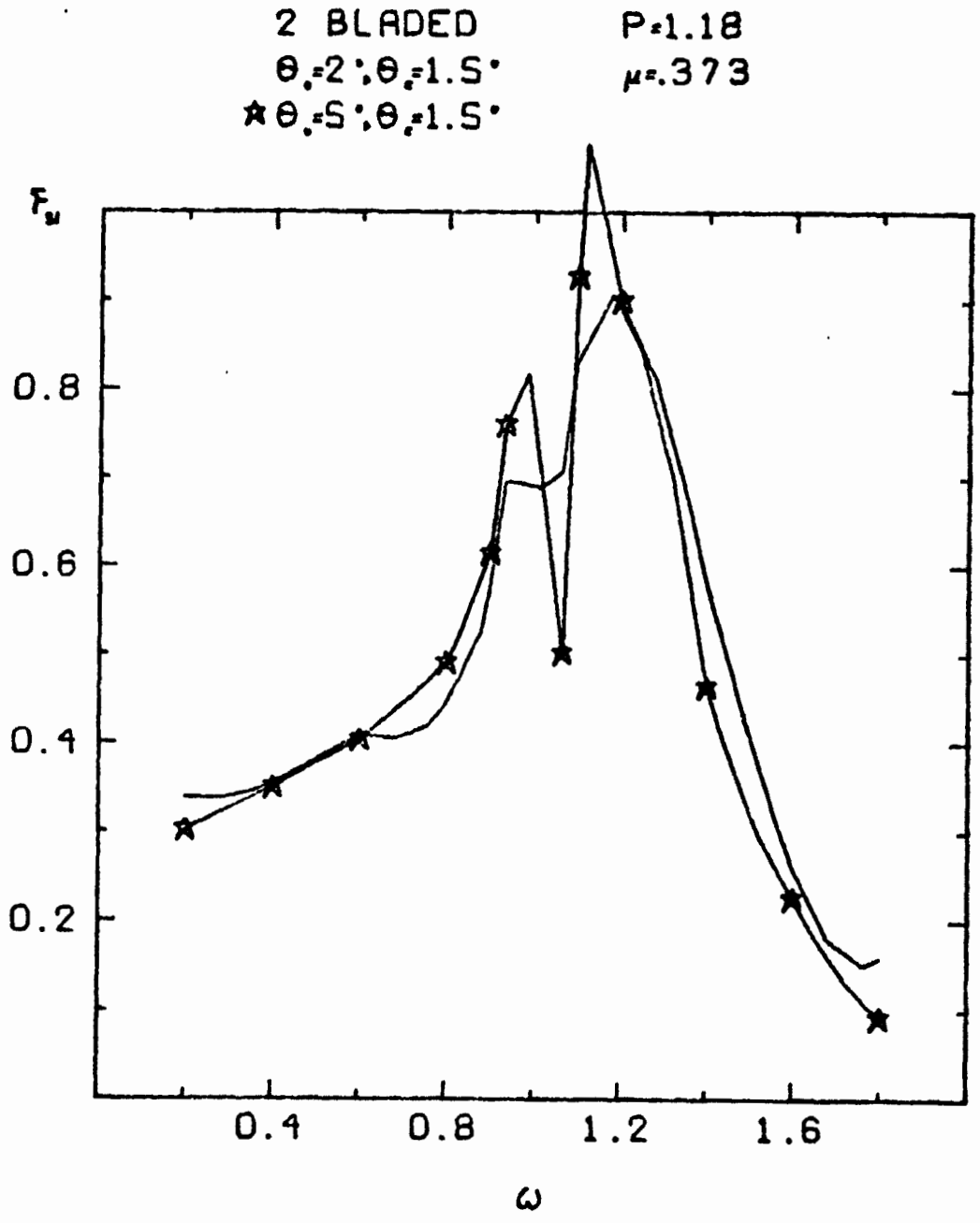

Figure 14d

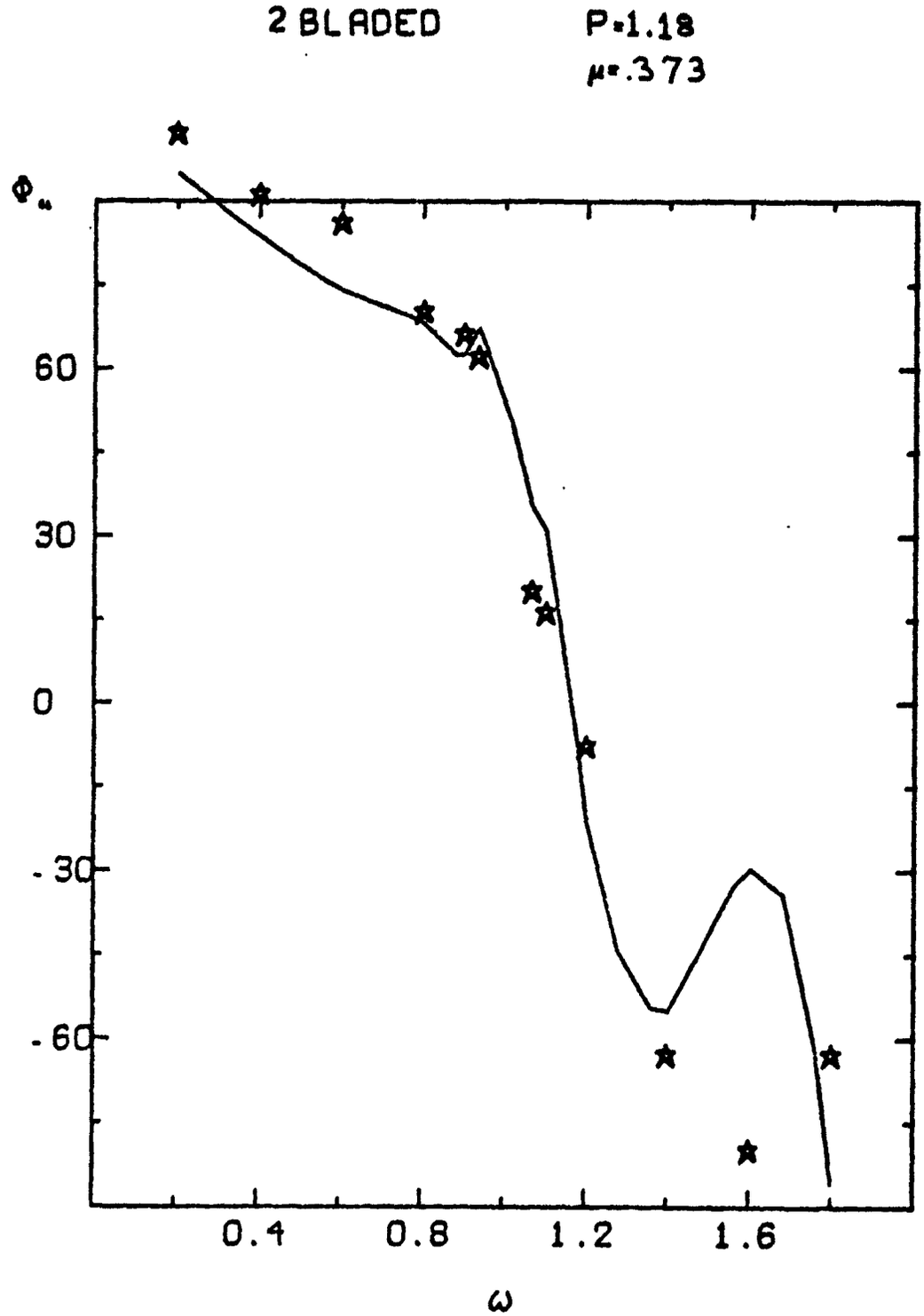

Figure 14e

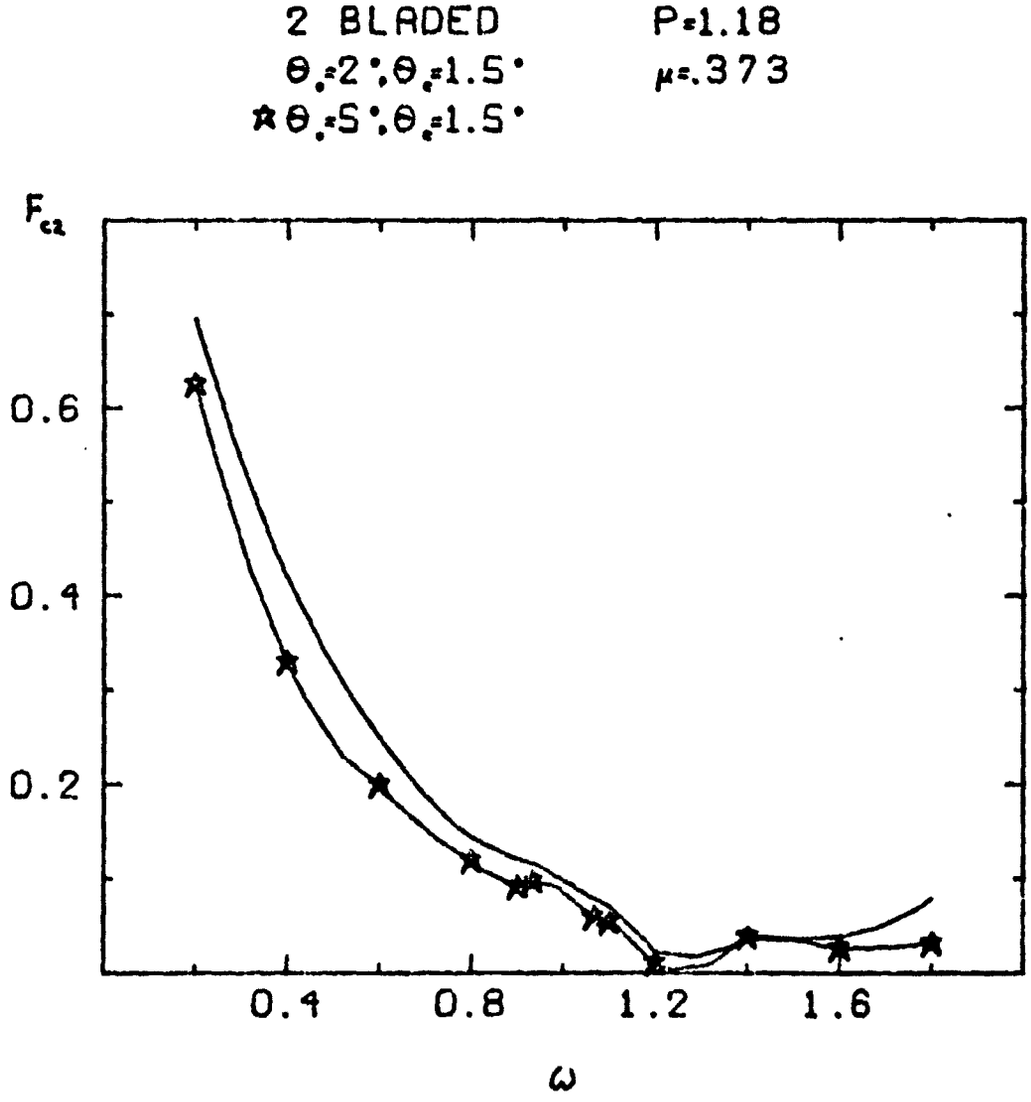
2 BLADED
θ_0=2°,θ_c=1.5°
★ θ_0=5°,θ_c=1.5°
P=1.18
μ=.373
F_{c_2}
0.6
0.4
0.2
0.4
0.8
1.2
1.6
ω

Figure 14f

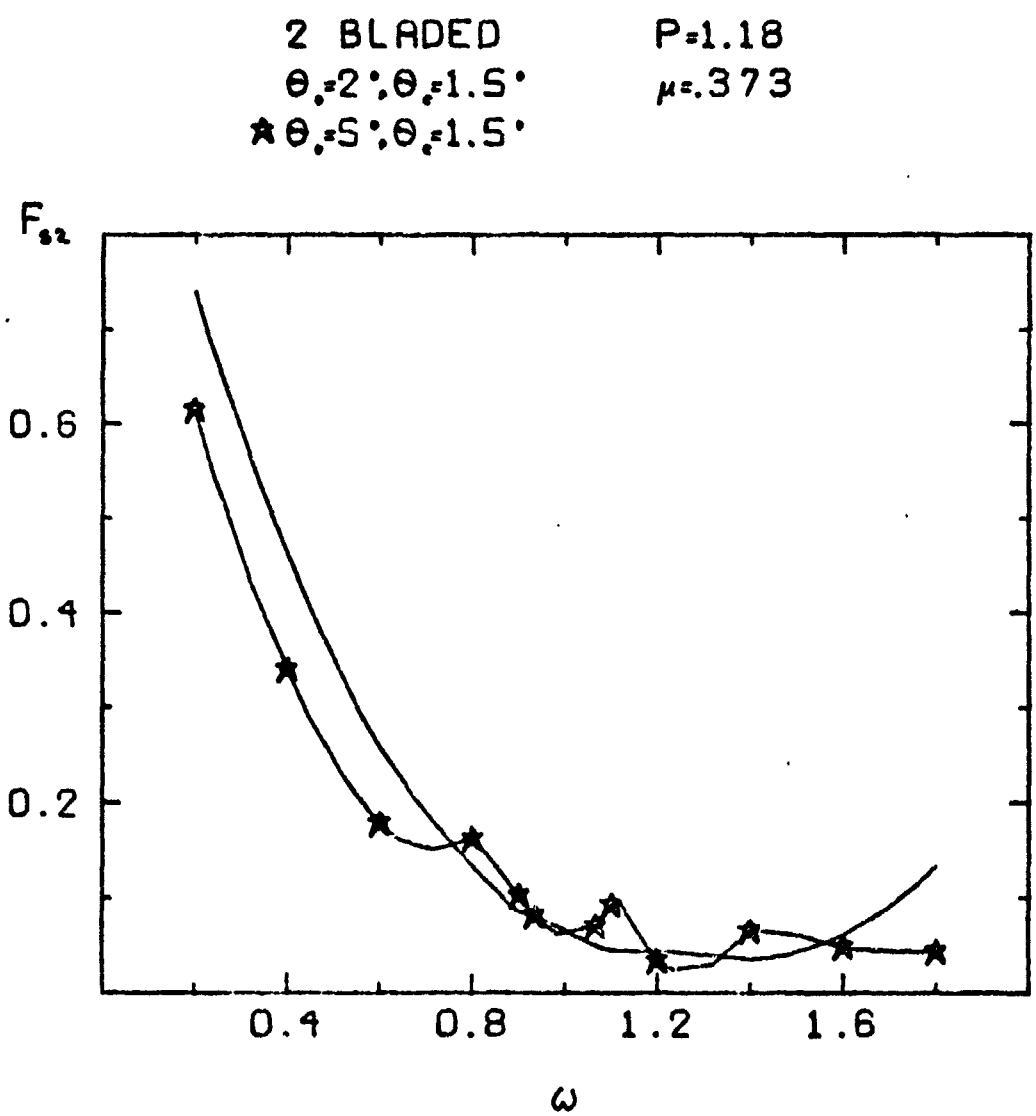
2 BLADED
θ_0=2°, θ_c=1.5°
★ θ_0=5°, θ_c=1.5°
P=1.18
μ=.373
F_{s2}
0.6
0.4
0.2
0.4
0.8
1.2
1.6
ω

Figure 14g

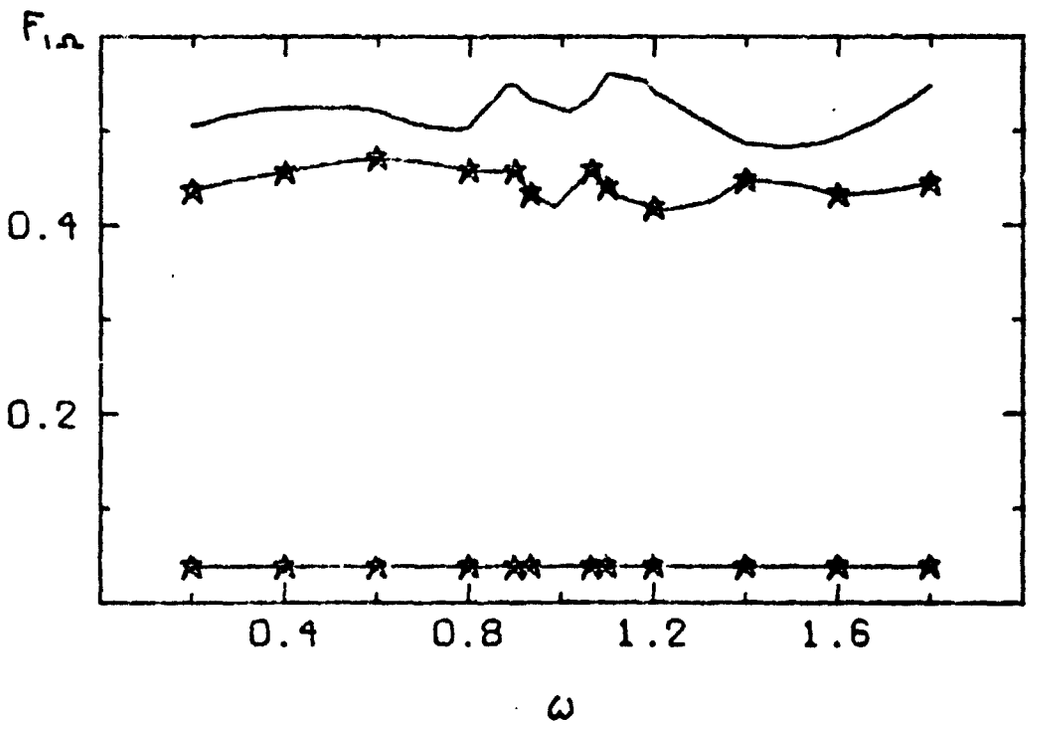

Figure 14h

2 BLADED $\quad P=1.18$

$\theta_0=2°, \theta_c=1.5°$ $\quad \mu=.555$

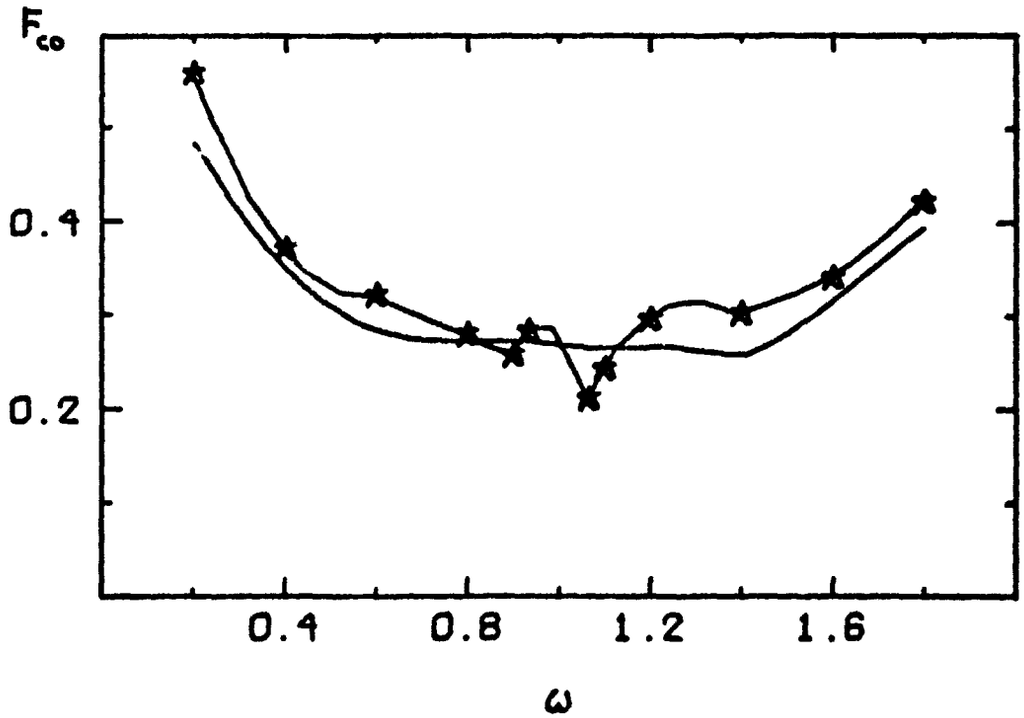

Figure 15a

2 BLADED P=1.18
θ_o=2°,θ_c=1.5° μ=.555

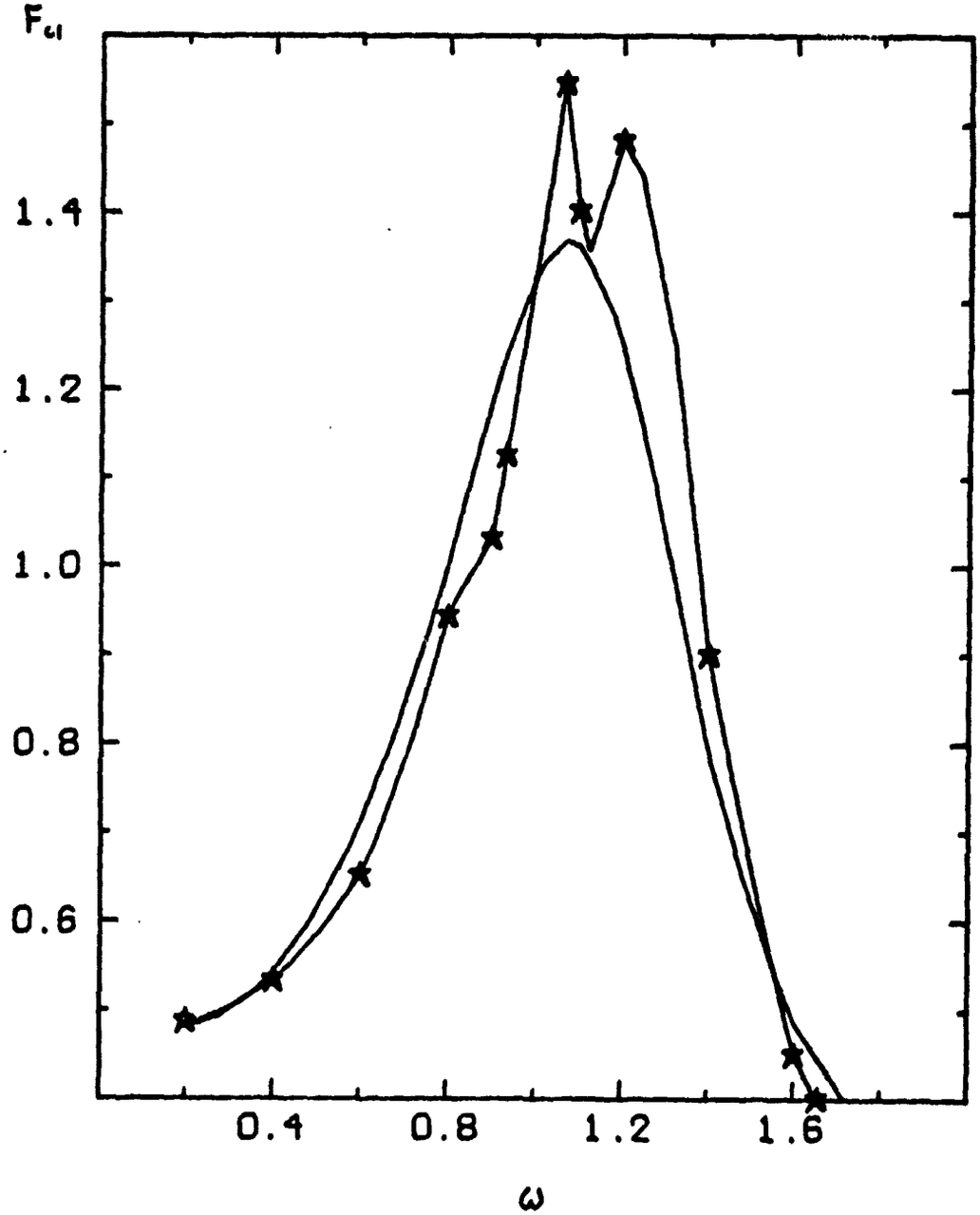

Figure 15b

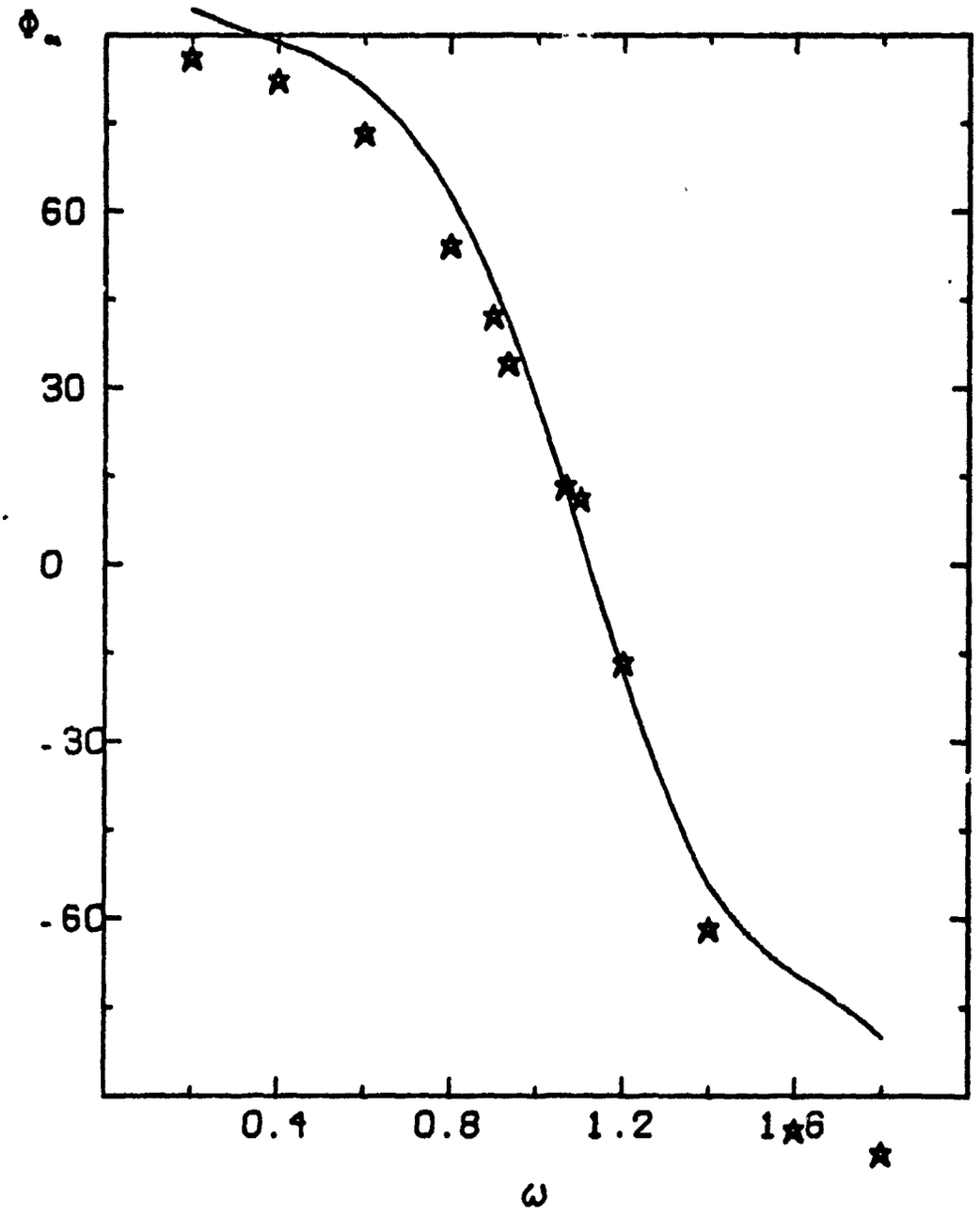

Figure 15c

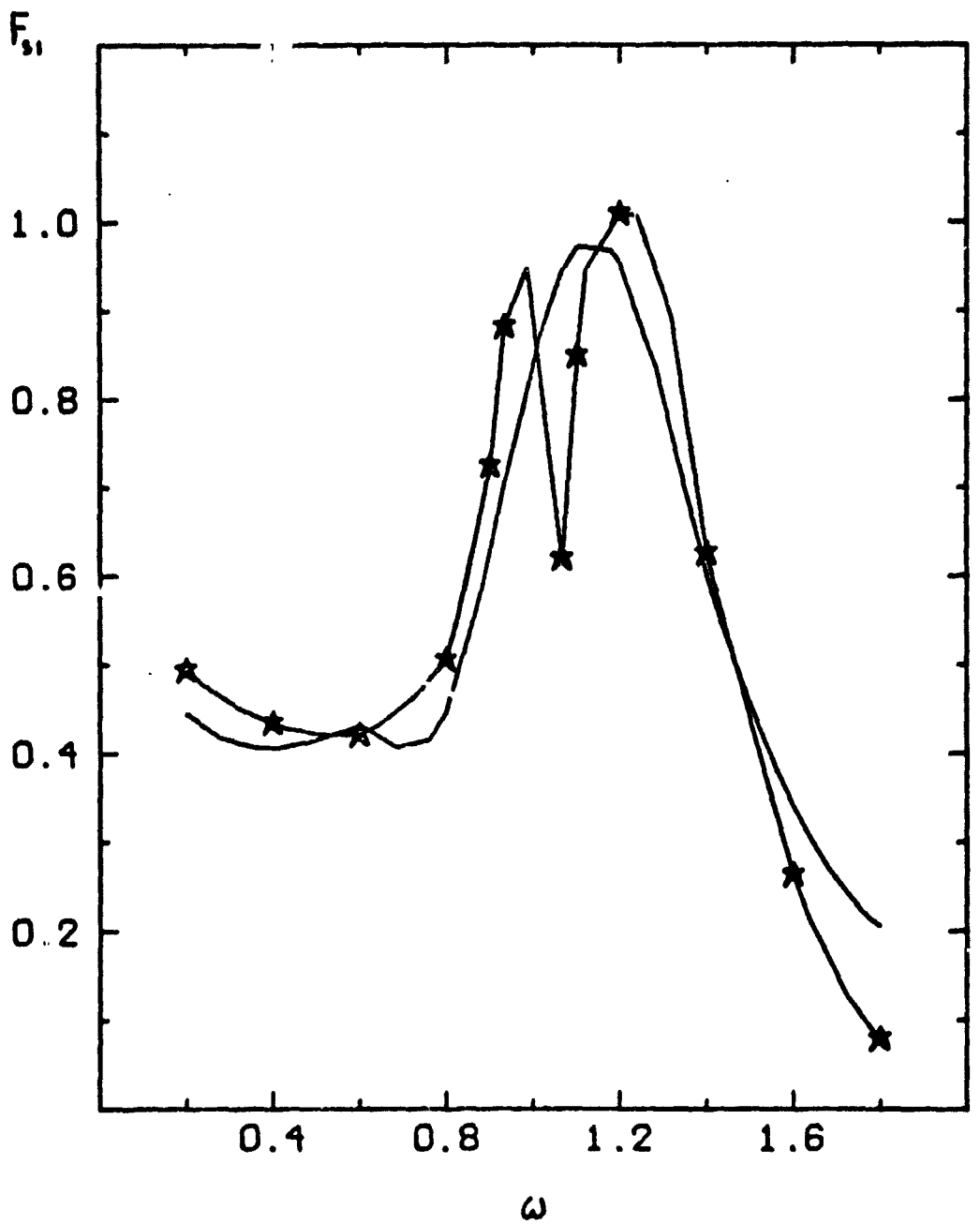

Figure 15d

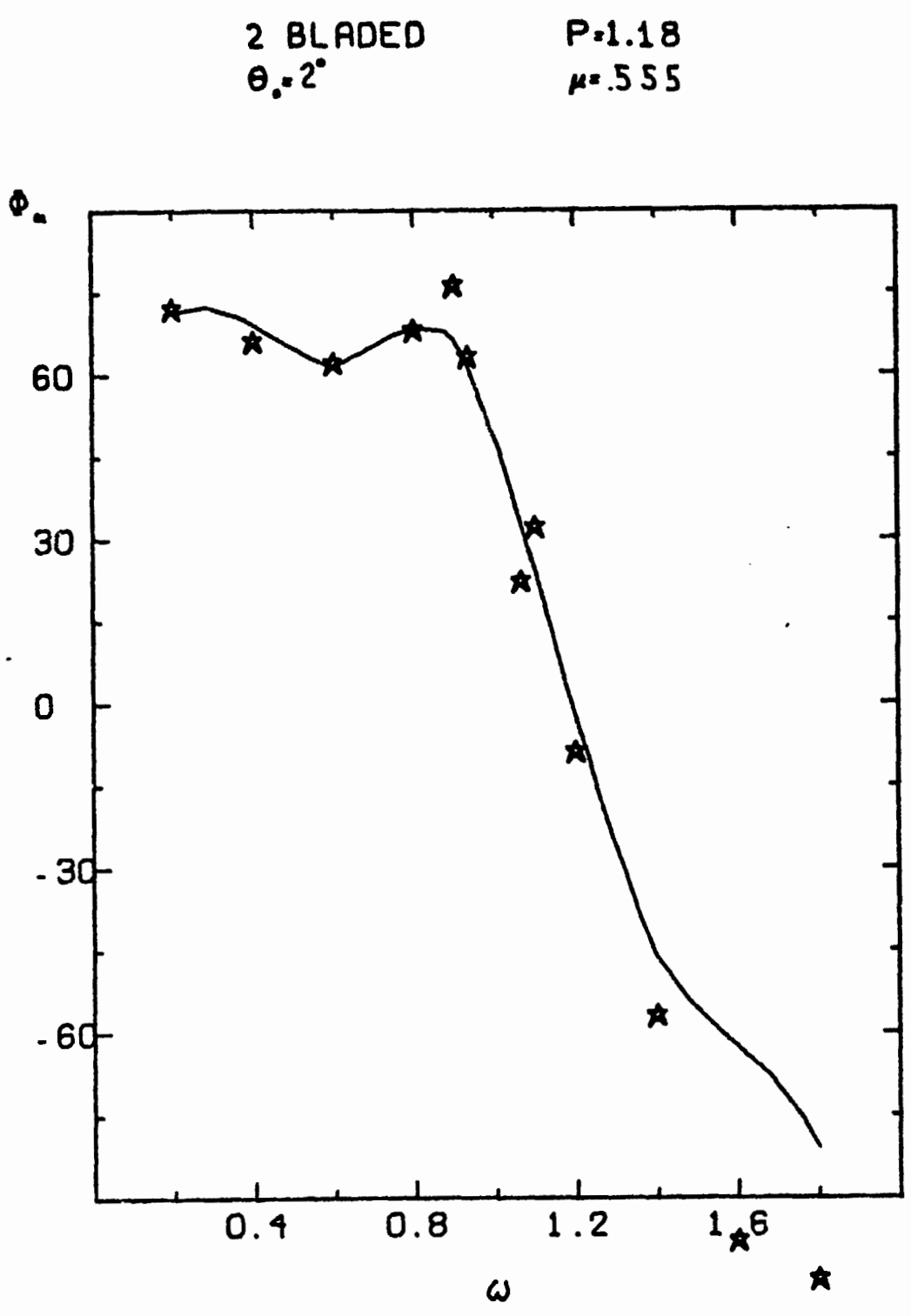

Figure 15e

2 BLADED $\theta_0=2°, \theta_c=1.5°$ $P=1.18$ $\mu=.555$

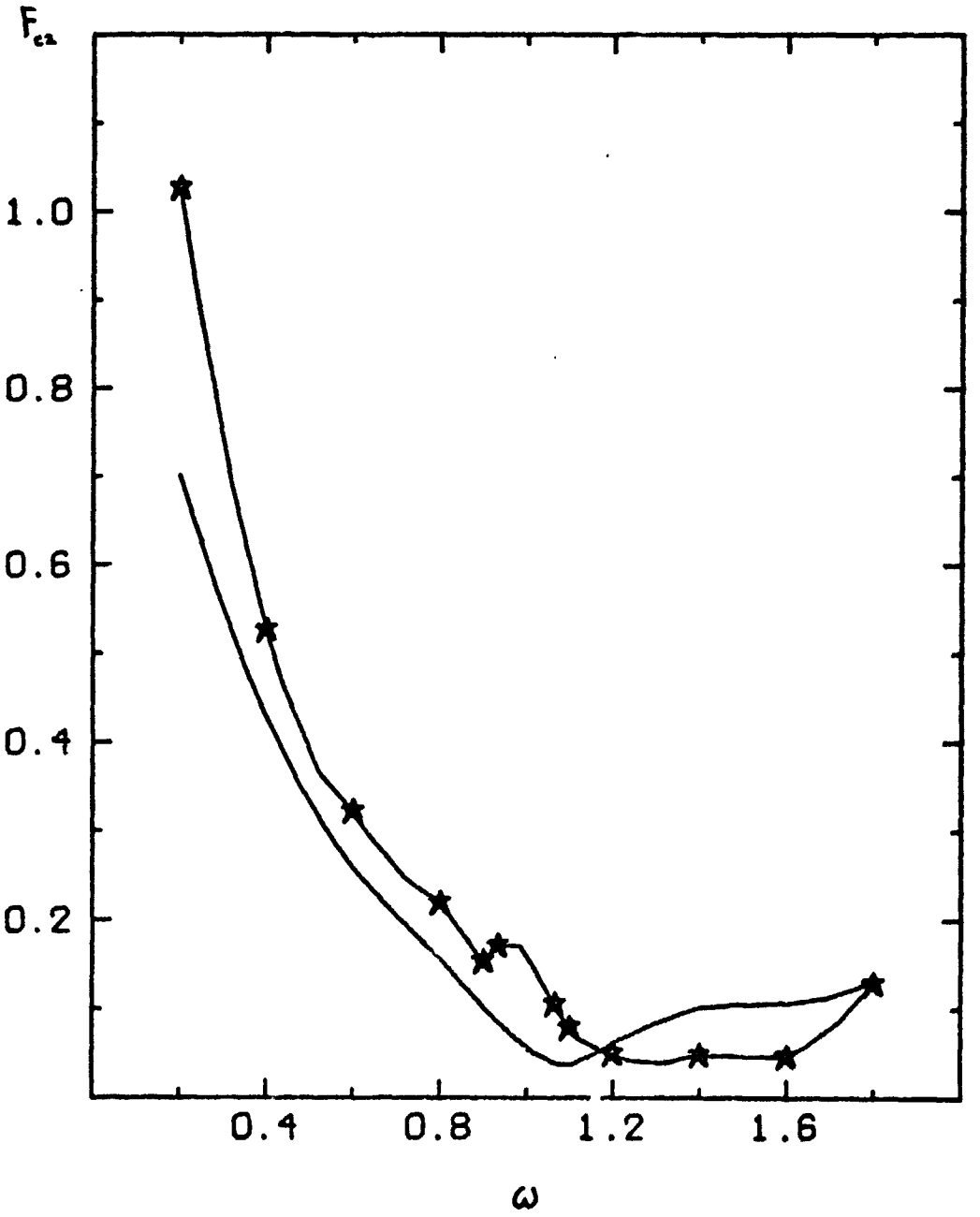

Figure 15f

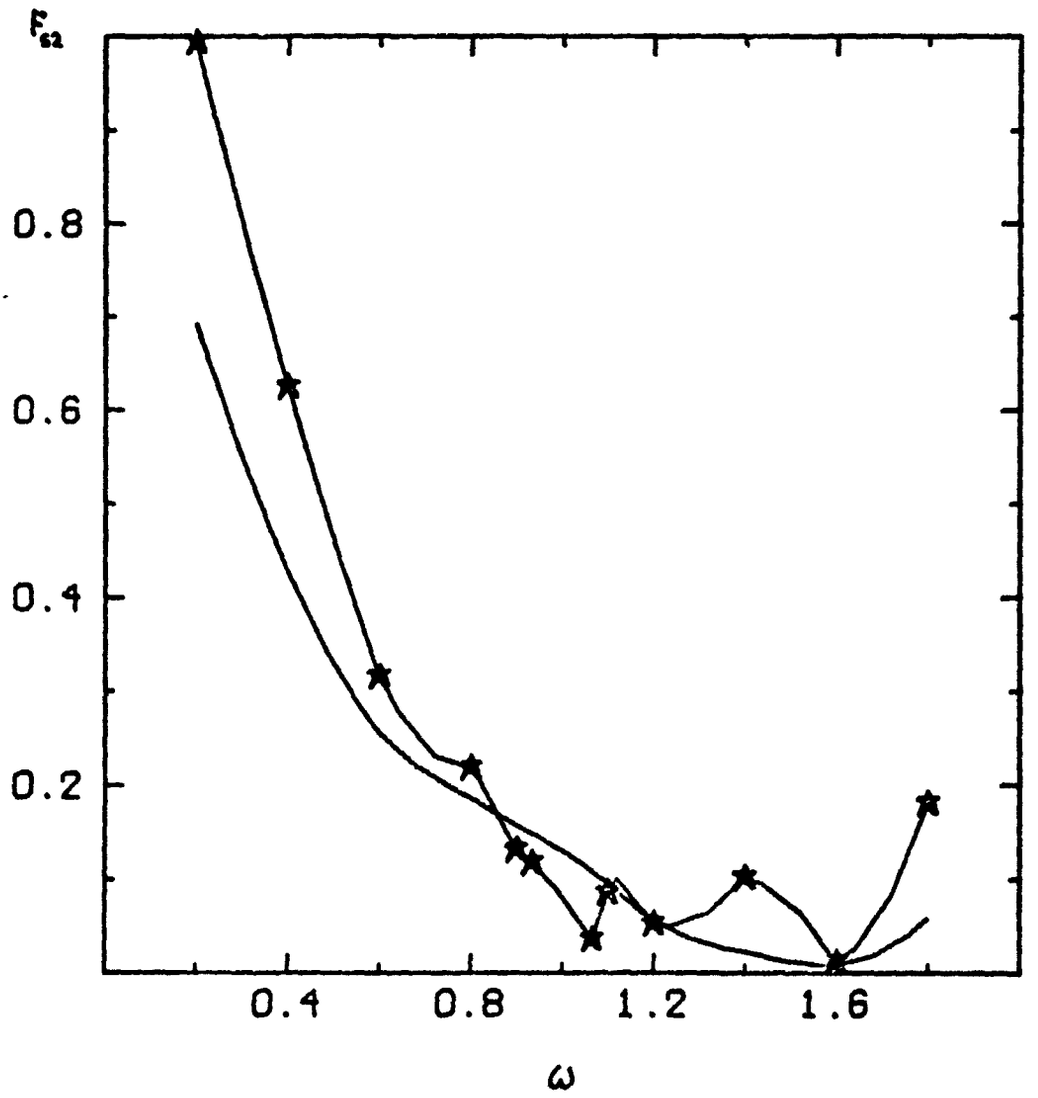

Figure 15g

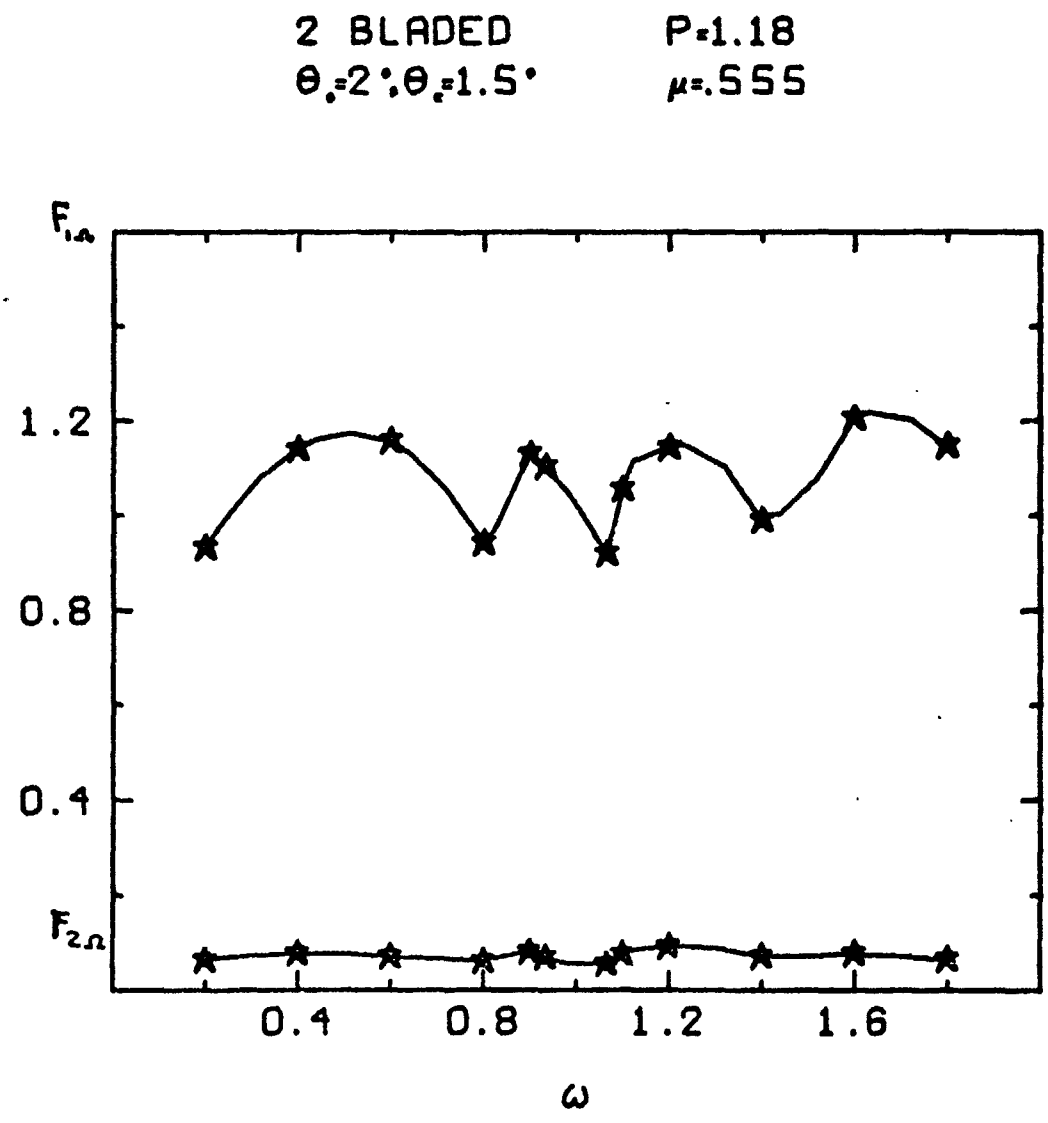

Figure 15h

2 BLADED P=1.18
θ_o=2°, θ_c=1.5° μ=. .74

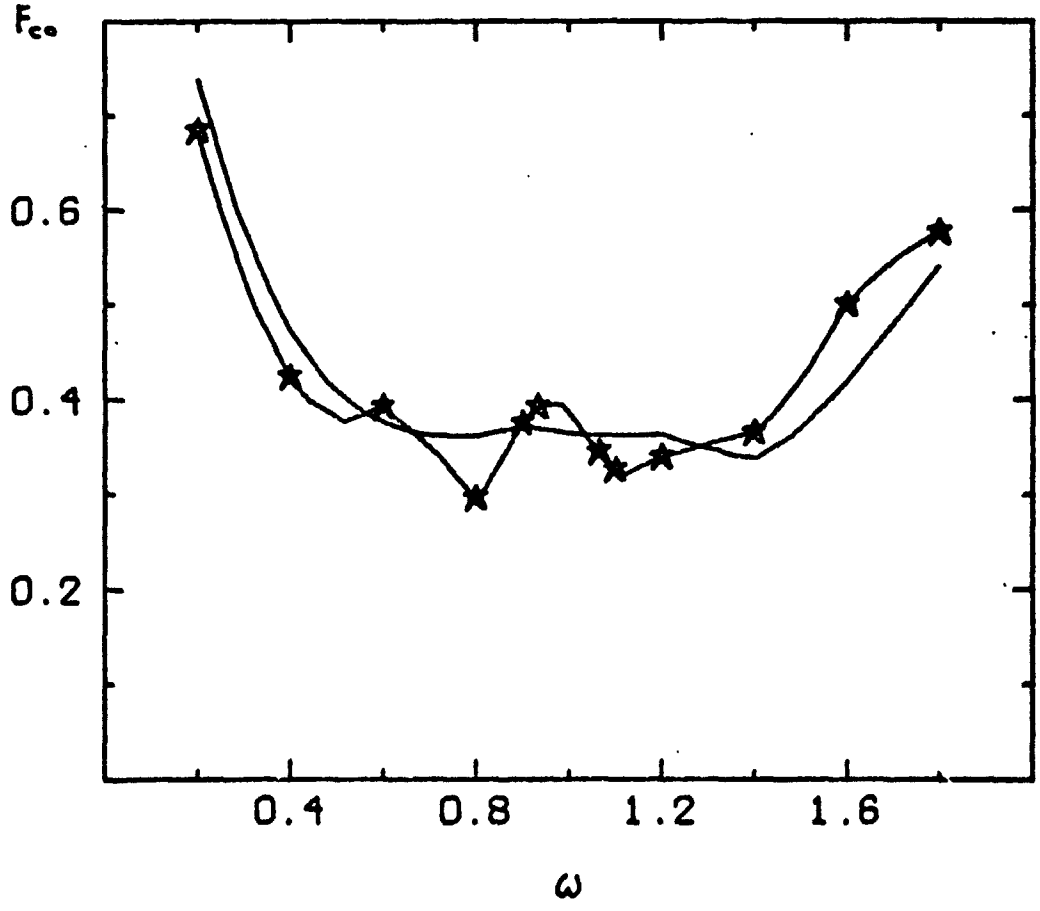

Figure 16a

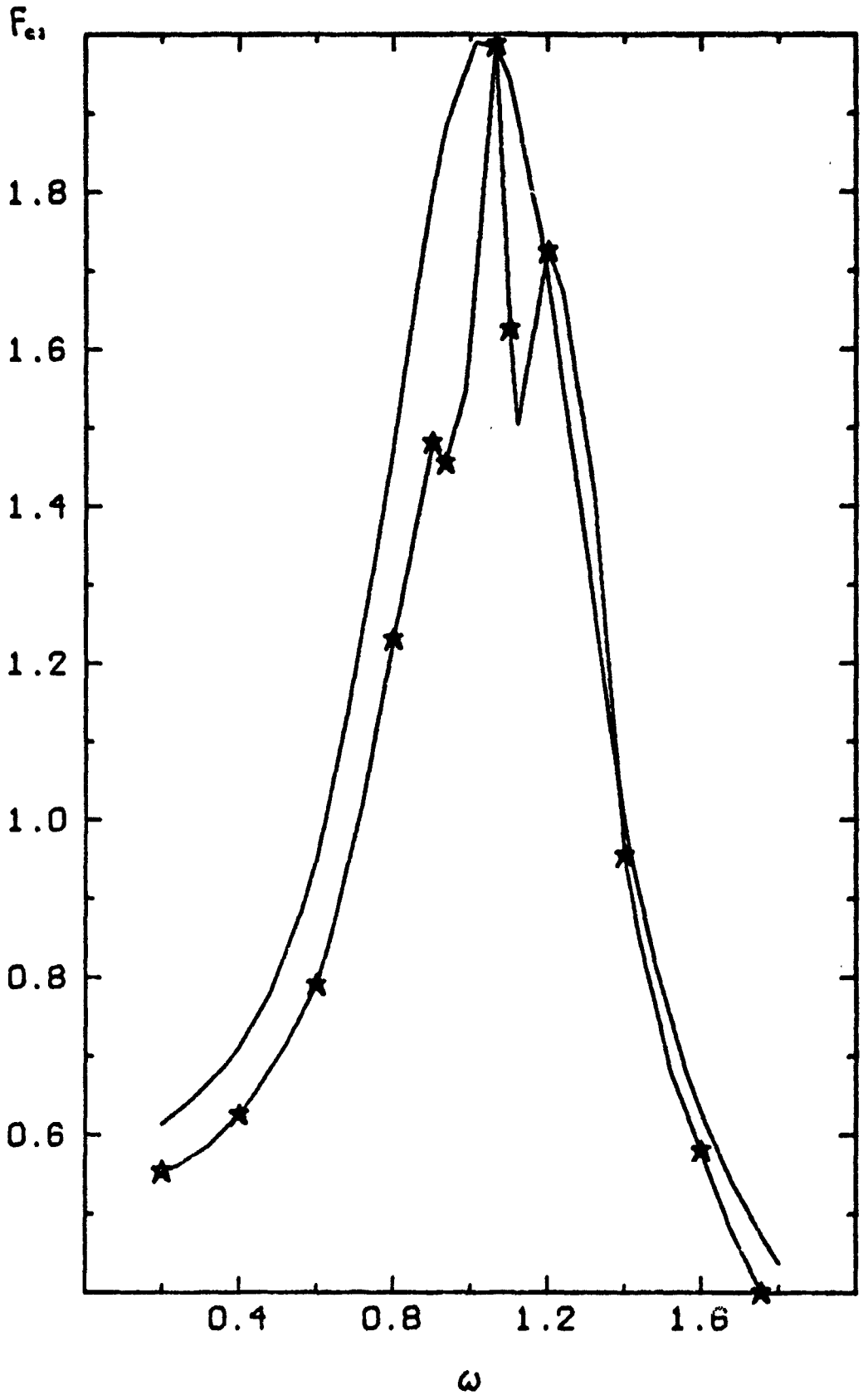

Figure 16b

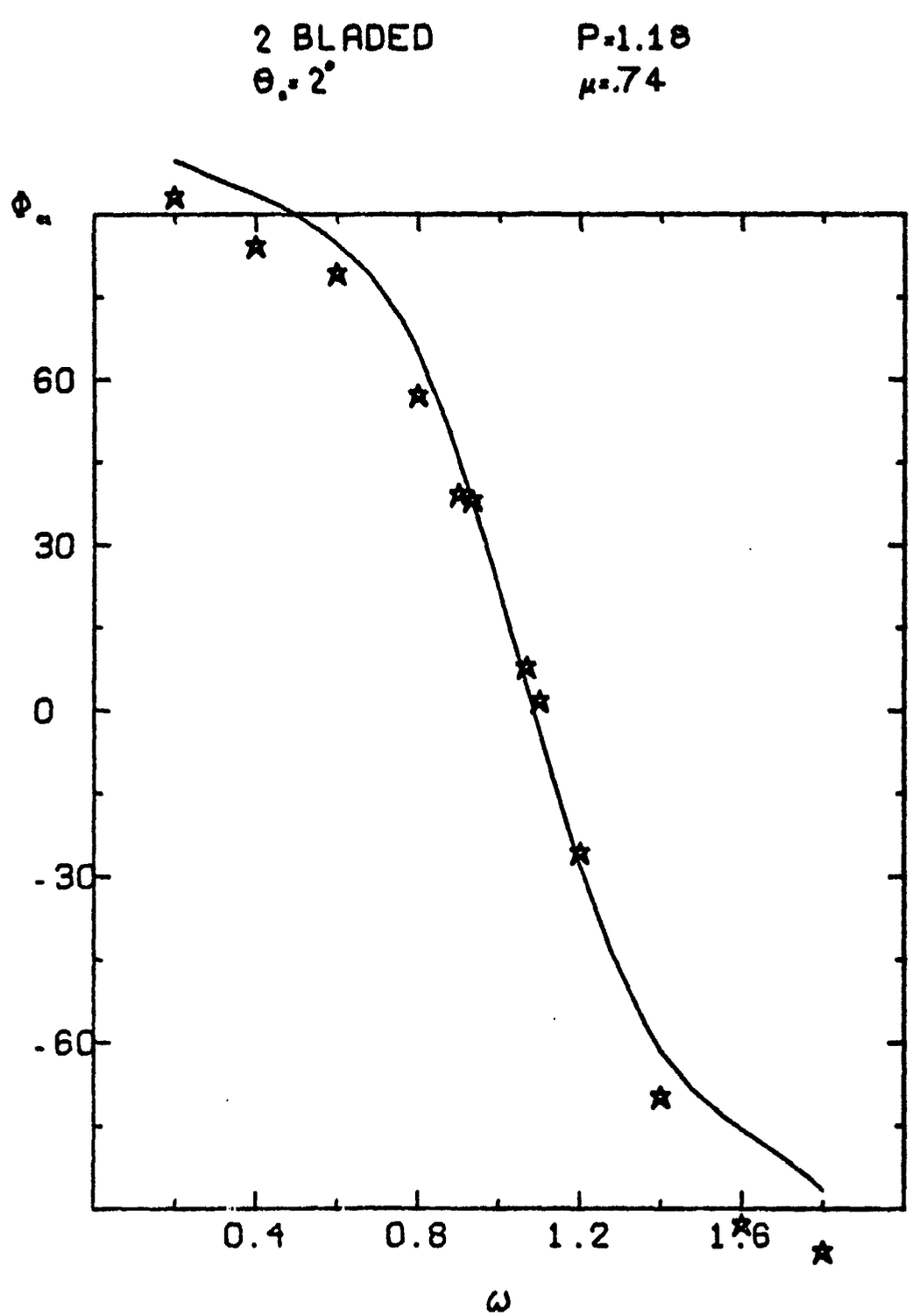

Figure 16c

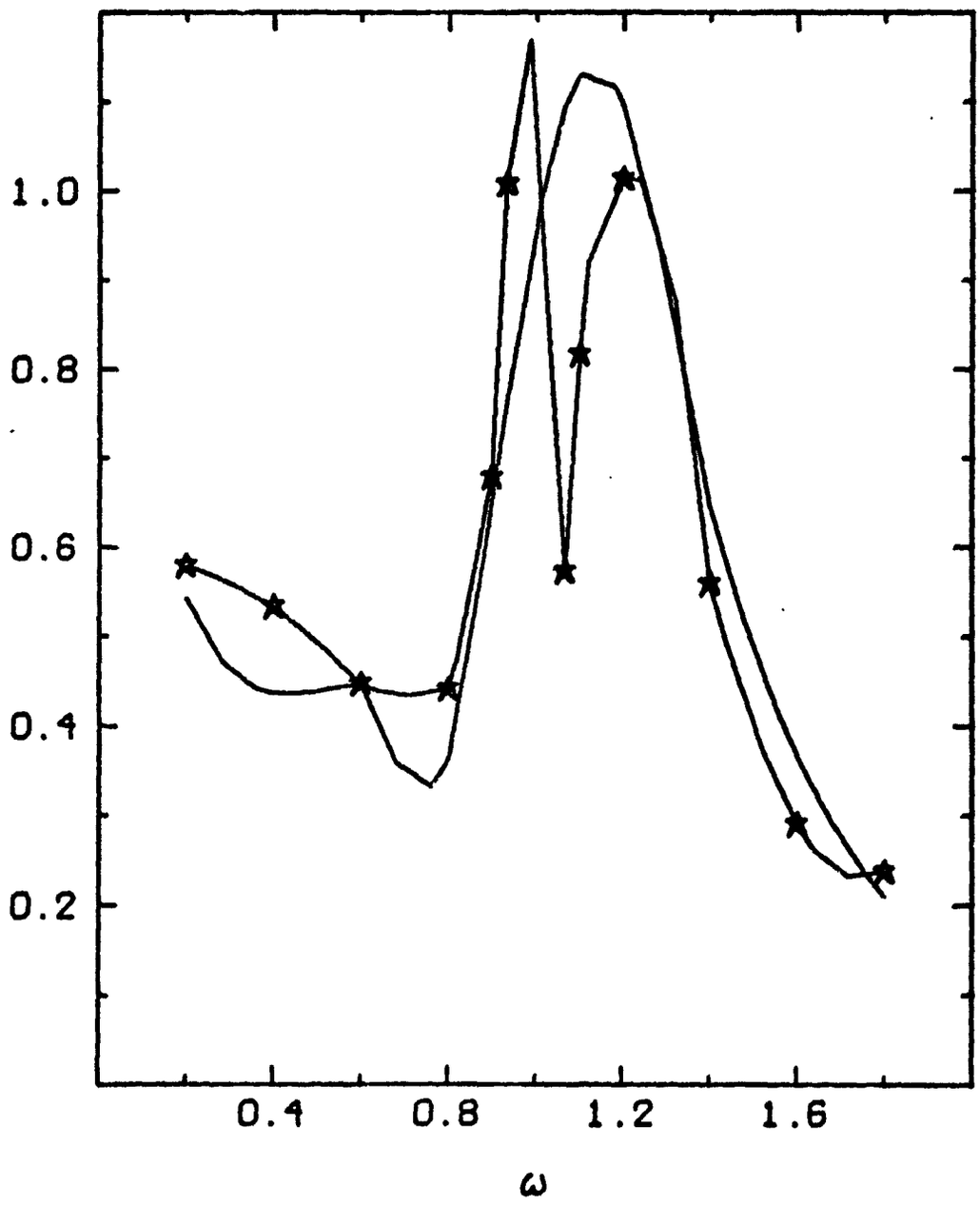

Figure 16d

2 BLADED P=1.18
θ_0=2 μ=.74

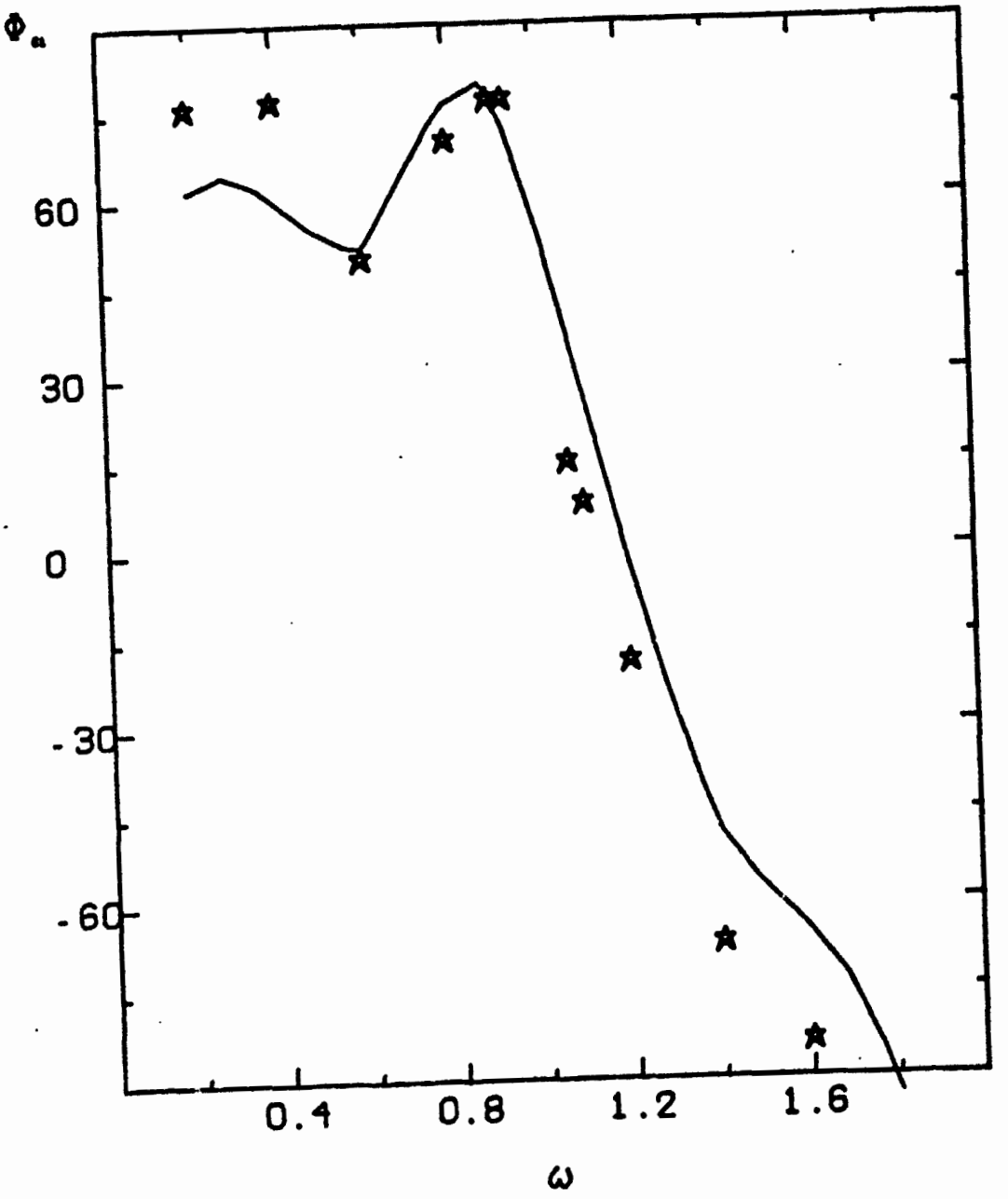

Figure 16e

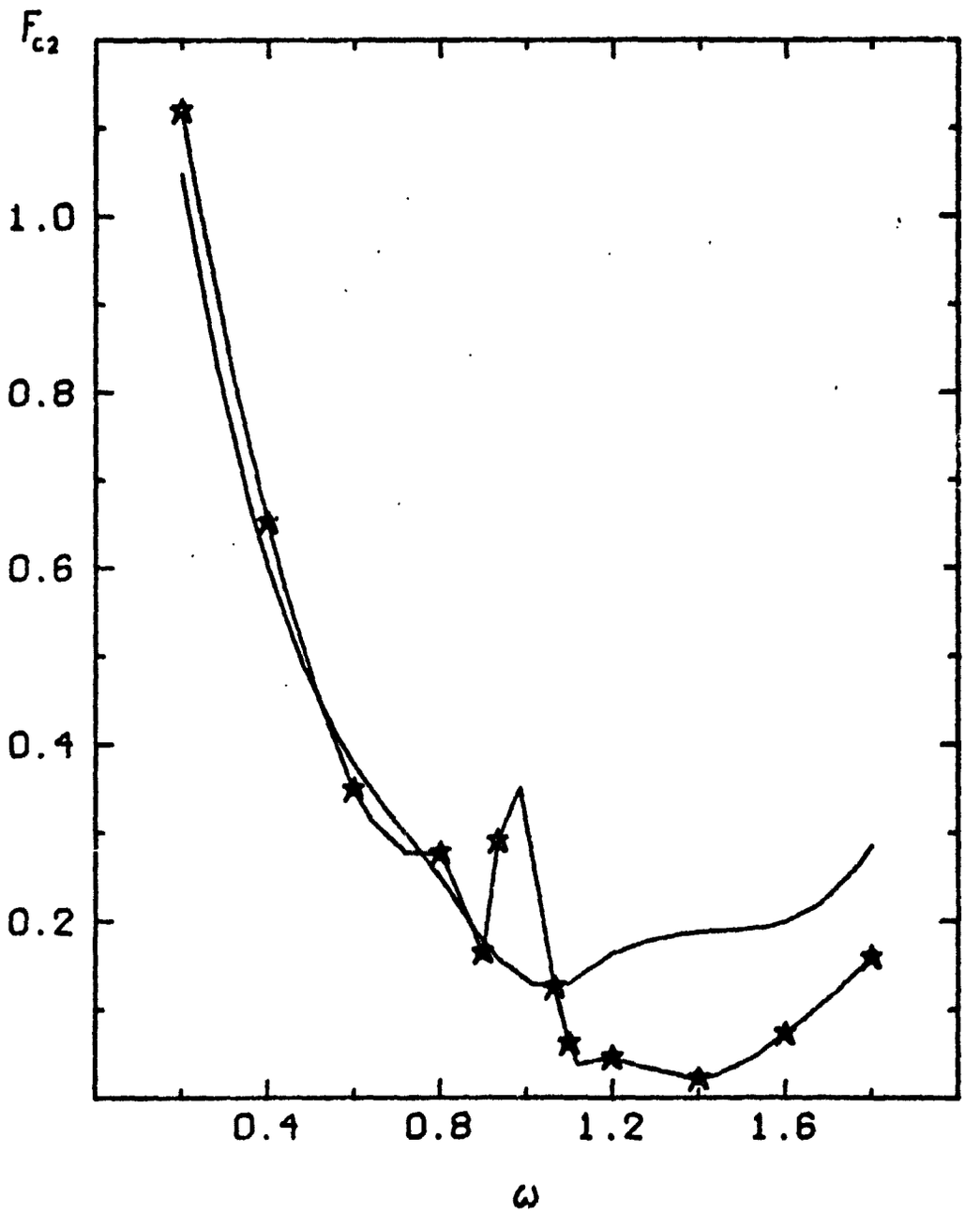

Figure 16f

2 BLADED $P=1.18$
$\theta_0=2°, \theta_1=1.5°$ $\mu=.74$

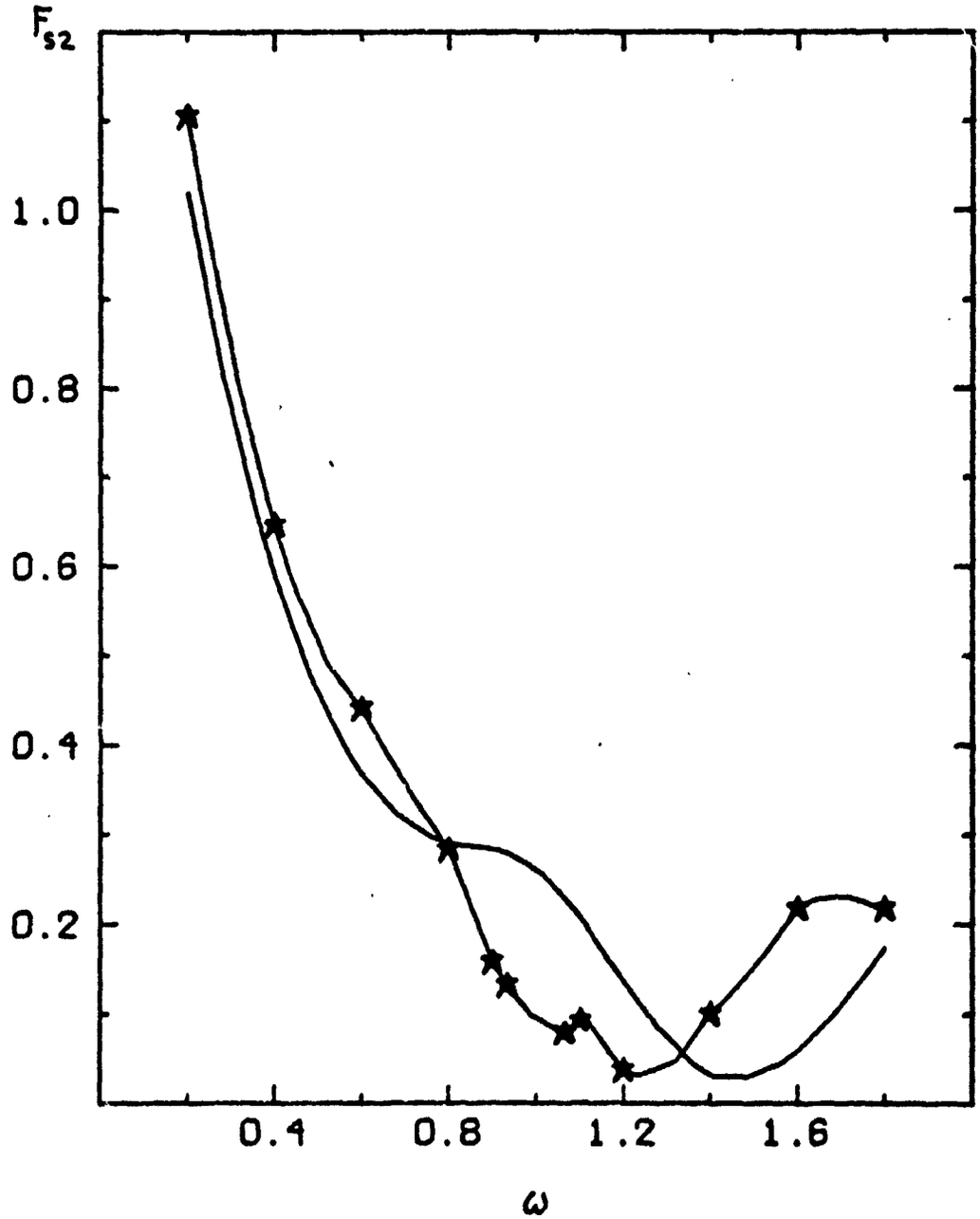

Figure 16g

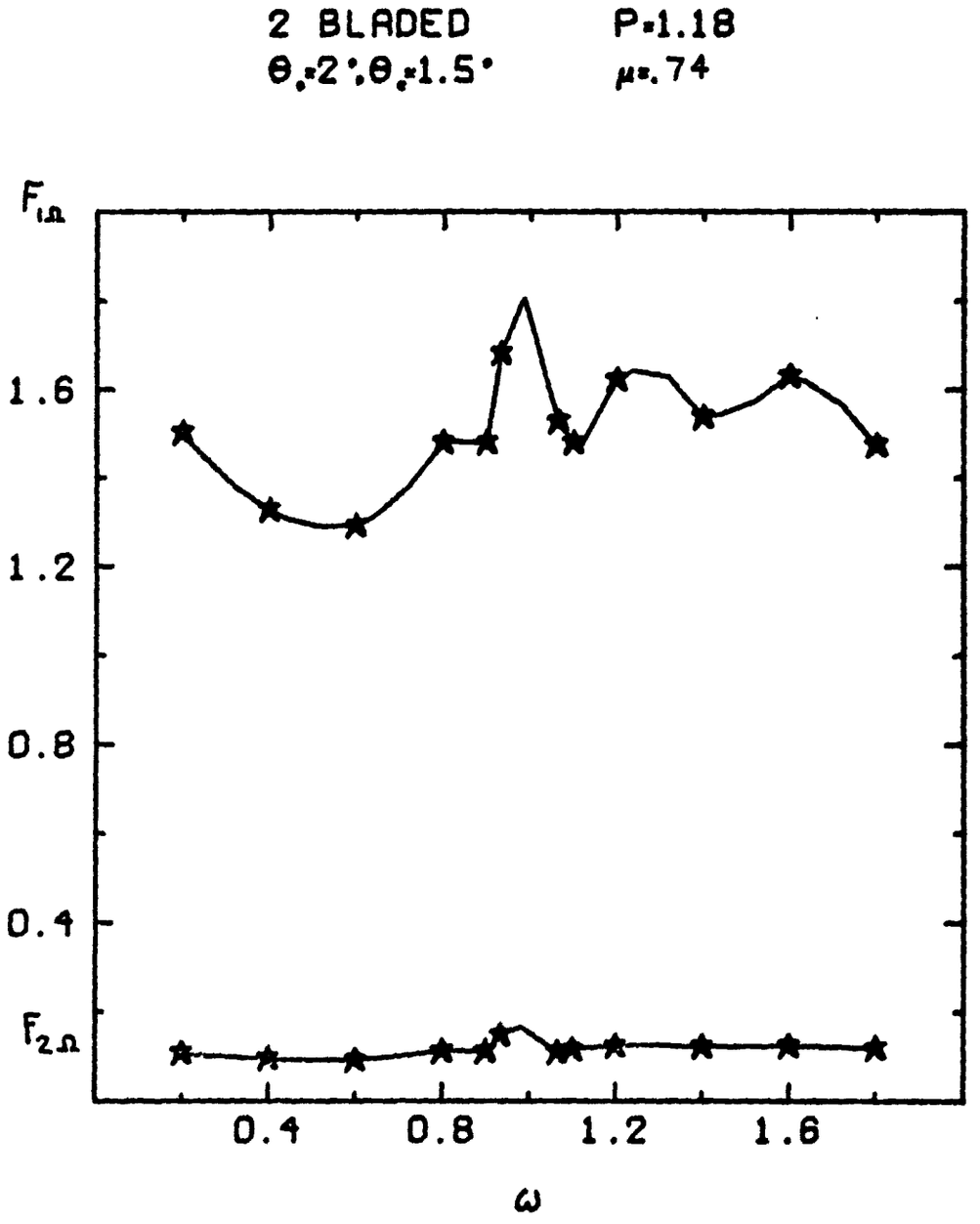

Figure 16h

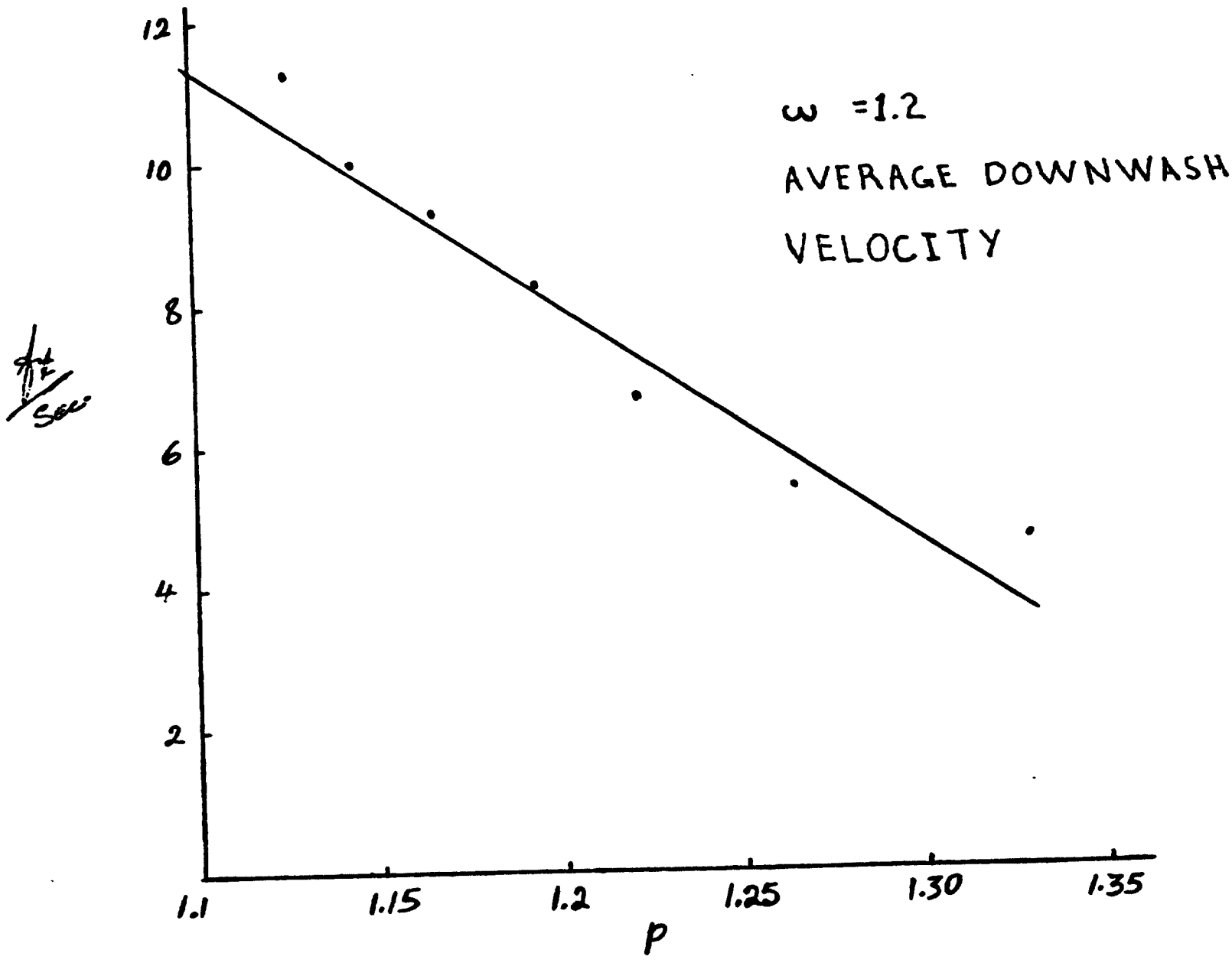
12
10
8
6
4
2
1.1
1.15
1.2
1.25
1.30
1.35
P
ω =1.2
AVERAGE DOWNWASH
VELOCITY
ft/sec

Fig. 17

$\omega = 12$

F_{ω_f} normalized with the average Down wash Amplitude

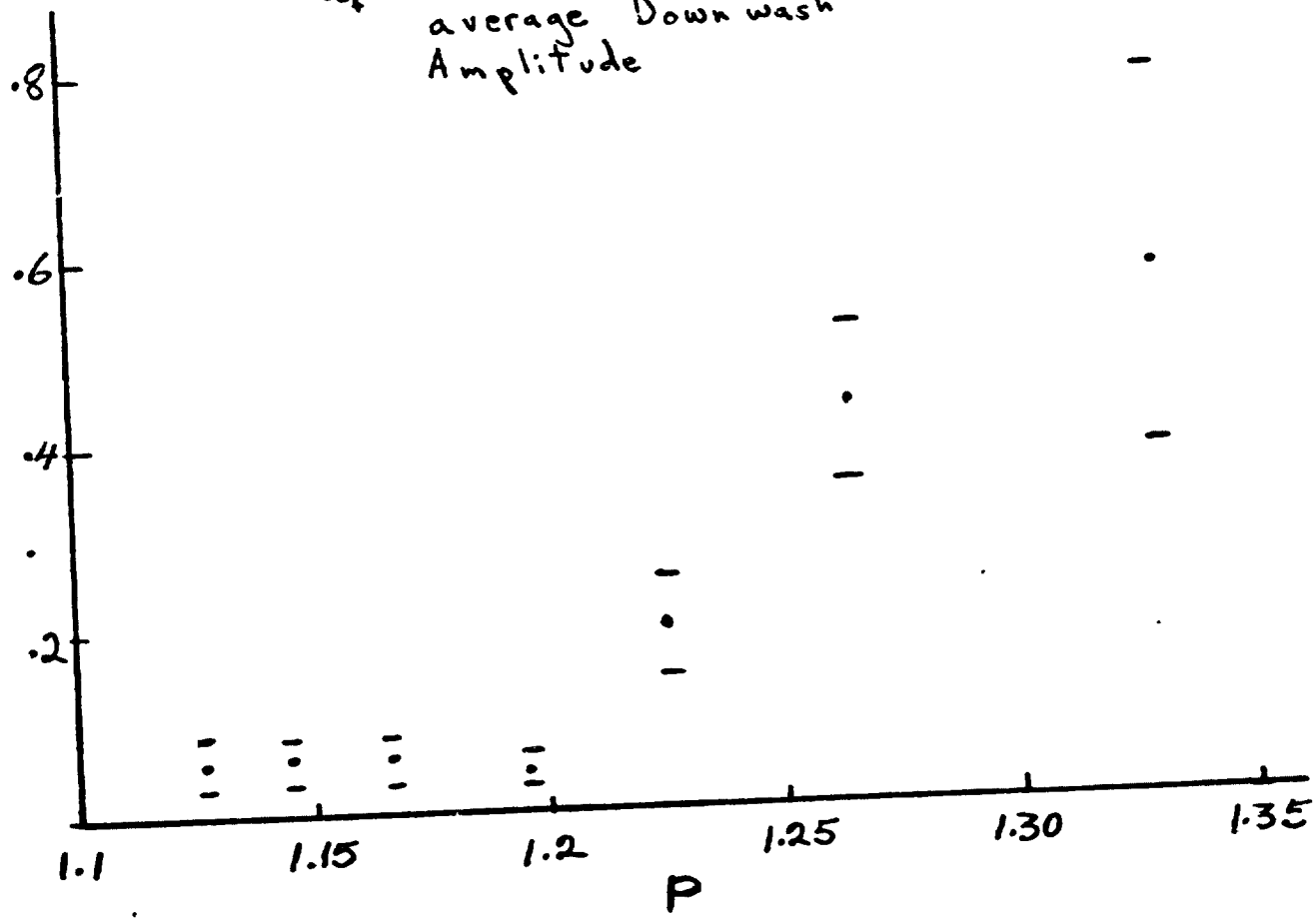

$\frac{F_{\omega_f}}{\text{Av. Down Wash}}$

Fig. 18

$\omega = 1.2$

Downwash

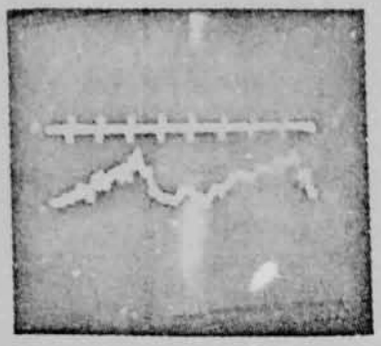

P = 1.33

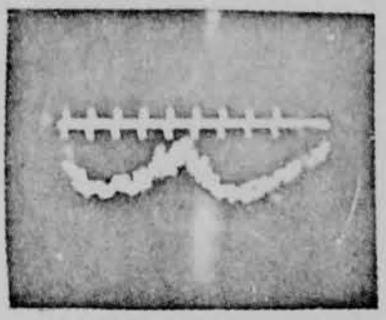

P = 1.265

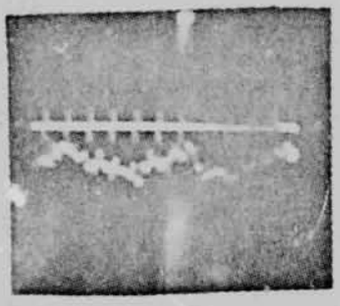

P = 1.224

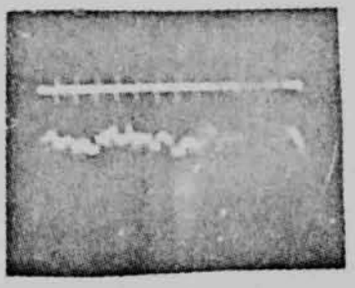

P = 1.195

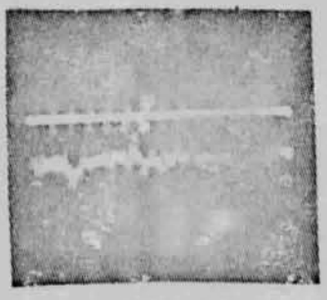

P = 1.167

Figure 19

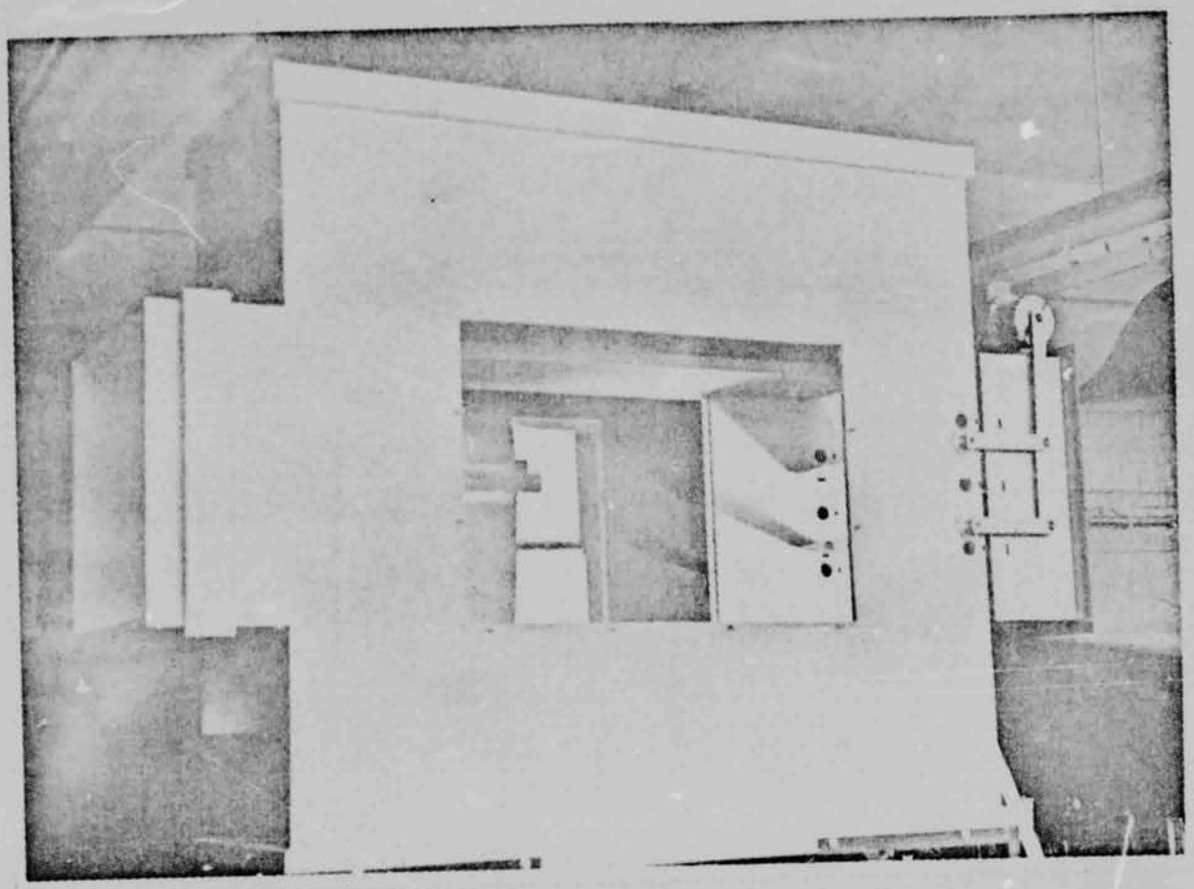

Figure 20a

Figure 20b

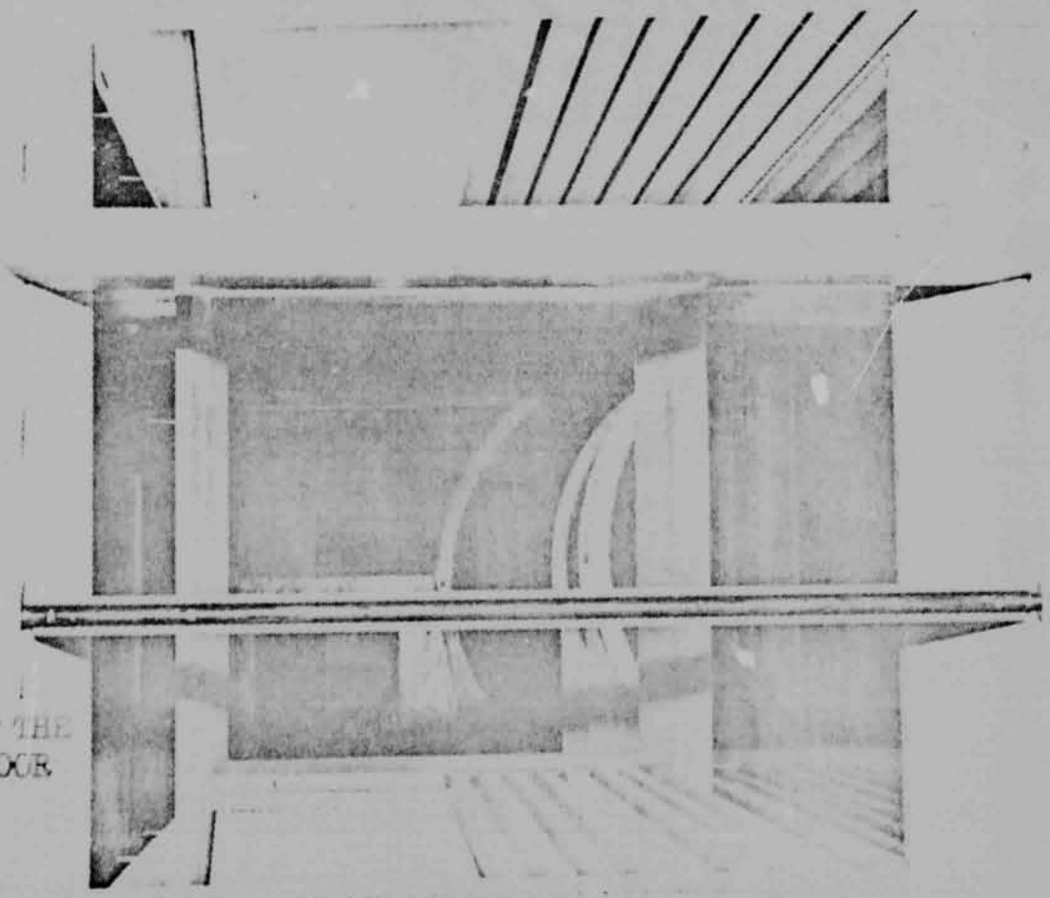

Figure 20c

Appendix A

List of Purchased and Borrowed Equipment

I. Equipment purchased under Contract NAS2-4151 and carried over to Contract NAS2-7613 with purchase price over $1,000.

1 - TSI Thermo Systems Incorporated Model 1050 Research Anemometer	$1,285.00
2 - TSI Model 1052 Polynomial Linearizers at $1,150 each	2,300.00
1 - TSI Model 1015C Correlator	1,075.00
SUM	$4,660.00

II. Equipment purchased under Contract NAS2-7613 over $300

1 - Digital Multimeter	$300.00
1 - Single Channel Helium Bubble Generator with 1 high speed and 1 low speed head	$700.00
	$1,000.00

III. Borrowed Equipment - over $1,000.00

1 - TSI Single Channel, non-linearized hot wire anemometry system	$3,600.00 (New value)
1 - Tektronix Type 502A Dual Beam Oscilloscope	$1,100.00 (New value)
1 - Ampex FR-1300 Recorder/Reproducer	$7,500.00 (New value)
1 - Hewlett Packard Thermal Recording System	$7,500.00 (New value)
1 - Consolidated Electrodynamics Corp. Type 5-124 Recording Oscillograph	$3,000.00 (New value)
1 - 2-channel adjustable high-low pass variable filter	$2,200.00
TOTAL	$26,700.00